FACULTY OF SCIENCE AND TECHNOLOGY

MASTER'S THESIS

Study programme / specialisation: Engineering Structures and Materials / Civil Engineering Structures	The spring semester, 2023 Open
Author: Mahdi Wahidi	
Supervisor at UiS: Dimitrios Pavlou Co-supervisor: Johan Andreas Håland Thorkaas	
Thesis title: Real-time Structural Health Monitoring of Engineering Structures	
Credits (ECTS): 30	
Keywords: Fatigue, fatigue damage accumulation, high-cycle fatigue, damage model, fracture, S355J2+N steel, fatigue life prediction S-N curve, linear, nonlinear	Pages: 93 + appendix: 15 Stavanger, 15.06.2023

Real-time Structural Health Monitoring of Engineering Structures

By

Mahdi Wahidi

Thesis is submitted to the Faculty of Science and Technology
University of Stavanger
In Fulfillment of the Requirements for the degree of
Master of Science (MSc) in Engineering Structures and Materials

FACULTY OF SCIENCE AND TECHNOLOGY

University of Stavanger

Year 2023

Abstract

In recent times, there is increasingly more focus on the environment. Structural Health Monitoring is about maintaining and extending the lifetime and safety of structures. This is a vital field of work. It is becoming more and more important to be efficient in the use of our planets resources. We do not have any resources to waste, and therefore we must maintain our structures, and extend their life for as long as safely possible. The structures must be able to maintain their safety at all times, and therefore, the field of Structural Health Monitoring is a vital field for a more environmentally friendly future for mankind. Instead of letting structures fall into decay, until they are demolished and build up again from scratch, we can monitor the structures during their lifetime, and discover damages real-time. This will not only enable us to have better control over our structures safety and properly maintain them, but in the long run, this will also save costs for our society.

This work of this thesis has mainly been about literature review about the field of Structural Health Monitoring, and fatigue, as well as fatigue damage model. An experimental program was made, and a fatigue test was performed.

The goal of this thesis has been to develop a better understanding about the field of Structural Health Monitoring and a better understanding about fatigue. By performing a fatigue test, the goal was to acquire a better understanding about fatigue behavior under two-level block loading. It is also important to gain a better understanding about linear and nonlinear fatigue, which is discussed in Chapter 3 of this thesis.

Acknowledgements

I would firstly like to thank my parents, for all the encouragement, and support that they have provided me, not just through my studies, but throughout my entire life. They are a source of inspiration to me, and have given me strength, even in the most challenging times. I would also like to thank the rest of my family, my brother and sister, my grandmothers, my aunts, uncles and my cousins. Everyone has encouraged me and supported me throughout my studies, and I will be forever grateful. Everything that I am, I owe to my family.

I would also like to extend a big thank you, to my great supervisor, professor Dimitrios Pavlou, who has shown endless patience with me and given me all the help and supervision necessary to finish this thesis work. He has throughout the entire semester, been a great source of inspiration to me, not only as a professor with vast knowledge about fatigue, but also as a person, endlessly patient and supportive.

A big thank you to my lab supervisor Johan Andreas Håland Thorkaas, as he has given me tremendous amount of help and support with my work in the machine lab. His supervision of the lab work was what enabled the experimental part of this thesis, and for that I am very grateful. A lot of the work done has been with the enormous help and great supervision of my two supervisors. Without them, I would've never been able to finish on my own.

Lastly, I would like to thank the University of Stavanger, for providing the facilities necessary to perform the thesis work. All members of the faculty as well as everyone working in the machine lab have been very supportive and helped in any way they can. I am forever grateful.

Table of Contents

List of figures

List of tables

List of appendixes

List of abbreviations

DCA	Damage curve approach
DDCA	Double damage curve approach
DLDR	Double linear damage rule
FDS	Fatigue driving stress
LDR	Linear damage rule
NDE	Non-destructive evaluation
NLDR	Nonlinear damage rule
SHM	Structural health monitoring
VTLC	Virtual target life curve

1. Introduction

1.1. Topic Relevance

According to the book Structural Health Monitoring: An International Journal, Structural Health Monitoring (SHM) is the continuous or regular monitoring of the condition of a structure. This is done by using built-in or autonomous sensory systems, and any intervention because of those to preserve structural integrity. [Chang et al., 2002]

Structural Health Monitoring will enable us to further lengthen the lives of the structures in our society. Not only saving us costs in demolishing and rebuilding from scratch, but also lowering usage of materials and makings us a more environmentally friendly society.
At the same time, monitoring of structures real-time will ensure we have the highest safety in terms of structural health. It will be cost efficient for us to become aware of damages to the structures as early as possible, to monitor further increase in damages and to assess the risk levels.

1.2. Objectives

The objectives of this master thesis are the following tasks:

- To give a brief overview of Structural Health Monitoring methods.
- To give an overview and understand fatigue damage accumulation methods.
- Implementation of linear and nonlinear fatigue models.
- Lastly, to perform fatigue tests.

1.3. Methodology

The work of this thesis has been done firstly, through literature review, and gaining a better understanding of Structural Health Monitoring and fatigue, as well as better understanding about fatigue damage accumulation methods.

Afterwards, the work was to prepare for the experimental part of the thesis project. Assigned by supervisors, I received 12 bars of steel and needed to find the material sheets for that specific material, so that I, with the supervision of Professor Dimitrios Pavlou could plan the experimental program. There were two material sheets, for the same material, and we had to do tensile tests, to determine the material properties. After the material properties were determined, an S-N curve was found from a study with the same material and used to plan the experimental program.

The experimental program planned by Professor Dimitrios, was planned as a two-level block loading sequence. Where two types of load sequences would be tested. A high-to-low fatigue loading tests, and a low-to-high fatigue loading test.

When learning about fatigue, one usually starts to learn about the linear model most people know as Miner's rule, and then work their way to learn about the other linear and nonlinear models. For the work in this thesis, it was chosen that the linear calculations would be done with Miner's rule and modified Goodman, and the nonlinear calculations would be done with the Rege-Pavlou model.

Lastly, after the theoretical understanding was in place, and the planning had been sufficiently done, I could, with the supervision of the lab supervisor of this work, Johan Andreas Håland Thorkaas, begin the experimental verification of the theoretical results.

1.4. Thesis structure

The project work that has been done during this thesis is discussed throughout six chapter (not counting chapter one).

Chapter 2 gives a brief overview of Structural Health Monitoring methods and tries to discuss different methods of Structural Health Monitoring for civil structures like bridges and building, as well as mechanical structures like planes and cars.

Chapter 3 gives an overview about fatigue damage models. This is the biggest chapter of this thesis as it contains an overview of both linear and nonlinear fatigue damage models. It does not contain all fatigue damage model, there are many and to limit the scope of this thesis, only the most widely accepted and recent ones have been discussed.

Chapter 4 is the experimental verification of the fatigue models, and discusses the formulas used to calculate the theoretical fatigue lives of the specimen of this thesis. The specimen is a steel bar S355J2+N grade steel and the material and chemical properties of the steel are explained as well as how the experimental program is planned to be carried out.

In chapter 5 the results from the fatigue life calculation are described both the linear and nonlinear ones. Then the result from the experimental work is presented and described. Lastly, graphs are made showing the damages and the cycle ratios.

In chapter 6, there is discussed the results described in chapter 5. The experimental work procedure and how the lab work went, as well as the issues that occurred are described. Lastly it discusses the most recent Structural Health Monitoring methods.

Chapter 7 is the last chapter of this thesis and will give a conclusion about this thesis work, as well as some suggestions for future work.

Lastly, there are three appendices that have more details about this thesis work, that is the experimental fatigue test data, the calculations and the tensile test results.

2. Structural Health Monitoring

2.1 Structural Health Monitoring: An Overview

This chapter will give an overview about Structural Health Monitoring. The continuous or regular monitoring of a structure with built-in or autonomous sensory systems and any resultant intervention to preserve structural integrity is called Structural Health Monitoring (SHM). SHM is a multidisciplinary and broad field because it is diverse in terms of technology and science as well as its varied application.

The technological developments needed for practical structural health monitoring originate from engineers and scientist of many different fields. For instance, from materials science, civil, mechanical, chemistry, physics, electrical, and aerospace engineering. SHM is used on diverse structures and systems like civil infrastructure, aircrafts, spacecrafts, ships, pipelines, biological systems, manufacturing and processing facilities, and for defense and protection of the environment [Chang et al., 2002].

SHM can increase the lifetime, safety, performance, and reduce maintenance needs of all types of structures, from nanostructures, to microstructures, to infrastructures. It is very important that knowledge is continuously shared and new technologies and ideas are integrated into new fields and applications. For instance, the integration of biological function with nanoscale precision also known as Bio-Nanotechnology is very promising and could produce major advancement in the field of SHM.

The integration of Nanotechnology, Biomimetics, Smart structures and SHM could perhaps during this century deliver vast improvements to material systems, communication architectures, sensors, and actuators. This could result in superelastic lightweight structures that can self-assemble, monitor their own health and performance, adapt and react to their environment, and self-heal in a way that new generations of structures may become autonomous and possibly almost unbreakable.

The socio-economic benefits of such enduring and autonomous structures would extend beyond all civil infrastructure systems and can further allow the human exploration and colonization of space [Chang et al., 2002].

Some damage detection methods are localized or visual methods using ultrasonic, acoustics, X-ray, magnetic fields, and thermal principles. To perform these techniques, knowledge about the vicinity of the damage is required and the area must be accessible. Human-based inspection procedures are very costly and therefore sparsely used.
The need for quantitative, global, damage detection methods that can be applied to complex structures has led to research into methods using changes in structural vibration characteristics. This has led to systems that can detect specific faults like bearings and gears.

For structural integrity damage, there has been research into both model-based methods and signal-based methods. The term “Model-based diagnostics” versus “Symptom-based diagnostics” was introduced [Natke & Cempel, 1997]. The focus of the research is on sensor technologies detection and localization methods [Van der Auweraer & Peeters, 2003].

2.1.1 Application Fields

In the civil engineering field, the main concerns for stakeholders are the increasing age of the civil infrastructure as well as the related costs of inspection and maintenance. There is a focus on bridges and high-rise structures. Global issues with respect to bridges has been researched [Prine, 1995] [Aktan et al., 2000]. The concept of global lifetime cost was introduced [Enright &

Frangopol, 2000]. The general condition of bridges is called “Bridge Management Systems” and the topic of bridge management is presented [Czepiel, 1994].

In the aeronautics sector the focus has been to increase efficiency of operation and support of an air vehicle fleet [Derriso et al., 2001] [Galea & Baker, 2000]. SHM is a component of a global Integrated Vehicle Health Management system (IVHM).

2.1.2 Distributed Measurement Systems

The instrumentations used in SHM are researched more and more. Previously, this topic was mainly focused on sensors, but more research has been done on the practical implications regarding the acquisition, collection, and processing of the data. The main critical elements appear to be:

- Sensor data collection. Sensors in civil structures can be distributed over large distances and therefore solutions based on smart cabling systems as well as wireless transmission had been researched [Strasser, 1998] [Fuhr, 2000] [Lemke, 2000].
- Power supply through cabling system, battery or solar [Oshima et al., 2000].
- Synchronization of the dynamic data to extract system models from multisensory data. The data must be sampled at the same time. This can be done by use of common triggers, extra synchronization cabling, or GPS based time tagging.
- The merging of the environmental data and dynamic data. To differentiate integrity related phenomena from temperature, wind or humidity effects, environmental data are essential [Oshima et al., 2000] [Peeters et al., 2000].
- Transferring the acquired data to a remote analysis station by use of either private server using Ethernet [Todoroki et al., 2000], Intranet [Mita, 2000] [Yamamoto et al., 1998] or public interests [Lemke, 2000] [Rahman et al., 2000].
- Finally, long-term monitoring in often harsh weather conditions puts heavy demands on the robustness of the instrumentation [Van der Auweraer & Peeters, 2003].

2.2 Health Monitoring of Civil Infrastructure

Civil infrastructures like buildings and bridges begin to deteriorate once they are built and used. Maintaining a safe and reliable civil infrastructure for daily use is important to the well-being of society. Knowing the integrity of a structure in terms of its age and usage, and its level of safety to withstand infrequent but high forces such as earthquakes, tornadoes or hurricanes is both important and necessary. Health monitoring is the process of determining and tracking the structural integrity and assessing nature of the damage in a structure.

Health monitoring of civil infrastructure consists of determining, with measured parameters, the location and severity of damages in buildings or bridges as they occur. However, using state-of-the-art methods of health monitoring, the information is not sufficiently accurate in determining the extent of the damage. These methods can determine whether damage is present in the entire structure or not. They are called “global health monitoring” methods. They are important because often just knowing that damage has occurred is enough to cause further examination of the structure to find the exact location and severity of the damage.

Non-destructive evaluation methods (NDE) are used to locate the damage. Methods like ultrasonic guided waves to measure the state of stress or eddy current techniques to locate cracks can determine the exact location and extent of the damage. These methods are called “local health monitoring” methods. NDE is often time-consuming and costly, and access is not always possible.

That is why both local and global health monitoring methods are important and necessary [Chang et al., 2003].

2.3 Real-time Health Monitoring of Mechanical Structures

Complex mechanical systems such as civil infrastructures, power plants, surface ships, aircrafts, and submarines, often vary widely in usage patterns. Because of the difficulty and costs of implementation in these complex structures, usage is often measured in different quantities such as years for roads and bridges, flight hours for aircrafts, and number of starts in diesel engines.

The state of damage in a mechanical structure is also assumed to bear a direct correlation with the amount of usage. This however depends on how a structure is used. One can be used in a benign manner while another is used in a way that drastically reduces its service life. For instance, engines in aircrafts used for pilot training experience higher levels of stress.

This makes it difficult and costly in logistics and maintenance efforts mainly because maintenance action and operation planning are based on usage and therefore as damages and anomalies are experienced over time, periodic maintenance and premature replacement of parts become more frequent to ensure the safety of the most heavily used structures. This can be solved by using on-line failure diagnosis and prognosis that allows for remaining life prediction for critical structural components of operating machinery under calculated load profiles.

Because of the random and nonstationary nature of fatigue crack propagation in ductile-alloy structures, it is difficult to determine the current state of damage and remaining service life of machinery components. For structures where failure can have catastrophic consequences the practice is to either estimate service life conservatively or frequent costly and time-consuming inspections or both. Real-time sensing of damage will allow on-going re-evaluation and extension of the service life and safety against unforeseen catastrophic failures.

If no inspection or on-line prediction of damage is available, it is important to repair or retire the structure when the worst possible crack trajectory reaches a critical length reduced by a safety margin. The trajectory of the crack should be determined for an acceptable risk level from observed statistics, but due to lack of an appropriate stochastic model of crack propagation, this is not commonly applied. More research needs to be done in extending the service life of mechanical structures while fulfilling their objective.

Meaning a trade-off must be achieved between service life and operational performance. Currently it is done by inspections and maintenance actions based on fixed usage intervals. On-line sensing of the damage state and remaining service life predictions will reduce the frequency of inspections and increase the mean time between major maintenance actions on serviceable structures [Keller & Ray, 2003].

2.4 Framework for Structural Health Monitoring

2.4.1 Real-time Strain Measurement

Measuring of the strain evolution real-time is going to allow us to have much more control of a structures fatigue life. There are many different types of sensors available for measurement of loads over a period of time. These are strain gauges, digital image correlation method (DIC) for strain measuring, fiber optic sensing of strains (FBG), vibrating string gauges (VSG) and so on. Each of these has their own advantages and disadvantages. For instance, the DIC method gathers

vast amounts of data, but this in turn also is a problem, it gathers too much data, and also requires high level of light intensity to be able to gather the relevant data. The FBG sensor have problems with the stability of the measure signal during a long-time monitoring process and the signal allocates unplanned changes in in magnitude offset. FBG sensor cannot, due to this, hold the right offset for a long period of time. The VSG sensor have problems with frequency range or higher measurement costs. To be able to focus on long-term monitoring and measuring of loads for any structure, the strain gauges seem to be the best and most practical solution to obtain relevant strain measurement data [Chmelko & Garan, 2016].

2.4.3 Transformation to cyclic loads with aim of Rainflow Counting Method

This part of the Structural health Monitoring process focuses on extracting cycles that are from complicated load histories where each cycle is associated with a closed stress-strain hysteresis loop. By using the original Rainflow cycle counting method, the cycles from complicated uniaxial loading situations can be extracted and then transformed into simpler cyclic loads [Lee & Tjhung, 2012].

2.4.4 Calculation of equivalent stress amplitude for each loading cycle

Stresses that are obtained directly from cycles, often cannot be used due to not being the same stress ratio as the S-N curve of the material in question. Therefore, the cyclic stress will be calculated into mean stress and stress amplitude, and then they will both be further calculated into an equivalent stress amplitude that can be used with an S-N curve. This will be further explained with necessary calculations in chapter 4.

2.4.5 Calculation of the damage due to each loading cycle

Every load will have a peak (maximum stress) and a bottom (minimum stress). As explained in 2.4.4, once the complicated loads are transformed into simpler cyclic loads, they will be calculated into mean stress and stress amplitude, and then an equivalent stress. This will happen for every load level. From each equivalent stress, and by using an S-N curve of a material, it is possible to obtain the number of cycles until failure. By knowing the number of fatigue cycles a specimen has been through and calculating with the use of an S-N curve, the number of cycles until failure, the damage from each loading cycle can be calculated. This is also explained in chapter 4 with calculations.

2.4.6 Damage summation of the all loading cycle

After calculating the damage from each loading cycle, all of the damage is summarized to calculate the damage that has been done to the specimen. This is often compared on a graph with the cycle ratio.

3. A Review on Fatigue

3.1 Introduction

Fatigue is defined as failure caused by a load lower than the load needed to induce a static failure. This can be a mechanical load, thermal load, or other types of loads. [Kamal & Rahman, 2018]. The American Society for testing and materials have given the definition:

"The process of progressive localized permanent structural change occurring in a material subjected to conditions that produce fluctuating stresses and strains at some point or points and that may culminate in cracks or complete fracture after a sufficient number of fluctuations" [ASTM International, 2013]

To characterize fatigue, we have some parameters and variables that we can use. One of them is called fatigue life and it is number of cycles until material failure. Stress ratio (R) is another one and is calculated by the algebraic ratio of the two loading parameters used in each cycle. To understand the stress ratio (R), we need to characterize some other parameters. These are: Maximum stress (σ_{max}), minimum stress (σ_{min}), the mean stress (σ_{mean}), and the stress amplitude (σ_a) [Lee et al., 2012] [ASTM International, 2013]. Figure 1 shows these parameters in a cyclic loading sequence and their relation to each other through the Equations (3.1), (3.2), and (3.3) [Dantas, 2019].

$$R = \frac{\sigma_{min}}{\sigma_{max}} \tag{3.1}$$

$$\sigma_a = \frac{\sigma_{max} - \sigma_{min}}{2} \tag{3.2}$$

$$\sigma_{mean} = \frac{\sigma_{max} + \sigma_{min}}{2} \tag{3.3}$$

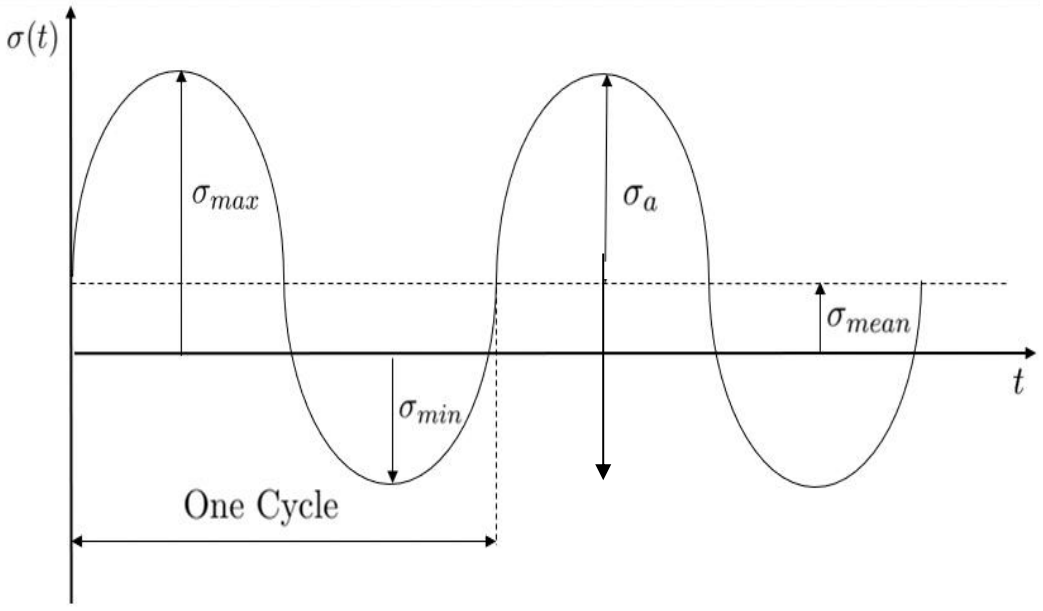

Figure 1: Cyclic loading [Dantas, 2019].

A fatigue stress cycle can by this be defined as three couples of parameters: Maximum stress and minimum stress, mean stress and stress amplitude, or stress amplitude and stress ratio. If we however want to characterize the fatigue stress cycle, we also need to define the loading wave shape. The loading spectrum shown in Figure 2 is a sinusoidal wave, but it can also have different shapes. In time dependent cases like corrosion or creep, the frequency and shape wave can affect the fatigue life strongly [Schijve, 2001].

We can classify the loading according to the mean stress value as: fluctuating (R > 0), repeated (R = 0), fully reversed (R = -1), and reversed (R < 0) [Fernandes et al., 1999].

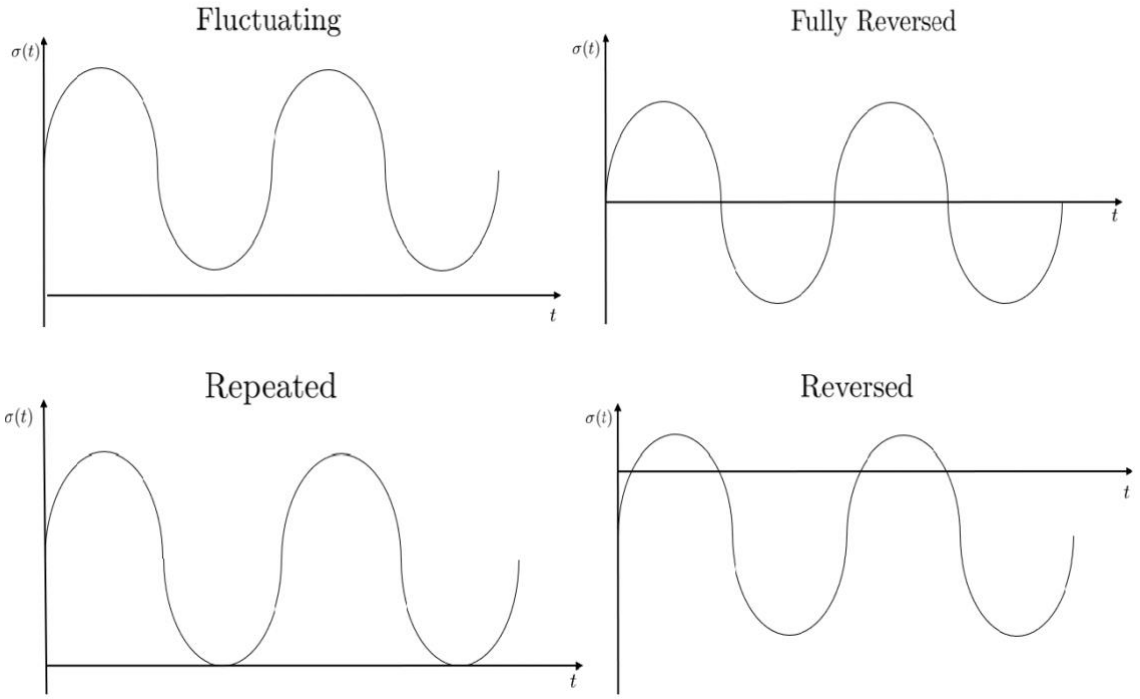

Figure 2: Stress ratios [Fernandes et al., 1999].

The fatigue limit (σ_{f0}) can be defined as the cyclic loading limit that does not cause a fatigue failure [Schijve, 2001].

3.2 Different Fatigue Stages, Factor and Regimes

The fatigue life can be divided into three different phases: the initiation/nucleation phase, the crack growth phase, and the final failure phase (see Figure 3). The different stages are affected by different factor. For instance, the surface condition only affects the first stage, and the corrosion affects both the crack initiation phase and the crack growth phase, but their degree of effect varies. Therefore, the prediction of fatigue life of initiation and crack growth are different stage [Schijve, 2001].

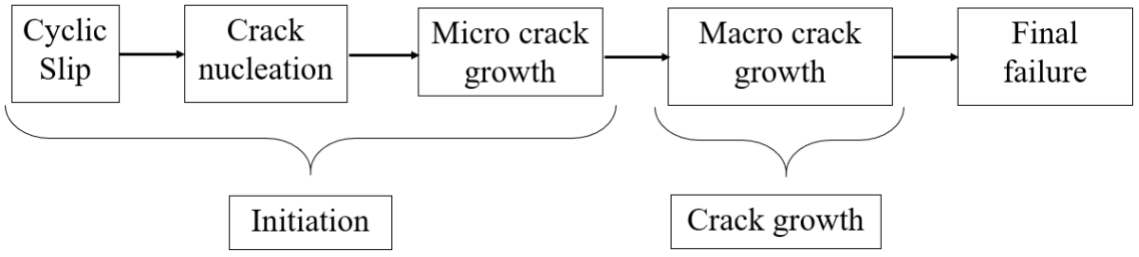

Figure 3: Fatigue phases [Schijve, 2001].

As shown in Figure 3, the initiation phase is the biggest phase in the fatigue life. The initiation phase is expected to include microcracks that cannot be seen with the naked eye until macro crack phase. Initiation of the crack at the material surface happens for several reasons, for instance, corrosion pits, surface roughness and lower restriction to the movement of slip bands. An important thing to note, is that fatigue damage is viewed as a consequence of the slip band dislocations as well as the microcracks that initiate along them. Normally after the initiation stage, the crack deviates from the direction of the slip band and grows perpendicular to the direction of loading [Schijve, 2001].

There are also material properties that affect the initiation phase and need to be accounted for like type of lattice crystal, shape and size of the grains, variation of crystal orientation, anisotropy, composition and presence of inclusions [Schijve, 2001].

The residual stresses also play a big role in the fatigue life that is positive when they are compressive and usually undesirable in tensile cases. In general, the ultimate tensile strength is also an important factor in the fatigue behavior of a material. We also need to pay attention to the geometry because a concentration of stresses due to the geometry will require us to apply a corrective factor like the stress concentration factor (K_f) [Boardman et al., 1990].

There mainly two types of fatigue: Low cycle fatigue (LCF) and high cycle fatigue (HCF), and each with their own characteristics. The two types are represented through the S-N curve in Figure 4. The S-N curve is a graphical representation of the fatigue life of a material or component and will be more explained in later sections. In recent years, other types of fatigue have been researched like ultra-low cycle fatigue or very-high cycle fatigue [Lee et al., 2012].

Low cycle fatigue is characterized by a high load and short fatigue life. Usually lower than 10^4 cycles. In this type of fatigue, the material suffers microplastic deformation from the first cycle. The opposite of this is high cycle fatigue which consists of an elastic deformation state and has a longer fatigue life usually between 10^4 and 10^7 cycles. Therefore, in high cycle fatigue, the crack initiation phase is the biggest phase [Dantas, 2019].

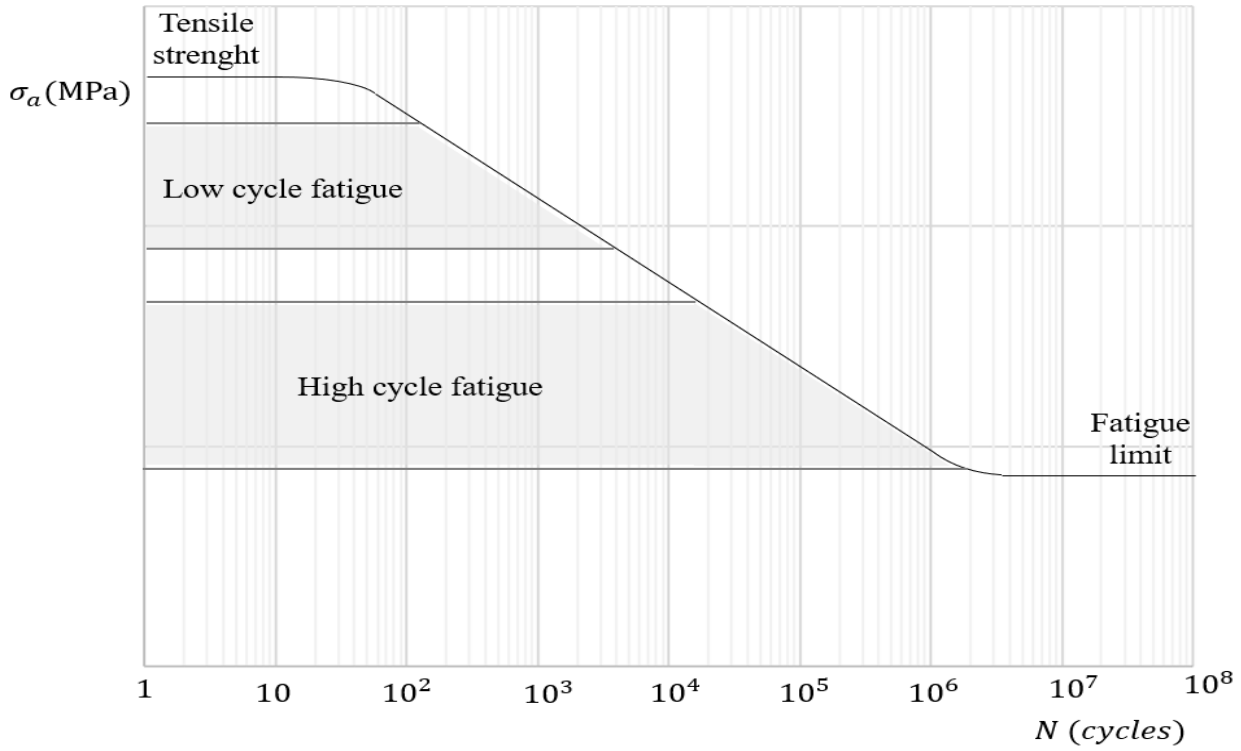

Figure 4: Fatigue life domains [Schijve, 2001].

The turning point from one phase to the other is not well established and the main difference is on the types of deformation previously been discussed. Therefore, due to these differences, each phase has its own suitable approaches and ways to evaluate fatigue life. For instance, a major part of HCF models use a stress approach, while LCF models use a strain approach [Schijve, 2001] [Socie, 1993].

The stress amplitude highly impacts the fatigue damage, and the mean stress is also equally important in the high cycle fatigue phase due to it influencing the opening and closing of microcracks. For instance, a compressive mean normal stress contributes to the closing of microcracks which in turn increases the resistance to fatigue, while a tensile mean stress has the opposite effect, and contributes to the opening of microcracks and decreases the resistance to fatigue. That is why many models, account for the mean stress effect which is explained in the next sections [Lee et al., 2012].

The focus of this thesis is high cycle fatigue and therefore, from this point onward, HCF approaches and models suitable to it will be presented and explained.

3.3 General Approaches

The first observed occurrence of fatigue happened in the nineteenth century, and it was first described by August Wöhler. He published the results from his fatigue tests, but also made important conclusions about them, such as, the most important parameter in fatigue being the stress amplitude, whereas the mean stress being the second most important parameter. Some years later, Basquin took Wöhler's work and improved upon it in a way that would represent and evaluate the fatigue life that is still relevant to date. This section will present and explain Basquin's work along with other relevant fatigue models that have been developed in the last century. [Schütz, 1996].

The models that will be discussed in this chapter assume a material without any defects or cracks. A perfect initial material. If one wishes to study the behavior of an imperfect material, with a defect or crack, a mechanic fracture approach should be applied [Fernandes et al., 1999].

3.3.1 S-N Curves

Basquin suggested that the fatigue data points be plotted for different levels of loading as stress amplitude (σ_a) versus numbers of cycles until failure (N_f). Because there are such large deviations in fatigue, he selected a logarithmic scale for the x-axis (number of cycles) and a logarithmic or linear scale for the y-axis (stress amplitude) (Fig. 3.5). This makes it possible to obtain a linear curve known as the S-N curve or Wöhler curve. Because the S-N curve is a mean curve, it represents every combination of stress amplitude and number of cycles that half the specimens fail. There are also S-N curves for every value of mean stress and for even higher values, the curve will be located lower on the graph to show them [Boardman et al., 1990] [Lee et al., 2012].

The equation for the S-N curve can be written as:

$$\sigma_a = \sigma_{f'} (2N_f)^b \tag{3.4}$$

Where b is a material constant and the slope of the linear regression, and $\sigma_{f'}$ is the fatigue strength during one cycle [Lee et al., 2012].

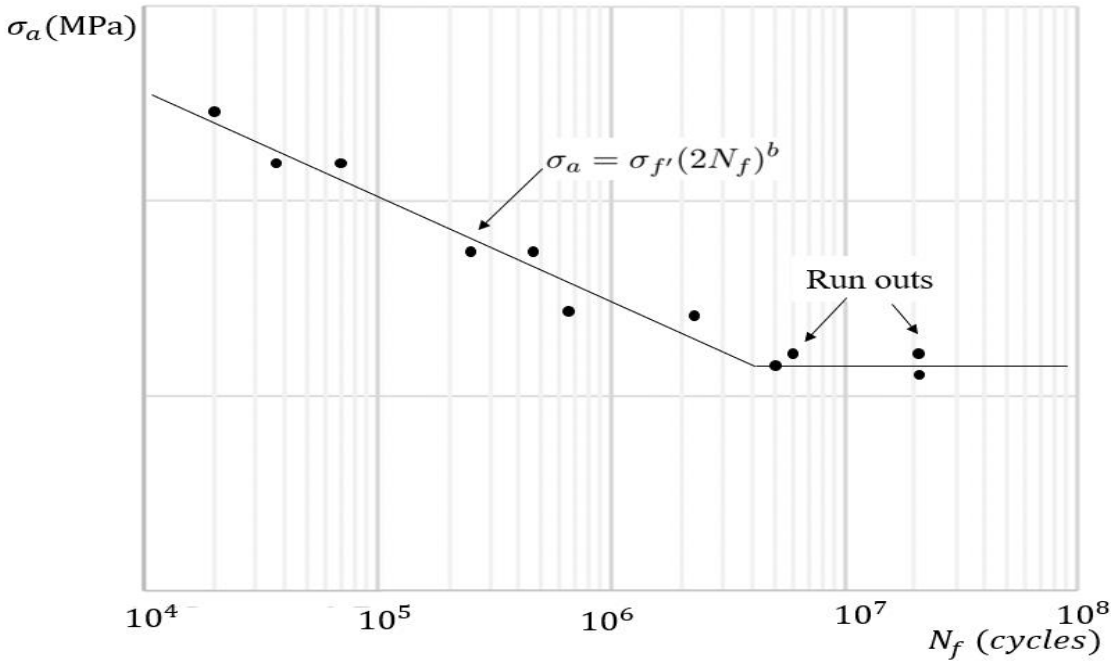

Figure 5: S-N curve (Wöhler curve) [Schijve, 2001].

The S-N curve of a material can be determined by doing fatigue tests on unnotched specimens. Due to most of the fatigue life (ca. 90 %) being the initiation phase, this curve can be used to predict the initiation crack phase of a notched specimen [Schijve, 2001].

3.3.2 Fatigue Diagrams

Fatigue diagrams plot the fatigue data for a specific number of cycles or for the fatigue limit of a single curve. Usually, the curve represents the stress amplitude, the maximum or the minimum stress as a function of the mean stress and can be compared to the S-N curves (see Figure 6). Furthermore, for a stress amplitude that is equal to zero, all curves generally converge to the yield strength or ultimate tensile strength [Schijve, 2001].

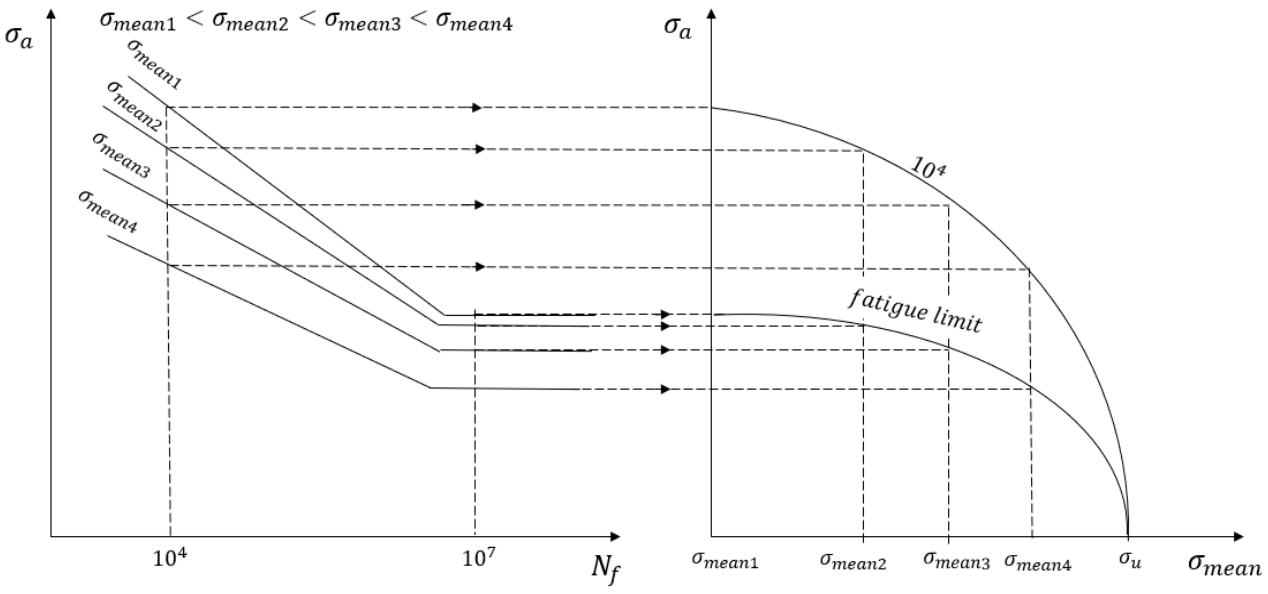

Figure 6: Conversion of S-N curves to a Fatigue Diagram [Schijve, 2001].

This is a general description about fatigue diagrams. There are several types of fatigue diagrams, and it's important to note that there are differences between each one of them. In the next sections, the most relevant fatigue diagrams will be presented and explained.

Gerber

Around the year 1880, Gerber proposed an equation as the criterion for fatigue:

$$\sigma_a = \sigma_{f0-1} \left(1 - \left(\frac{\sigma_{mean}}{\sigma_u}\right)^2\right) \tag{3.5}$$

where σ_{f0-1} is the fatigue limit for R = – 1.

As shown in Figure 7, the Gerber diagram is a parable, and it considers the fatigue limit and the ultimate strength [Dantas, 2019].

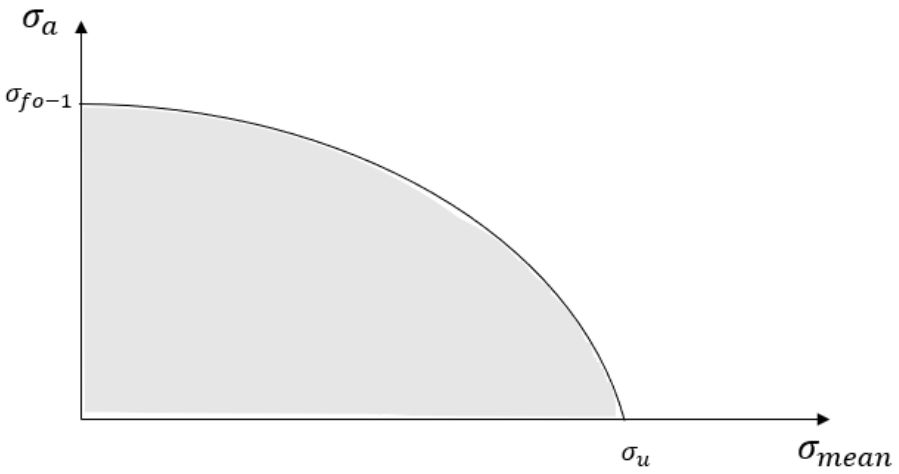

Figure 7: Gerber Fatigue Diagram [Dantas, 2019].

Goodman

A few years after Gerber, around the year 1900, Goodman proposed as the criterion for fatigue the expression from Equation (3.6). Later however this was modified by adding a second condition to avoid the plastic deformation zone. These equations are known as "modified Goodman" and are expressed by Equation (3.7).

The original Goodman diagram and the modified Goodman diagram are both shown in Figure 8. We can see that the safety area is reduced from the first diagram to the modified diagram due to the results being the area below the intersection of the two lines defined [Dantas, 2019].

$$\sigma_a = \sigma_{f0-1} \left(1 - \frac{\sigma_{mean}}{\sigma_u}\right) \tag{3.6}$$

$$\begin{cases} \sigma_a = \sigma_{f0-1} \left(1 - \dfrac{\sigma_{mean}}{\sigma_u}\right) \\ \sigma_{mean} + \sigma_a = \sigma_y \end{cases} \tag{3.7}$$

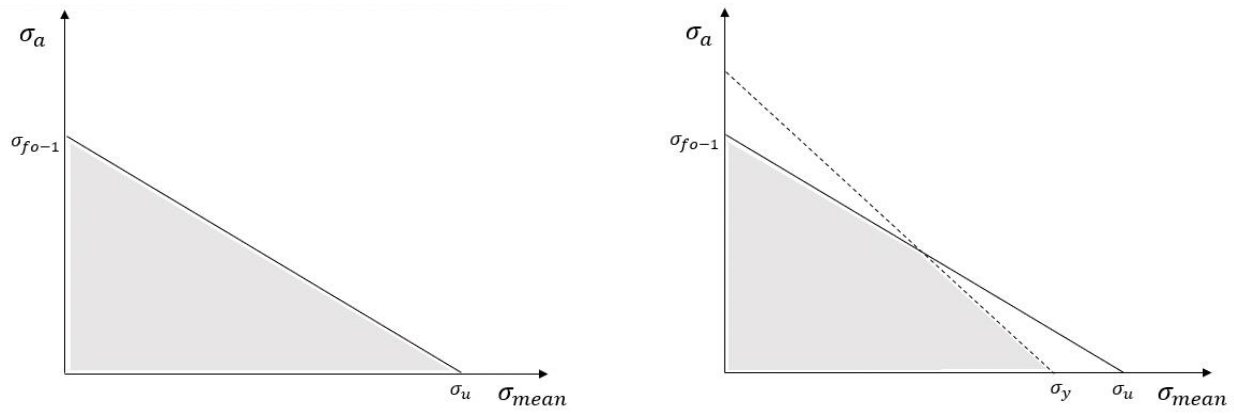

(a) Original Goodman Fatigue Diagram (b) Modified Goodman Fatigue Diagram

Figure 8: Goodman Fatigue Diagrams [Dantas, 2019].

Soderberg

The Soderberg diagram was described around 1930 and is the one that's most conservative and has the highest safety. That is because it limits the maximum mean stress value to be equal the yield strength. Meaning, it proposes the following linear relation as the criterion of fatigue:

$$\sigma_a = \sigma_{f0-1}\left(1 - \frac{\sigma_{mean}}{\sigma_y}\right) \tag{3.8}$$

Through the Soderberg diagram in Figure 9, the linear relation that is established between σ_a and σ_{mean} can be verified [Dantas, 2019].

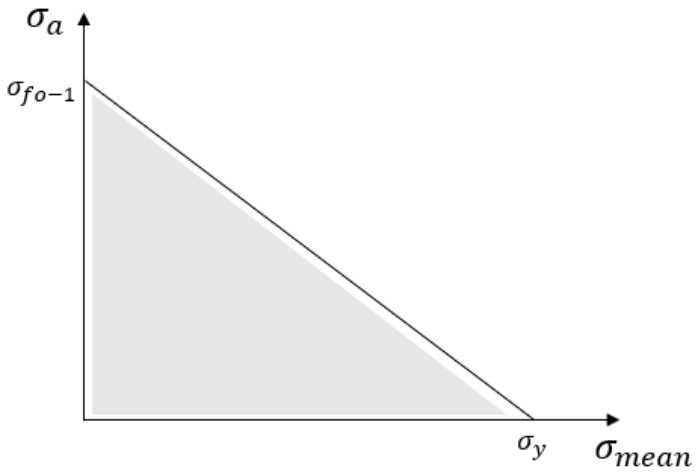

Figure 9: Soderberg Fatigue Diagram [Dantas, 2019].

3.3.3 Multiaxial Fatigue State

The fatigue state has, until now, been viewed as a uniaxial state and all the approaches presented and explained in the previous section have been elaborated for that state. The reality, however, is that fatigue is not a uniaxial state, but most of the time, it is a complex, multiaxial stress state. Many engineering structures like offshore structures, wind turbines and bridges suffer damages from this fatigue state. Unfortunately, damage caused by a multiaxial fatigue stress state and how to assess it, is still unknown. That is why it is an open topic and the focus of research to this day [Ellyin & Kujawski, 1993] [Dang-Van, 1994].

There are two types of multiaxial loading, proportional and non-proportional. For the first type, the principal stress directions do not change due the loads being in phase. During the second type, while under non-proportional loading, the directions are always changing because of out-of-phase loads (see Figure 10). These types of loads have their own distinct fatigue behavior and therefore, the models that are suitable for proportional loading are sometimes not suitable for non-proportional loading. Generally, a non-proportional loading is more damaging and requires a more complex understanding and prediction of fatigue life [Kamal & Rahman, 2018] [Lee et al., 2012].

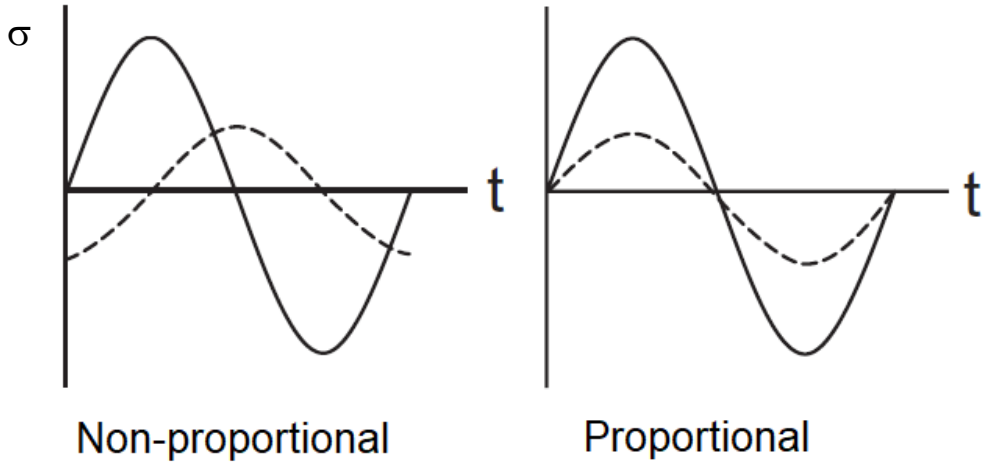

Figure 10: Non-proportional loading & Proportional loading [Lee et al., 2012].

3.3.4 Multiaxial Fatigue

The multiaxial fatigue state is a complex phenomenon, and it should not be simplified into an equivalent uniaxial fatigue state by simple static hypotheses. Many variables need to be considered, for instance, material cyclic properties and different effects of normal and shear stress. [Margetin et al., 2016]. Due to this, many multiaxial fatigue models which consider different factor have appeared in the last century. Each of these models attempt to present the multiaxial fatigue state process and damage in a mathematics condition.

The development of the multiaxial fatigue models is a fairly new and open topic. In the literature, there are many different models and points of views. Sometimes, even contradictory ideas are presented, which makes it even harder to establish a solid idea about multiaxial fatigue. Due to this, only the most accepted and discussed models and views will be mentioned.

There is no consensual classification of the multiaxial fatigue models, but they are usually divided into three main types, stress, strain, or energy-based models. The last two types are also

known as the strain-energy models and are sometimes included in the strain models [Lee et al., 2012].

The stress models are based on stress tensors and are suitable for high cycle regimes due to being known as an elastic deformation state. The strain models, however, are related to strain tensors and are usually used in low cycle regimes, but they can also be used in high cycle regimes, which makes them a good choice for assessing both. The energy models rely on energy quantities and are associated to plastic deformation energy. Therefore, they are also more suited and applied to low cycle regimes [Maktouf et al., 2016].

The next section will discuss the most relevant and discussed models, established in the last decades. Due the experimental work of this thesis being stress based, only the stress-based models will be presented.

3.3.4.1 Multiaxial Fatigue Models

The stress-based models can be divided into three types, equivalent stress, empirical formula, and critical plane models [Lee et al., 2012]. They all have different characteristics.

Empirical Formula Models

The first of the models and the ones that are heavily related to experimental fatigue data, were the empirical models. Their main drawback being their limited applicability to biaxial fully reversed stress state [Lee et al., 2012].

Gough and Pollard

It was around 1930 that Gough and Pollard conducted many in-phase fatigue tests under bending and torsional loads. Around the 1950s they were able to formulate an empirical model. The proposed formula established different failure conditions for ductile and brittle materials:

$$\left.\begin{array}{ll} \left(\frac{\sigma_a}{\sigma_{a,R=-1}}\right)^2 + \left(\frac{\tau_a}{\tau_{a,R=-1}}\right)^2 = 1 & \text{for ductile materials} \\ \left(\frac{\sigma_a}{\sigma_{a,R=-1}}\right) + \left(\frac{\tau_a}{\tau_{a,R=-1}}\right)^2 = 1 & \text{for brittle materials} \end{array}\right\} \quad (3.9)$$

where the $\sigma_{a,R=-1}$ is the fully reversed fatigue limit for pure bending, and $\tau_{a,R=-1}$ is the fully reversed fatigue limit for pure torsion [Lee et al., 2012].

Equivalent Stress Models

The equivalent stress models are based on the static yield criteria, and they consist of transforming a multiaxial state into an equivalent uniaxial fatigue stress state. A major part these models cannot be applied to a non-proportional loading and are ineffective to incorporate the fatigue phenomenon. The reason for their frequent use is that they are simple and easy to applicate [Kallmeyer et al., 2002].

Maximum Principal Stress

The maximum principal stress model states that fatigue crack initiation begins when the maximum principal stress amplitude ($\sigma_{1,a}$) is equal or greater than the normal stress fatigue limit of a uniaxially fully reversed test ($\sigma_{1,R=-1}$) [Lee et al., 2012]:

$$\sigma_E = \sigma_{1,a} \geq \sigma_{1,R=-1} \tag{3.10}$$

Maximum Shear Stress (Tresca)

The Tresca criterion can also be used in fatigue, and it states that a crack initiation will happen when following condition is verified:

$$\tau_E = \tau_{a,max} = \frac{\sigma_{1,a} - \sigma_{3,a}}{2} \geq \tau_{a,R=-1} \tag{3.11}$$

where $\sigma_{1,a}$ is the maximum principal amplitude and $\sigma_{3,a}$ is the minimum principal amplitude [Lee et al., 2012].

von Mises

The von Mises model is also applicable to fatigue and tell us that a fatigue crack will occur when Equation (3.12) is verified:

$$\sigma_{VM,a} + \alpha_{VM} * \sigma_{VM,m} \geq \sigma_{a,R=-1} \tag{3.12}$$

$\sigma_{VM,a}$ is the von Mises stress amplitude, the α_{VM} is the mean stress sensitivity factor, and $\sigma_{VM,m}$ is the von Mises mean stress.

The $\sigma_{VM,a}$ and the $\sigma_{VM,m}$ are calculated with Equations (3.13) and (3.14):

$$\sigma_{VM,a} = \frac{1}{\sqrt{2}} \sqrt{(\sigma_{1,a} - \sigma_{2,a})^2 + (\sigma_{2,a} - \sigma_{3,a})^2 + (\sigma_{1,a} - \sigma_{3,a})^2} \tag{3.13}$$

$$\sigma_{VM,m} = \sigma_{1mean} + \sigma_{2mean} + \sigma_{3mean} \tag{3.14}$$

where $\sigma_{1,a}$, $\sigma_{2,a}$, and $\sigma_{3,a}$ are the principal stress amplitudes and σ_{1mean}, σ_{2mean}, and σ_{3mean} are the principal mean stresses [Lee et al., 2012].

Sines

Two extensive studies were conducted by Sines in 1955 and 1959 where experimental fatigue data for bending, torsional, and combined bending and torsional, resulted in the Equation (3.15) [Sines, 1955] [Sines, 1959]. Failure will occur when the left side of the equation is larger than the constant s.

$$\tau_{a,oct} + k_s * (3\sigma_{hmean}) = s \tag{3.15}$$

where the constant s is a material constant proportional to the fatigue limit, k_s is another material constant that accounts for value of static stress, σ_{hmean} is the hydrostatic stress for the mean stresses shown in Equation (3.16):

$$\sigma_{hmean} = \frac{\sigma_{1mean} + \sigma_{2mean} + \sigma_{3mean}}{3} \tag{3.16}$$

and $\tau_{a,oct}$ is the octahedral shear stress amplitude calculated by Equation (3.17):

$$\tau_{a,oct} = \frac{1}{3}\sqrt{(\sigma_{1,a} - \sigma_{2,a})^2 + (\sigma_{2,a} - \sigma_{3,a})^2 + (\sigma_{1,a} - \sigma_{3,a})^2} \tag{3.17}$$

These constants can both be calculated with two tensile fatigue tests, one for R = 0 and, one for R = – 1 [Sines, 1959].

The octahedral shear stress amplitude and hydrostatic mean stress were therefore calculated for R = – 1:

$$\tau_{a,oct,R=-1} = \frac{\sqrt{2}}{3}\sigma_{1,a} = \frac{\sqrt{2}}{3}\sigma_{a,R=-1} \tag{3.18}$$

$$\sigma_{hmean,R=-1} = 0 \tag{3.19}$$

we then get:

$$s = \tau_{a,oct,R=-1} = \frac{\sqrt{2}}{3}\sigma_{a,R=-1} \tag{3.20}$$

Then we do the same calculations for R = 0:

$$\tau_{a,oct,R=0} = \frac{\sqrt{2}}{3}\sigma_{1,a} = \frac{\sqrt{2}}{3}\sigma_{a,R=0} \tag{3.21}$$

$$\sigma_{hmean,R=0} = \sigma_{1mean} = \sigma_{1,a} \tag{3.22}$$

we substitute with Equation (3.15):

$$k_s = \frac{\sqrt{2}}{3}\left(\frac{\sigma_{a,R=-1} - \sigma_{a,R=0}}{\sigma_{a,R=0}}\right) \tag{3.23}$$

This model may include the effects of the mean stress; however, it cannot be applied to non-proportional loading [Lee et al., 2012].

Crossland

The Crossland models is almost identical to the Sines model, only different being, instead of the hydrostatic mean stress, the maximum hydrostatic stress (σ_{hmax}) is used. This model can therefore be applied to non-proportional loading:

$$\tau_{a,oct} + k_c * (3\sigma_{hmax}) = c \tag{3.24}$$

where the c and the k_c are material constants and σ_{hmax} is the maximum hydrostatic stress that can be calculated with Equation (3.25):

$$\sigma_{hmax} = \frac{\sigma_{1max} + \sigma_{2max} + \sigma_{3max}}{3} \tag{3.25}$$

Critical Plane Models

The critical plane method presents the concept of the critical plane where the probability of crack initiation is higher. Each model is characterized by the definition of critical plane and should consider the physical mechanisms of fatigue damage and microcracking [McDowell & Ellis, 1994] [Kallmeyer et al., 2002].

Findley

The first one to propose a critical plane approach was Findley in 1958. The criterion stating that shear stress is the primary mechanism of fatigue damage, and that normal stress is a secondary mechanism. That means it is the shear stress that is responsible for nucleation and initiation of small cracks, while the normal stress is responsible for the materials capability to withstand cyclic loadings. This model considers the effect of the mean stress, and states that, in ductile metals, the means stress is not very relevant for torsion, but has a major influence on bending [Findley, 1958].

Due to this criterion, the critical plane is defined as the plane where a certain damage parameter achieves the maximum value. This damage parameter is the maximum value of a linear relation between alternating shear stress on a θ plane ($\tau_{\theta a}$) and the maximum normal stress ($\sigma_{\theta a}$) on the same plane, multiplied by a factor k_f that manages the influence of the stress on the fatigue life. When the damage parameter is equal to the material constant f, failure will occur [Findley, 1958]:

$$(\tau_{\theta a} + k_f * \sigma_{\theta a} = f) \tag{3.26}$$

It is important to note that the factor k_f and material constant f are constants for a certain number of cycles until failure.

This can only be applied to proportional loadings, which means that Equation (3.27) needs to be verified:

$$\frac{\tau_a}{\sigma_a} = \frac{\tau_{max}}{\sigma_{max}} = a \tag{3.27}$$

Findley also defined other equations to determine the material constant f in certain cases of combined bending/axial loads and torsion, or pure bending/axial loads and pure torsion. The first case being:

$$f = \sqrt{((\frac{\sigma_a}{2})^2 + \tau_a^2 + k_f^2 * \left(\left(\frac{\sigma_{max}}{2}\right)^2 + \tau_{max}^2\right)} + k_f * \frac{\sigma_{max}}{2} \tag{3.28}$$

For pure bending or axial loads, it is known that $\tau_{max} = \tau_a = 0$, then f is defined as:

$$f = \sqrt{(\frac{\sigma_a}{2})^2 + k_f^2 * (\frac{\sigma_{max}}{2})^2} + k_f * \frac{\sigma_{max}}{2} \tag{3.29}$$

For pure torsion loads, $\sigma_{max} = \sigma_a = 0$:

$$f = \sqrt{\tau_a^2 + k_f^2 + \tau_{max}^2} \tag{3.30}$$

since the $\tau_{max} = \tau_a + \tau_{mean}$, Equation (3.30) can be written as:

$$f = \sqrt{\tau_a^2 + k_f^2 * (\tau_a + \tau_{mean})^2} \tag{3.31}$$

As mentioned before, the mean shear stress has little relevance for the fatigue life in the case of torsion loads. We can therefore ignore it in Equation (3.31):

$$f = \sqrt{1 + k_f^2} * \tau_a \tag{3.32}$$

The value of the factor k_f or the method to determine it, is not well established, by Findley or any other authors. However, Socie developed in 2018, some expressions related to the stress fatigue limit in the case of pure axial/bending or pure torsion loads [Socie, 2018]:

$$\frac{\sigma_{a,R=-1}}{\tau_{a,R=-1}} = \frac{2}{1 + \frac{k_f}{\sqrt{1+k_f^2}}} \tag{3.33}$$

$$\frac{\sigma_{a,R=0}}{\sigma_{a,R=-1}} = \frac{k_f + \sqrt{1+k_f^2}}{2k_f + \sqrt{1+(2k_f)^2}} \tag{3.34}$$

$$\frac{\sigma_{a,R=0.5}}{\sigma_{a,R=-1}} = \frac{k_f + \sqrt{1+k_f^2}}{4k_f + \sqrt{1+(4k_f)^2}} \tag{3.35}$$

In the above Equations (Eqs. (3.33), (3.34), (3.35)), $\sigma_{a,R=-1}$ is the fatigue limit in an axial or bending fatigue test, performed with a stress ratio equal to -1. $\sigma_{a,R=0}$ is the fatigue limit in an axial or bending fatigue test, performed with a stress ratio equal to zero. Lastly, $\tau_{a,R=-1}$ is the fatigue limit in a torsion fatigue test, performed with a stress ratio equal to -1. Therefore, to determine the fatigue limit and be able to calculate k_f, only two different types of uniaxial fatigue tests are necessary [Socie, 2018].

McDiarmid

In 1991 and 1994, McDiarmid presented a critical plane approach for the multiaxial high-cycle fatigue, that includes the mean stress effect and can be applied to non-proportional loading. According to its criterion, the critical plane is the plane where the shear stress amplitude achieves the maximum value. The model defines two different scenarios: the first one (case A) is that cracks grow along the surface of the material, and the second one (case B) that the cracks grow inwards, from the surface of the material [McDiarmid, 1991] [McDiarmid, 1994].

Fatigue failure is therefore achieved when Equation (3.36) is verified:

$$\frac{\tau_{\theta a}}{t_{A,B}} + \frac{\sigma_{\theta max}}{2\sigma_u} = 1 \tag{3.36}$$

where $t_{A,B}$ is a material constant defined as:

$$\begin{cases} t_{A,B} = t_A & \text{for case A} \\ t_{A,B} = t_B & \text{for case B} \end{cases} \tag{3.37}$$

where the t_A and the t_B are the reversed shear fatigue limits for the two cases A and B.

In Equation (3.38), the criterion is rewritten as:

$$\tau_{\theta a} + \frac{t_{A,B}}{2\sigma_u}\sigma_{\theta max} = t_{A,B} \tag{3.38}$$

Dang-Van's Multi-scale Approach

Dang-Van presented in 1994, an approach based on "micro-macro" scale analysis and local variables. Two scales were defined:

- The macroscopic scale: is used by engineers and is characterized by an elementary volume V (M) surrounding the point M where the fatigue analysis is made. The macroscopic stress ($\bar{\sigma}_{macro}(t)$) and the macroscopic strain ($\bar{\varepsilon}_{macro}(t)$) are homogenous in the elementary volume at any time t (see Figure 11) [Dang-Van, 1994].

- The mesoscopic scale: is a subdivision of the elementary volume V (M) and of the order of grain size. The mesoscopic strain ($\bar{\sigma}_{meso}(t)$) and the mesoscopic strain ($\bar{\varepsilon}_{meso}(t)$) are not assumed to be homogenous and are different from the macroscopic variable (see Figure 11) [Dang-Van, 1994].

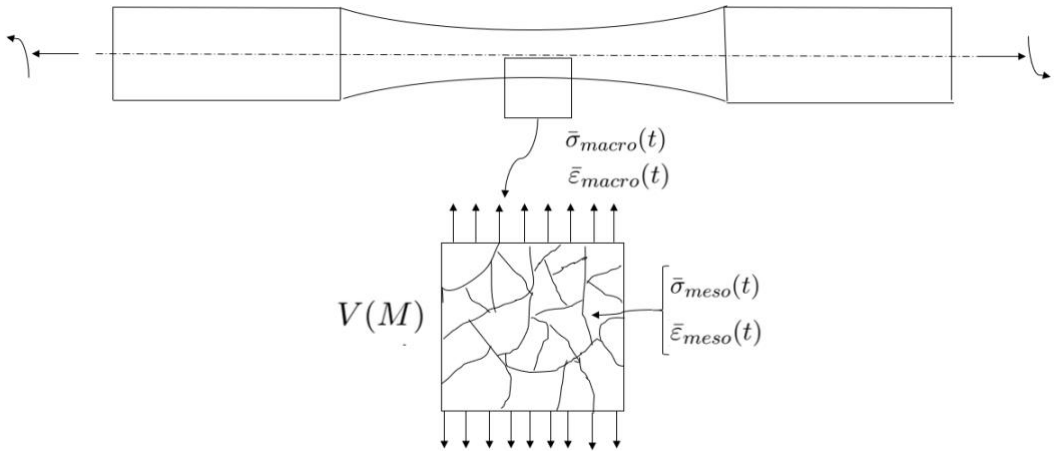

Figure 11: Macroscopic and mesoscopic scales [Dang-Van, 1994].

The criterion applies to the elastic shakedown principles of the mesoscopic scale and assumes that an elastic shakedown happens before a crack initiation [Desimone et al., 2006]. This phenomenon is associated to high-cycle fatigue because it represents a stabilized elastic response which only happens when the yield strength is not achieved [Lee et al., 2012]. By using the principles discussed above, the conditions in Equation (3.39) between the macroscopic and the mesoscopic variables can be established:

$$\bar{\varepsilon}^e_{macro}(t) = \bar{\varepsilon}^e_{meso}(t) + \bar{\varepsilon}^p_{meso}(t) \tag{3.39}$$

where the $\bar{\varepsilon}^{e}_{meso}(t)$ is the elastic mesoscopic stran tensor, and the $\bar{\varepsilon}^{p}_{meso}\ (t)$ is the mesoscopic plastic strain tensor.

Applying Hooke's law to Equation (3.39) will give us:

$$\bar{\varepsilon}^{e}_{macro}(t) = \frac{\bar{\sigma}_{macro}(t)}{E_{macro}} \tag{3.40}$$

$$\bar{\varepsilon}^{e}_{meso}(t) = \frac{\bar{\sigma}_{meso}(t)}{E_{meso}} \tag{3.41}$$

where the E_{macro} is the macroscopic Young's modulus, and the E_{meso} is the mesoscopic Young's modulus.

After a certain number of cycles, the mesoscopic plastic strain stabilizes and becomes independent of the time t. That means by rewriting Equation (3.39) the mesoscopic stress tensor can be redefined as:

$$\bar{\sigma}_{meso}(t) = \frac{E_{meso}}{E}\bar{\sigma}_{macro}(t) - E_{meso}\bar{\varepsilon}^{p}_{meso}\ (t) \tag{3.42}$$

Assuming that $\frac{E_{meso}}{E_{macro}} = 1$:

$$\bar{\sigma}_{meso}(t) = \bar{\sigma}_{macro}(t) - E_{meso}\bar{\varepsilon}^{p}_{meso}\ (t) = \bar{\sigma}_{macro}(t) + p \tag{3.43}$$

where p is a deviatoric tensor and a mesoscopic residual stress.

Both the mesoscopic stress tensor and the macroscopic stress tensor can be divided into a deviatoric stress tensor ($\bar{\sigma}_{meso,d}(t)$ or $\bar{\sigma}_{macro,d}(t)$) and a hydrostatic stress tensor ($\bar{\sigma}_{meso,h}(t)$ or $\bar{\sigma}_{macro,h}(t)$). For the first scale we get the Equation (3.44):

$$\bar{\sigma}_{macro}(t) = \bar{\sigma}_{macro,h}(t) + \bar{\sigma}_{macro,d}(t) \tag{3.44}$$

in Equation (3.44), the hydrostatic tensor is defined as:

$$\bar{\sigma}_{macro,h}(t) = \begin{bmatrix} \sigma_h(t) & 0 & 0 \\ 0 & \sigma_h(t) & 0 \\ 0 & 0 & \sigma_h(t) \end{bmatrix} \tag{3.45}$$

$$\sigma_h(t) = \frac{\sigma_1(t) + \sigma_2(t) + \sigma_3(t)}{3} \tag{3.46}$$

for the mesoscopic stress tensor, we get the Equation (3.47):

$$\bar{\sigma}_{meso}(t) = \bar{\sigma}_{meso,h}(t) + \bar{\sigma}_{meso,d}(t) \quad (3.47)$$

The microscopic and the mesoscopic hydrostatic stress tensors are equal:

$$\bar{\sigma}_{meso,h}(t) = \bar{\sigma}_{macro,h}(t) \quad (3.48)$$

the mesoscopic deviatoric stress tensor is defined as:

$$\bar{\sigma}_{meso,d}(t) = \bar{\sigma}_{macro,d}(t) + p \quad (3.49)$$

In the case of a proportional loading:

$$p = average(\bar{\sigma}_{macro,d}(t)) \quad (3.50)$$

According to this model, failure will occur when Equation (3.51) is verified:

$$\max\left(\bar{\tau}(t)_{meso,max,d} + k_d * \bar{\sigma}(t)_{meso,h}\right) = d \quad (3.51)$$

where the $\bar{\tau}(t)_{meso,max,d}$ is:

$$\bar{\tau}(t)_{meso,max,d} = \frac{\bar{\sigma}(t)_{meso,1,d} - \bar{\sigma}(t)_{meso,3,d}}{2} \quad (3.52)$$

According to Dang-Van, the cracks initiate in transgranular slip bands, generally because of local shear stress and due to the influence of hydrostatic tension [Dang-Van, 1994] [Desimone et al., 2006].

A few years later, a simplified version of this model was proposed for engineering applications [Dang-Van & Maitournam, 2003]. According to this version, fatigue failure will occur when Equation (3.53) is verified:

$$\tau_{a,max} + k_d \sigma_{h,max} = d \quad (3.53)$$

where the k_d and the d are material constants.

It is important to note that the mean stresses do not affect the value of $\tau_{a,max}$, whereas the value of the hydrostatic stress, includes the mean stress.

By performing two fatigue tests at different stress ratios, both material constants k_d and d can be obtained. If the torsional and fully reversed are applied to Equation (3.53), the value of d can be determined:

$$d = \tau_{a,max} = \tau_{a,R=-1} \tag{3.54}$$

By combining Equation (3.54) with the fully reversed axial test, the value of k_d can be determined:

$$k_d = 3\left(\frac{\tau_{a,R=-1}}{\sigma_{a,R=-1}} - \frac{1}{2}\right) \tag{3.55}$$

The two material constants can also be determined by performing two random tests at the fatigue limit by plotting the test data and applying linear regression [van Lieshout et al., 2017].

3.3.5 Estimation of The Fatigue Life - Multiaxial Criterion

By combining the models presented in the previous section with the basquin model, we can calculate the fatigue damage in the finite life region, using the following equations:

- Tresca

$$\frac{\sigma_{1,a} - \sigma_{2,a}}{2} = \tau_f'(2N_f)^b \tag{3.56}$$

- von Mises

$$\sigma_{V\,M,a} + \alpha_{V\,M}\sigma_{V\,M,m} = \tau_f'(2N_f)^b \tag{3.57}$$

- Sines

$$\tau_{a,oct} + k_s\left(3\sigma_{h,mean}\right) = \tau_f'(2N_f)^b \tag{3.58}$$

- Crossland

$$\tau_{a,oct} + k_c\left(3\sigma_{h,max}\right) = \tau_f'(2N_f)^b \tag{3.59}$$

- Findley

$$(\tau_{\theta a} + k_f\sigma_{\theta max})_{max} = \tau_f'(2N_f)^b \tag{3.60}$$

- McDiarmid

$$(\tau_{\theta a} + \frac{t_{A,B}}{2\sigma_u}\sigma_{\theta max} = \tau_f'(2N_f)^b \tag{3.61}$$

- Dang-Van

$$\tau_{a,max} + k_d \sigma_{h,max} = \tau'_f (2N_f)^b \tag{3.62}$$

By using this method, it is possible to obtain a design curve and determine the theoretical fatigue life of a specimen, at a certain state of loading [Socie, 1993].

3.3.6 Nonlinear Damage Curve and Two-Stage Linearization Models

3.3.6.1 Introduction

It was in 1948 that Richard and Newmark introduced the concept that the damage curve correlates to the cycle ratio. Their goal was to try and overcome the shortcomings of Palmgren-Miner rule, the linear Damage Rule (LDR). They thought that the D-r curves (r being the cycle ratio n/N) is dependent on the stress level [Richard & Newmark, 1948]. From this concept, along with empirical evidence, the nonlinear damage rule (NLDR) was proposed by Marco and Starkey. The NLDR expresses the damage as a power function that is load-independent:

$$D = \sum \left(\frac{n_i}{N_i}\right)^{x(\sigma_i)} \tag{3.63}$$

The exponent x being a function of the stress amplitude. Of course, the Palmgren-Miner rule is a special case of Equation (3.62) where the x is equal to one for all σ_i. The concept of the damage curve is shown in Figure 12. It shows the accumulated damage in a D-r diagram for both the linear damage rule. and the nonlinear damage rule. It also shows the predicted number of cycles to failure is lower in the case of nonlinear damage accumulation as the accumulation n / N ≅ 0.7 when the damage is D = 1, while for the linear damage accumulation the n / N = 1 when the D = 1 [Marco & Starkey, 1954].

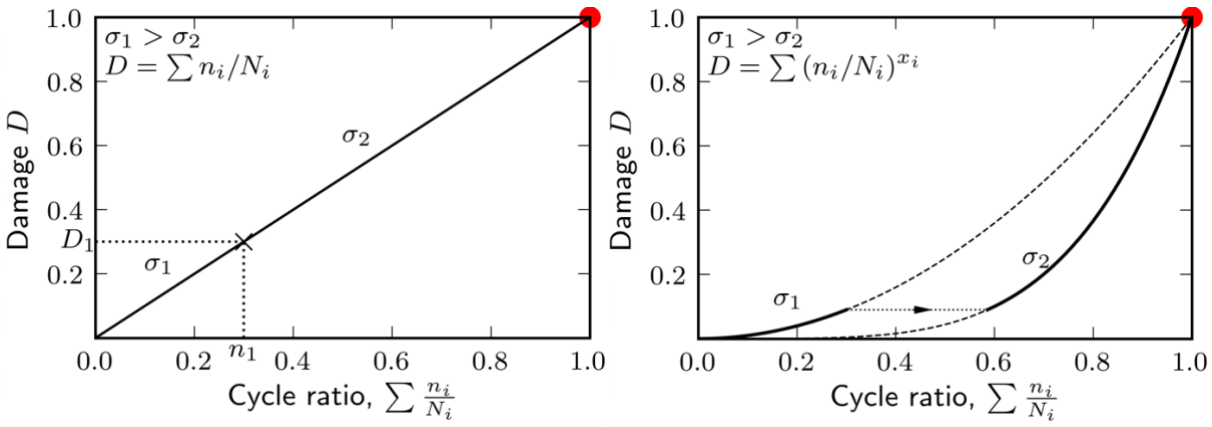

Figure 12: Linear damage rule (LDR) (left) vs nonlinear damage rule (NLDR) (right) for a high-to-low loading sequence. Red dot is point of failure where D = 1 [Marko & Starkey, 1954].

In 1960, Grover presented that damage accumulation should be analyzed by using two linear damage rules. He suggested a two-stage linear damage rule building on observations from a fracture mechanics viewpoint. The first stage being the crack initiation stage and the second stage being the crack propagation stage. His work was qualitative and any quantitative formulation for separation of the total life into initiation and propagation was not provided [Grover, 1960].

In the year 1966, Manson proposed the double linear damage rule (DLDR) building on Grover's work, which later in 1967 was changed so that the concept of crack initiation and crack propagation were literally altered to represent two effective phases of the fatigue process. The alteration proposed that the double linear damage rule became load and material dependent. This was to overcome some of the original limitation of the double linear damage rule. [Manson, 1966] [Manson et al., 1967].

Later, Manson and Halford began experimenting to compare the double linear damage rule with the linear damage rule. They found that in the case of the linear damage rule, the results showed an average overestimation of 37%. Compared to that, the double linear damage rule showed an average overestimation of only 12%. Shortly after the proposal of the double linear damage rule, Manson and Halford proposed the damage curve approach (DCA), which built on the concept of the damage curve approach by Marco and Starkey. Marco and Starkey did not provide a specific functional form for the exponent $x(\sigma_i)$ which severely limits its practicability. Based on a model of empirically formulated effective crack growth, Manson and Halford proposed an analytical formulation for the damage curve. The damage model for a multi-level loading sequence can be expresses as:

$$[[[(\frac{n_1}{N_1})^{\alpha_{1,2}} + \frac{n_2}{N_2}]^{\alpha_{2,3}} + \frac{n_3}{N_3}]^{\alpha_{3,5}} \dots + \frac{n_{i-1}}{N_{i-1}}]^{\alpha_{i-1,i}} + \frac{n_i}{N_i} = 1 \quad with \quad \alpha_{i-1,N_i} = (\frac{N_{i-1}}{N_i})^{0.4} \qquad (3.64)$$

where the 1, 2, …, i – 1,i are the load components sequence numbers. Manson and Halford found out that the difference between the double linear damage rule and damage curve approach were relatively small for two-level and three-level block loading tests. This was as expected as the double linear damage rule should be viewed as a linearization of the damage curve concept. If the loading conditions are more realistic however, a larger difference is expected due to the results of the double linear damage rule not being affected by the load changes within a single phase, compared to the damage curve approach that is affected by all changes in the load sequence [Marko & Starkey, 1954] [Manson & Halford, 1981].

An experimental study by Costa et al. of the behavior of aluminum alloy friction stir welds (AA6082) subjected to variable amplitude loading, compared the double linear damage rule to Mine's rule. It was concluded that the double linear damage rule was significantly more accurate, but that both were very non-conservative for a fully reversed loading condition (R = -1) [Costa et al., 2012].

The double linear damage rule and Miner's rule were implemented by Inoma et al. for a fatigue life prediction of offshore drilling top-drive tie rods and found out that Miner's rule consistently overestimated the fatigue life. More accurate estimates were obtained with the double linear damage rule. In general, the double linear damage rule is thought to be an improvement to Miner's rule since the required input is the same [Inoma et al., 2019].

The first damage curve approach model by Manson and Halford was empirically defined based on results from two-level loading sequences that did not involve very small values of n_1 / N_1. Later, Manson and Halford noticed that there is a rapid drop of n2 / N2 for a very small n_1 / N_1 in a high-low loading sequence with an $N_2 >> N_1$. To achieve more accurate results at very low n_1 / N_1, a new term was added to the damage curve approach equation which is significant for low values of n_1 / N_1, but relatively small for higher values. This model is referred to as the

double damage curve approach (DDCA) and is a combination of the most accurate parts of double linear damage rule and the damage curve approach. In Figure 13, the double linear damage rule, the damage curve approach, and the double damage curve approach are shown for three values of N_{ref} / N_i with N_{ref} being a reference life level [Manson & Halford, 1981] [Manson & Halford, 1986].

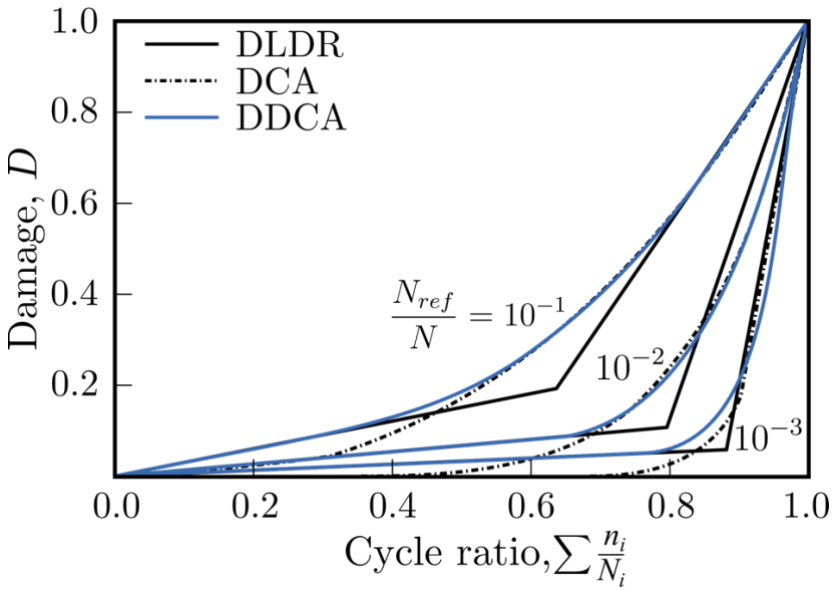

Figure 13: The double damage curve approach (DDCA) blends with the damage curve approach (DCA) at high cycle ratios, and with the double linear damage rule (DLDR) at low cycle ratios [Manson & Halford, 1986].

The models of DLDR, DCA and the DDCA, all have similar characteristics as they are load level-dependent, but do not account for the load interaction and the cycles with an amplitude below the fatigue limit. The most known method to account for load interactions is by using an interaction factor that depends on the load ratio. The first to propose this were Corten and Dolan in 1956. They performed hundreds of tests with constant amplitude and two-level block loading on cold-drawn steel wires, and proposed a cumulative damage model that is expressed as:

$$D = m\, r\, n^{a} \tag{3.65}$$

with the m being the number of damage nuclei, r the damage propagation rate coefficient, which is a function of the stress condition, the n the number of applied cycle and the exponent a is a material constant. The damage model assumes that damage happens as the nucleation of microscopic voids that eventually form cracks. The rate of the damage increases with the number of applied cycles and the stress amplitude. The damage can also propagate at stress levels that are lower than the stress required to initiate the damage [Corten & Dolan, 1956].

From these two-level block loading experiments, Corten and Dolan established an empirical relation between the stress dependent ratio R = r_1 / r_2, the damage exponent a, and the stress ratio through a material property d. The empirical relation is given by $R^{1/a} = (\sigma_2 / \sigma_1)^d$ and has been used to determine Equation (3.66) where N_g is the total number of cycles to failure. It is assumed that failure will occur when D reaches unity. The parameter d represents the slope of a

linear curve in a log ($R^{1/a}$) – log (σ_2 / σ_1) diagram, where the R = r_1 / r_2 and can be determined via experiments:

$$N_g = \frac{N_1}{\sum \alpha (\frac{\sigma_i}{\sigma_1})^d} \tag{3.66}$$

the life prediction model from Equation (3.66) takes load interaction effects into account through the load ratio (σ_2 / σ_1) [Corten & Dolan, 1956].

3.3.6.2 Models based on The Damage Curve Approach

Chen et al. studied the effects of sequential loading on fatigue damage of grade 304SS stainless steel subjected to tension-compression, followed by torsion, then tension-compression again, in-phase loading followed by 90° out-of-phase loading, and 90° out-of-phase loading followed by in-phase loading. These fatigue tests were performed with a cycle range between 10^3 and 10^4 and with several rules, such as Miner's rule, the DCA, and the DLDR. All the models yielded non-conservative results. It was hypothesized that the fatigue resistance of the material was influenced by the sequential loading which caused further hardening. Considering the results of the experiments, to consider the loading path in the sequential loading, a non-proportionality function J was introduced into the DCA exponent α. Then, the exponent α for a two-level block loading was expressed as:

$$\alpha = (\frac{1}{1+\beta J})(\frac{N_1}{N_2})^{0.4} \quad with \quad J = \frac{1.57}{T_{\varepsilon_{1,max}}} \int_T^0 |sin\zeta(t)| \varepsilon(t) dt \tag{3.67}$$

the $\varepsilon_1(t)$ is the absolute value and the $\zeta(t)$ is the angle of the maximum principal strain at time t. The $\varepsilon_{1,max}$ is the maximum value of $\varepsilon(t)$ in a cycle, and the T is the time for a cycle. Because only a few tests have been performed, and there is a relatively large scatter in the experimental data, further validation is needed. The preliminary results have shown an improvement over existing models [Chen et al., 2000] [Itoh et al., 2006].

Few years later it was discovered by Xu et al. the need for the DCA rule to account for load interaction effects. It was suggested that parameter $\alpha_{i-1,i}$ of the DCA model (Equation (3.64)) could be modified to include the load amplitude and effective stress related to the loading. Based on this, Gao et al. proposed a modification to the parameter $\alpha_{i-1,i}$ by adding a term that represents the minimum ratio of the applied stress amplitude. The parameter $\alpha_{i-1,i}$ is then expressed as:

$$\alpha_{i-1,i} = (\frac{N_{i-1}}{N_i})^{0.4 min\left\{\frac{\sigma_{i-1}}{\sigma_i}, \frac{\sigma_i}{\sigma_{i-1}}\right\}} \tag{3.68}$$

Gao et al., reported a near 80% higher accuracy with their modified DCA model predictions than those of the original Manson and Halford DCA model for the two-level block loading tests on C45 and 16Mn steel [Xu et al., 2012] [Gao et al., 2014].

Aside from accounting for the load sequence and the load interaction effects, Yuan et al. argue that an accurate fatigue model should also account for strength degradation. Based on the

work of Gao et al. they further modified the DCA model to account for the residual strength degradation by introducing a function for the residual strength degradation. The induce damage by the n_i applied number of cycles at the stress amplitude σ_i can be expressed as:

$$D_i = \gamma\left(\frac{n_i}{N_i}\right)^{\left(\frac{N_{i-1}}{N_i}\right)^{0.4min\left\{\frac{\sigma_{i-1}}{\sigma_i},\ \frac{\sigma_i}{\sigma_{i-1}}\right\}}} \quad with \quad \gamma = exp\left[\alpha\left(\frac{1}{A} - 1\right]\right. \tag{3.69}$$

the α being a material coefficient obtained from experimental data, A the coefficient for residual strength degradation reflecting the relation between the strength degradation and fatigue damage accumulation [Gao et al., 2014] [Yuan et al., 2015].

Few years later, in 2019, Zhou et al. presented a new cumulative damage model that is a combination of a DCA model and the Corten and Dolan model. The verification of their work is based on a single experiment for a multi-level block loading sequence model that is expressed as:

$$D = \left\{\left[\left(\frac{n_1}{N_1}^{\left(\frac{N_1}{N_2}\right)^{\alpha\left(\frac{\sigma_{max,1}}{\sigma_f}\right)}}\right) + \frac{n_2}{N_2}\right]^{\left(\frac{N_2}{N_3}\right)^{\alpha\left(\frac{\sigma_{max,2}}{\sigma_f}\right)}} + \cdots + \frac{n_{i-1}}{N_{i-1}}\right\}^{\left(\frac{N_{i-1}}{N_i}\right)^{\alpha\left(\frac{\sigma_{max,i-1}}{\sigma_f}\right)}} + \frac{n_i}{N_i} \tag{3.70}$$

with the $\sigma_{max,i}$ being the maximum stress at the i_{th} stress level, and the σ_f being the fatigue limit. The α_i is the same as in Equation (3.64) [Corten & Dolan, 1956] [Zhou et al., 2019].

3.3.6.3 Nonlinear Damage Accumulation Models Based on the S-N Curve

A new concept based on the Basquin equation was proposed by Kwofie and Rahbar which they called the fatigue driving stress (FDS). Their proposal was that the FDS is the driver of fatigue damage and that it can be used to predict the remaining fatigue life of a structure subjected to variable amplitude loading. The FDS increases in a nonlinearly with every cycle, causing cumulative damage to the material. Failure is assumed to occur when the FDS reaches a critical value. The critical fatigue driving stress is independent of the applied stress or any other load interactions. The value obtained by the previous FDS loads, is used to calculate an equivalent life-fraction that would be expended by the current load only and used to predict the remaining life. The FDS can based on the applied cyclic stress σ_i be expressed as:

$$S_{D_i} = \sigma_i N^{\frac{b n_i}{N_i}} \tag{3.71}$$

where the n_i being the number applied of cycles, and the N_i number of applied cycles at stress amplitude σ_i. While b is the fatigue strength exponent. The cumulative fatigue damage for

variable amplitude loading can, according to the model by Kwofie and Rahbar, be expressed as Equation (3.72):

$$D = \sum \frac{n_i}{N_i} \frac{\ln (N_i)}{\ln (N_1)} \tag{3.72}$$

with the N_1 is the fatigue life for the first applied load that initiates the fatigue damage. The ratio $\ln (N_i) / \ln (N_1)$ considers the load sequence and interaction effects. The FDS in Equation (3.71) is clearly a nonlinear function, but Equation (3.72) is a piece-wise function. Note that for $N_i = N_1$, Equation (3.72) will be reduced to the linear damage rule. The remaining life for variable amplitude loading is shown in Equation (3.73) [Kwofie & Rahbar, 2011] [Kwofie & Rahbar, 2013].

$$\frac{n_i}{N_i} = \frac{\left(1 - \frac{n_i}{N_i}\right) \ln(N_1) - \frac{n_2}{N_2} \ln(N_2) - \frac{n_3}{N_3} \ln(N_3) - \cdots - \frac{n_i}{N_i} \ln (N_{i-1})}{\ln (N_i)} \tag{3.73}$$

Later, Zhu et al. improved upon Kwofie and Rahbars concept and proposed an improved damage model for fatigue driving stress. They added an interaction factor that is a function of subsequent stress levels with the aim to account for the load interaction effects. Then the modified remaining lifetime function is expressed as [Zhu et al., 2019]:

$$\frac{n_i}{N_i} = \left(1 - \frac{n_1}{N_1} - \frac{n_2}{N_2} - \cdots - \frac{n_{i-1}}{N_{i-1}}\right) \left(\frac{\ln (N_1)}{\ln (N_{i-1})}\right)^{\frac{\sigma_{i-1}}{\sigma_i}} \tag{3.74}$$

Aeran et al. presented in 2017, that there is a need for a model that is based on commonly available S-N curves. The reason being that none of the models available at the time were readily applicable due to the need to determine other material parameters or a modification of the S-N curve. Their proposal was a damage model solely based on the S-N curves without any need for additional parameters. A new damage index was proposed and is expressed in Equation (3.75). The parameter δ_i can be determined by using an available S-N curve because it is only dependent on N_i. That means it can be calculated for any design detail where the S-N curve is available. The fatigue damage D can be expressed by the absolute value of the proposed index, meaning $D = D_i$:

$$D_i = 1 - \left[1 - \frac{n_i}{N_i}\right]^{\delta_i} \quad with \quad \delta_i = \frac{-1.25}{\ln (N_i)} \tag{3.75}$$

A more reliable estimation of the fatigue life under variable amplitude loading, a new damage transfer concept was also proposed by Aeran et al. to account for the load sequence and load interaction effects. A new interaction factor, μ, was proposed [Aeran et al., 2017] [Aeran et al., 2017]. For a loading block $i + 1$, the interaction factor is expressed as:

$$\mu_{i-1} = (\frac{\sigma_i}{\sigma_{i-1}})^2 \tag{3.76}$$

where the new damage transfer concept is based on using the fatigue damage evolution curves and the proposed load interaction factor μ. This means the damage at a given stress level can be determined by using the damage evolution curve of the considered material. Generally, for a material subjected to n_i cycles with a stress amplitude σ_i, the fatigue damage can be calculated by using Equation (3.75). In the case of the material being further loaded for n_{i+1} number of cycles with a stress amplitude value of σ_{i+1}, the damage can be transferred from σ_i to σ_{i+1} by using the interaction factor μ_{i+1} together. The effective number of cycles $n_{(i+1),eff}$ is calculated that corresponds to σ_{i+1} by using Equation (3.77). This means the damage state of the material does not change while transferring the loading state from one level of stress to the next one [Aeran et al., 2017].

$$n_{(i+1),eff} = N_{i+1} \left[1 - (1 - D_i)^{\frac{\mu_{i+1}}{\delta_{i+1}}}\right] \tag{3.77}$$

A number of cycles $n_{(i+1),eff}$ at a stress amplitude σ_{i+1} would result in the same damage D_i, assuming it had been present from the start. The total number of cycles at the loading $i + 1$ can be calculated by using Equation (3.78). After the loading step $i + 1$, the cumulative damage can then be determined by using Equation (3.79) and Equation (3.80) [Aeran et al., 2017]:

$$n_{(i+1),total} = n_{(i+1),eff} + n_{(i+1)} \tag{3.78}$$

$$D_{i+1} = 1 - \left[1 - \frac{n_{(i+1),total}}{N_{i+1}}\right]^{\delta_{i+1}} \tag{3.79}$$

$$D = |D_{i+1}| \tag{3.80}$$

In Figure 14, is the flowchart proposed by Aeran et al. of the damage transfer concept illustrated. The proposed model can also be applied to design details using an appropriate S-N curve defined in standards. Practicing engineers can easily implement it.

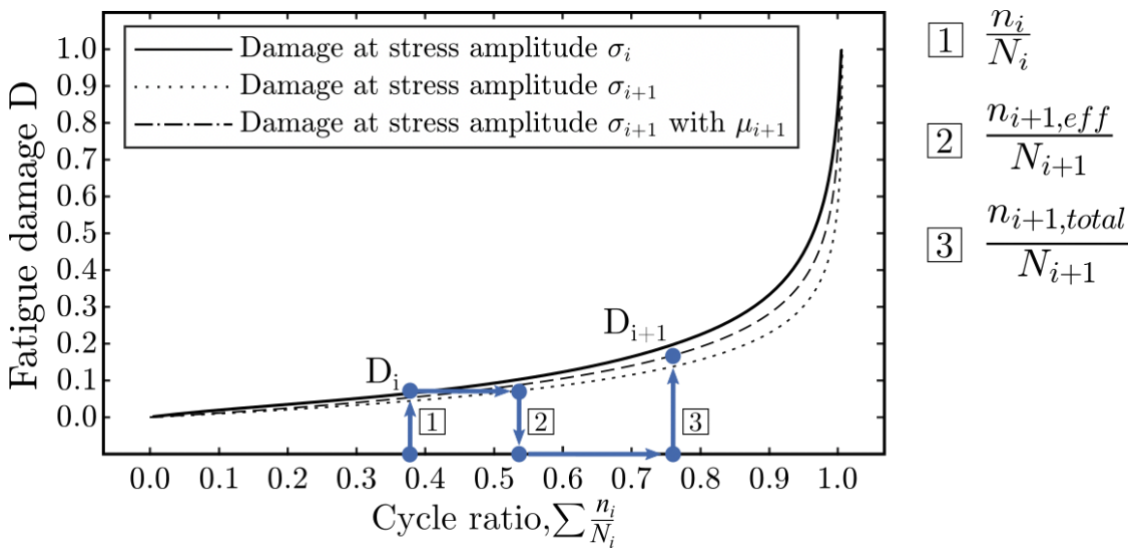

Figure 14: Illustration of the damage transfer concept. Figure adopted from work in [Aeran et al., 2017].

Si-Jian et al. proposed a new damage accumulation model where the only an S-N curve is required as input. This damage model is based on Miner's rule and Basquins equation. They derived Equation (3.81) for the cumulative damage [Si-Jian et al., 2018]:

$$D = 1 - \left[\left(\frac{n_1}{N_1}\right)^{\frac{\sigma_2}{\sigma_1}} + \frac{n_2}{N_2}\right]^{\frac{\sigma_3}{\sigma_2}} + \cdots + \frac{n_{i-1}}{N_{i-1}}\Bigg]^{\frac{\sigma_i}{\sigma_{i-1}}} + \frac{n_i}{N_i} \tag{3.81}$$

Theil proposed a new fatigue life prediction model based on the linearized damage growth curves of a double linear S-N diagram where the S-N curve corresponds to failure. The reason for this was to account for the effects of overload blocks with stress levels around ca. 0.2% ~ 10 % of the yield strength. This lifetime prediction model is based on an iterative calculation, which is explained based on Figure 15. Assume a four-level block loading sequence, as shown in Figure 3.15, that is characterized by the σ_{ai}, n_i pairs shown. The linear dash and dotted lines, represent the linearized damage growth curves, and their slope depends on the corresponding stress. When the fatigue life associated with the damage growth curve of the current stress level is reached (meaning N_i for the i_{th} load block), failure will occur. Theil proposed that the damage growth is linear for a constant amplitude. In Figure 15, the line OW_1 represents the damage growth curve at the first load level. This is expressed in Equation (3.82) [Theil, 2016]:

$$\sigma_1 = w_1 N_1 \rightarrow w_1 = \frac{\sigma_1}{N_1} = \frac{\zeta_{11}}{n_1} \quad with \quad \zeta_{11} = w_1 n_1 \tag{3.82}$$

where the n_1 is the applied number of cycles and N_1 is the fatigue life at σ_{a1}. The ζ_{11} is the corresponding stress level to n_1 on current damage curve, and the w_1 is the slope of the damage curve OW_1. The calculation continues in the same manner for following load blocks. It is important to note that the damage growth for following load blocks happens on a damage curve OW_i', parallel to the damage curve OW_i. To calculate the remaining fatigue life at a given stress

amplitude, the intersection between the relevant linearized damage growth curve and the S-N curve must be determined. In Figure 15, this is shown by the blue are for the fourth load block. Theil validated his proposal by using experimental data available in literature of aluminum alloys, a fine grain low alloy structural steel, and austenitic steel bolt joints. He realized that the estimations of these models were better than those obtained with Miner's rule. He also noted that better lifetime estimations could be obtained by using nonlinear damage growth curves, but that this in return would increase the number of required parameters and thus make it less applicable for practicing engineers [Theil, 2016].

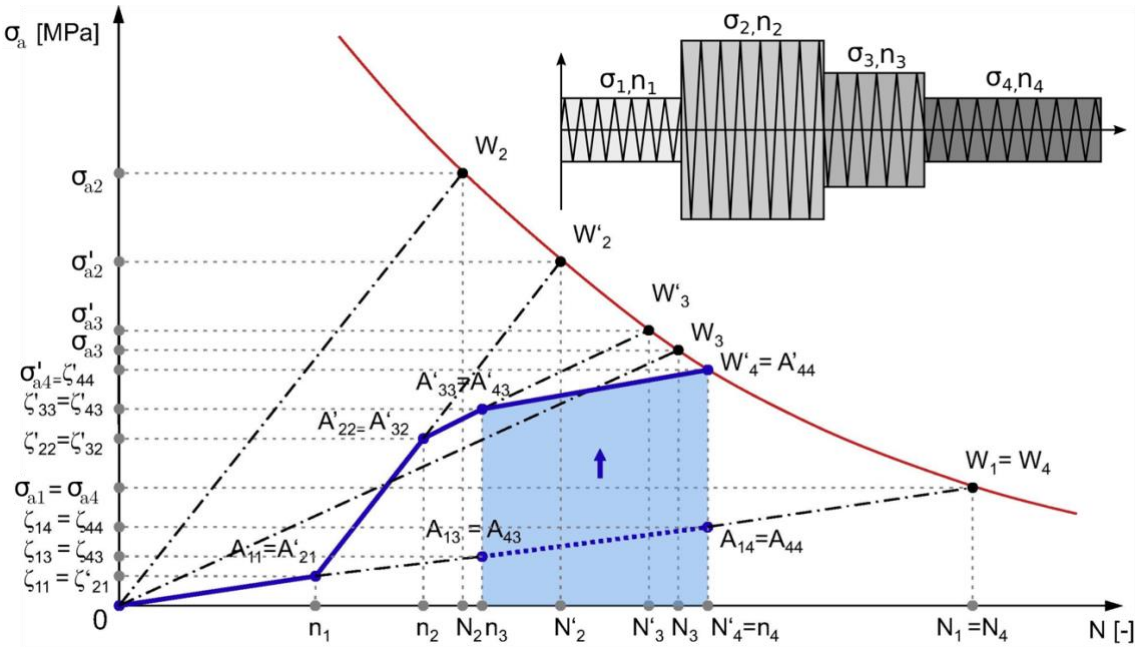

Figure 15: Graph of the linearized damage growth curve approach for fatigue life prediction in a four-level block loading. Figure adopted from work in [Theil, 2016].

3.3.7 Life Curve Modification Models

The life curve modification models modify the S-N curve to consider the different effects, such as the interaction effects and load sequence. There are mainly two types of life modification models. The first type being based on the models by Corten and Dolan and Freudenthal and Heller [Corten & Dolan, 1956] [Freudenthal & Heller, 1959]. The second type is based on the concept of the isodamage lines mentioned by Hunter and Fricke [Hunter & Fricke, 1954].

3.3.7.1 Life Curve Modification Models Based on Model of Corten & Dolan

The models by Corten and Dolan, and Freudenthal and Heller both represent a clockwise rotation of the S-N curve around a point of reference. The models may be similar in application, but they are based on different assumptions and therefore use different point of reference for the rotation. Corten and Dolan presented the idea that larger numbers of damage nuclei that are produced at higher stress amplitudes will cause an increased growth rate of damage nuclei at following lower stress levels [Kaechele, 1963].
Freudenthal and Heller proposed that the damage rate is independent of the load level. For the Corten and Dolan model, the point corresponding to the highest stress amplitude in the load spectrum is chosen as the point of reference. The Freudenthal and Heller model defines the point

of reference as the stress level where the low-cycle fatigue region transitions to the high-cycle fatigue region. This is mentioned to be between 10^3 and 10^4 cycles [Corten & Dolan, 1956] [Freudenthal & Heller, 1959].

Leipholz agreed with the thought that life-reducing interaction effects between cycles of variable amplitude could be accounted for by modifying the original S-N curve. Leipholz proposed a new model where the original S-N curve was replaced with a modified $S - \widehat{N}_i$ curve, that accounted for the load interaction effects. The new model is expressed in Equation (3.83) as [Leipholz, 1983] [Leipholz 1985] [Leipholz, 1986]:

$$N = \left[\sum_{i=1}^{k} \frac{\beta_i}{\widehat{N}_i}\right]^{-1} \quad with \quad \beta_i = \frac{n_i}{N_i} \tag{3.83}$$

where N is the total accumulated fatigue life, and the $\widehat{N}_i$ is the modified life at stress amplitude σ_i. Generally, the original curve and the modified curve deviate at low loading levels and converge at high loading levels. Using the Leipholz model of fatigue life prediction have been found reasonably accurate, when comparing to Miner's rule, there was a reduction of greatly non-conservative results observed [Dowdell et al., 1986].

Many researchers have studied the empirically determined parameter d, defined by Corten and Dolan as a material parameter. Spitzer and Corten suggested that the slope of the modified S-N curve (meaning the parameter d), could be determined from the average slope of a few S-N curves determined from two-level block loading tests. This approach was validated with fully reversed (R = –1) bending tests on 7075-T6 aluminum alloy wire and 2024-T4 [Spitzer & Corten, 1956]. The Corten and Dolan model has been shown to be suitable for a wide range of applications with good precision, but lifetime estimations are strongly dependent on the value of the parameter d [Zhao, 2000]. Rao et al. have reported that the value of d for steels, ranges from between 6.2 and 6.9 with an average value of 6.57 [Rao et al., 2001]. Peng et al. reported values of 4.8 for high strength steels and 5.8 for other materials [Peng et al., 2018]. Zhu et al. discuss that determination of the parameter d is semi-empirical, meaning many experiments are required to gather experimental data, and that the theoretical basis is lacking [Zhu et al., 2012]. Three experiments were performed with spherical welded joints from Q235B grade steel the calculated values of d were 3.39, 18.69, and 27.09. This indicated that it was difficult to obtain a consistent value for d [Jiao et al., 2018]. Spitzer and Corten theorized that d could be obtained from a two-level block loading and used for multi-level block loading conditions, but this was proven wrong by Marsh and Mackinnon. They showed that his often lead to unsafe predictions. Even so, the Corten and Dolan model is superior to Miner's rule since it considers the effects of low amplitude loading and load interactions [Spitzer & Corten, 1956] [Marsh & Mackinnon, 1968].

Zhu et al., proposed in 2012, a new way of calculating the exponent d. They proposed that d is a function of the applied stresses instead of a material constant. The modified parameter d is expressed in Equation (3.84) as:

$$d(\sigma_i) = \mu \frac{\sigma_1^{\lambda} \delta_f^{1-\lambda}}{\sigma_i} \tag{3.84}$$

where the μ is a material constant, the λ is a factor accounting for the load sequence effects with $0 < \lambda < 1$ (for a constant amplitude loading, $\lambda = 0$, meaning no load interaction). The value of λ can be estimated ad $\lambda = n_1 / N_1$. The δ_f is the parameter for the initial strength of the specimen which can be obtained through experiments. It was proposed that δ_f can be obtained for metal only, as $\delta_f \approx \sigma_b$ + 350 MPa, σ_b being the ultimate tensile strength. Even considering the

σ_b being equal to the yield strength, this expression makes little sense. The ratio δ_f / σ_i characterizes the effect of the material properties of the fatigue life, the ratio σ_1 / σ_i being the interaction factor. Experimental data from low-to-high and high-to-low block load sequences on 16Mn and C45 steels were compared to the predicted fatigue lives. The results verified that the proposed model would provide better lifetime predictions than Miner's rule for two-level block loading conditions. It was stated that this model can also be used for multi-level block loading conditions, however no verification was presented [Zhu et al., 2012].

Gao et al. presented a new expression for d that is based on the work of Zhu et al. which suggests that fatigue failure is influenced by a combination of the effects of stress conditions and the degree of damage. They suggested this can be done by an exponential function of the cycle ratio and loading ratio. They further modified the expression by Zhu et al. and added a material parameter γ. The γ is a material constant which can be found from experimental data and the chosen failure criterion (for instant n / N = 1) [Zhu et al., 2008] [Gao et al., 2015].

$$d = \exp\left[\left(\frac{n_i}{N_i}\right)^{\sigma_i/\sigma_{max}}\right] + \gamma \tag{3.85}$$

Gao et al. compared their model to the model of Corten and Dolan for normalized 16Mn steel, Hot-rolled 16Mn steel, and normalized C45 steel. The errors for the lifetime prediction model were all within a 50% error margin, which was not the case when using Miner's rule for predictions [Gao et al., 2015]. Equation (3.85) was then modified to consider the effects between stress ratios of consecutive load blocks [Xue et al., 2019].

$$d = \frac{\sigma_i}{\sigma_{i-1}}\left[exp\left(\frac{n_i}{N_i}\right)^{\frac{\sigma_i}{\sigma_{max}}} + \gamma\right] \tag{3.86}$$

Then, Equation (3.86) was further modified by Liu et al.:

$$d = \left(\frac{\sigma_i}{\sigma_{i-1}}\right)^k \left[\exp\left(\frac{n_i}{N_i}\right) + \gamma\right] \tag{3.87}$$

where the exponent k is a natural integer. Liu et al. validated their model with experimental data for two-level and multi-level block loading, available in the literature. They compared their model to the models of Gao et al. as well as Xue et al. and found that the lifetime predictions based on their model was significantly better than both other models. Although they did not give any clear guidance on how the value of the exponent k is determined. The values $k = 2$ and $k = 3$ both gave good results. It was reported that to find the best value for k, further study is needed [Gao et al., 2015] [Xue et al., 2019] [Liu et al., 2020].

3.3.7.2 Life Curve Modification Models Based on Isodamage Lines

The simplest way to assess the fatigue life of a structure free of damage is to use an S-N curve. This concept can be translated into a remaining lifetime assessment after a certain number of load cycles. After a number of cycles n_i, at a stress amplitude σ_i, the remaining fatigue life is equal to N_{iR}. The isodamage lines concept assumes that the S-N curve of a material corresponds

to a state of 100% fatigue damage, while the combinations of the cycles n_i and the stresses σ_i with identical values of damage, fall on smooth curves when plotted. Subramanyan presented a set of straight isodamage lines in an S-log(N) diagram, that converge close to the knee-point of the S-N curve (Figure 16). The damage is defined as the ratio of the slope of an isodamage line to the limiting value of the slope of the S-N curve. This is expressed in Equation (3.88). Due to the damage being expressed as a logarithmic function of the load cycles, means that the number of cycles needed to cause a certain amount of damage will increase when the stress amplitude decreases and vice versa. Meaning the model will account for observed increase in lifetime for a high-to-low block loading sequences, and likewise for the observed decrease in lifetime for the low-to-high block loading sequences [Subramanyan, 1976].

$$D_i = \frac{\tan(\theta_i)}{\tan(\theta_f)} = \frac{\log(N_f) - \log(N_i)}{\log(N_f) - \log(n_i)} \tag{3.88}$$

Where the N_f is the number of cycles to failure at the S-N curves knee-point. The N_i is the fatigue life for a constant stress amplitude σ_i, and the n_i is the number of cycles with the stress amplitude σ_i applied in the load step i. When there is applied a new loading step to the stress amplitude σ_{i+1}, the isodamage line is then followed to the new stress amplitude. Then, it is possible to define an equivalent number of cycles $n_{i,i+1}$ at the stress amplitude σ_{i+1}, where the damage is the same as after n_i number of cycles at stress amplitude σ_i. The equivalent number of cycles $n_{i,i+1}$ can be expressed as.

$$n_{i,i+1} = N_{i+1} \left(\frac{n_i}{N_i}\right)^{\alpha_i} \tag{3.89}$$

$$\alpha_i = \frac{\log(N_f) - \log(N_{i+1})}{\log(N_f) - \log(N)} = \frac{\sigma_{i-1} - \sigma_f}{\sigma_i - \sigma_f} \tag{3.90}$$

The remaining fatigue life $N_{(i+1)R}$ at the loading step $i + 1$ is expressed as:

$$N_{(i+1)R} = N_i - n_{i,i+1} \tag{3.91}$$

This procedure is shown in Figure 16 [Subramanyan, 1976].

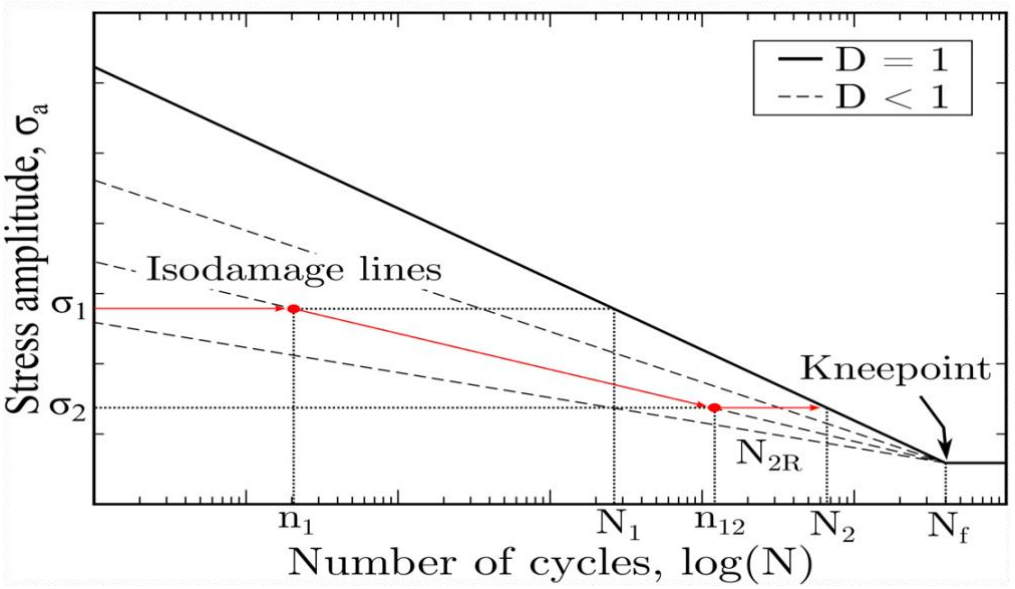

Figure 16: The isodamage path for a two-level block loading sequence [Subramanyan, 1976].

Hashin and Rotem presented a different method based on the isodamage lines concept. They proposed that the isodamage lines should converge at the point where the S-N intersects with the S-axis. This is illustrated in Figure 17. Note that the isodamage lines defined by Hashin and Rotem intersect the N-axis for $\sigma_a = 0$. This means that the fatigue life is lower for a two-stage block loading sequence, with the $\sigma_{a,1} = 0$ and $\sigma_{a,2} > 0$, than the fatigue life at a constant stress amplitude $\sigma_{a,2}$ [Hashin & Rotem, 1978]. The method by Subramanyan is favourable due the isodamage lines defined by Hashin and Rotem becoming invalid at low stress amplitudes. Also, Subramanyans model has been proven to successfully predict the fatigue lives of specimens under two-level block loading, made from aluminum alloy Al-2024-T42 [Pavlou, 2002]. Compared to Miner's rule, both models are an improvement, but they have been found to be slightly non-conservative [Lee et al., 2014]. Subramanyans model also does not consider cycles below the fatigue limit [Subramanyan, 1976].

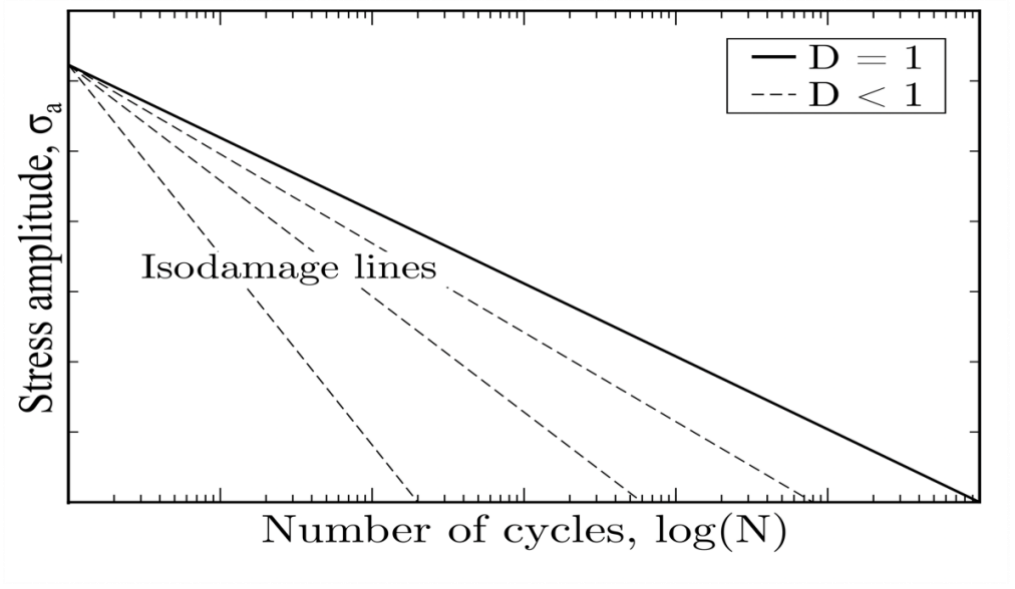

Figure 17: Hashin and Rotems model of the isodamage lines [Hashin & Rotem, 1978].

El Aghoury and Galal presented a new concept called the Virtual Target Life Curve (VTLC) to overcome the shortcomings of the previous models that were based on the isodamage lines. They proposed that every material has a theoretically infinite, virtual expected life that is greater than the real failure life under constant amplitude loading. The expected life will be reduced as the number of cycles increases and the damage rate will depend on the stress level. Overloading effects caused by the stress level transitions can abruptly increase the damage. The importance of this increase in damage depends on the ratio of the two stress levels. The criterion for failure in the VTLC model is reached when the accumulated number of cycles, reaches the virtual target life at a specific stress level. In Figure 18, the VTLC model is shown. As the number of cycles increases, the slope b_v of the VTLC, decreases. Failure will occur, when the VTLC rotates around the focal point (shown in Figure 18) until it is parallel with the original S-N curve (meaning $b_v = b$), and the fatigue life is assumed to be exhausted [El Aghoury & Galal, 2013].

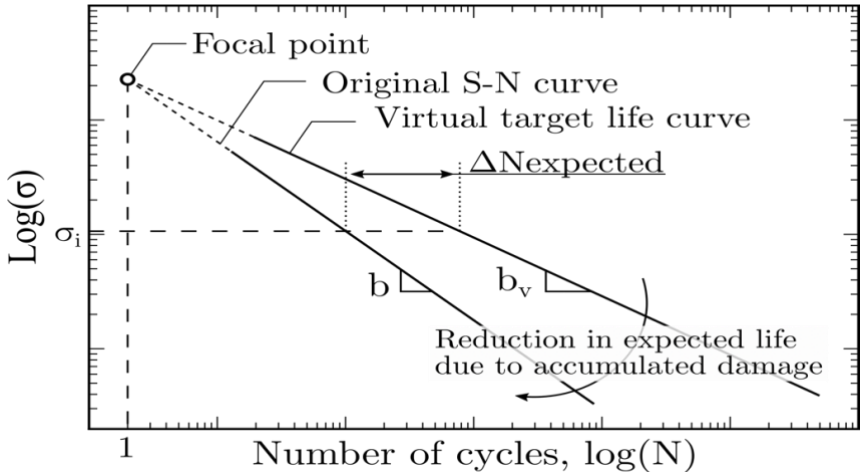

Figure 18: Illustration of the Virtual Target Life Curve [El Aghoury & Galal, 2013].

Rege and Pavlou proposed the concept of nonlinear isodamage curves based on the model of Subramanyan [Subramanyan, 1976]. This is shown in Figure 19. Their goal was to improve the non-conservative predictions by the previous model of Subramanyan, and Hashin and Rotem [Subramanyan, 1976] [Hashin & Rotem, 1978]. They made a one-parameter model that practicing engineers can apply easily. By using the Equation (3.92) and (3.93), the damages up to and including load step i, can be calculated for a multi-level block loading sequence.

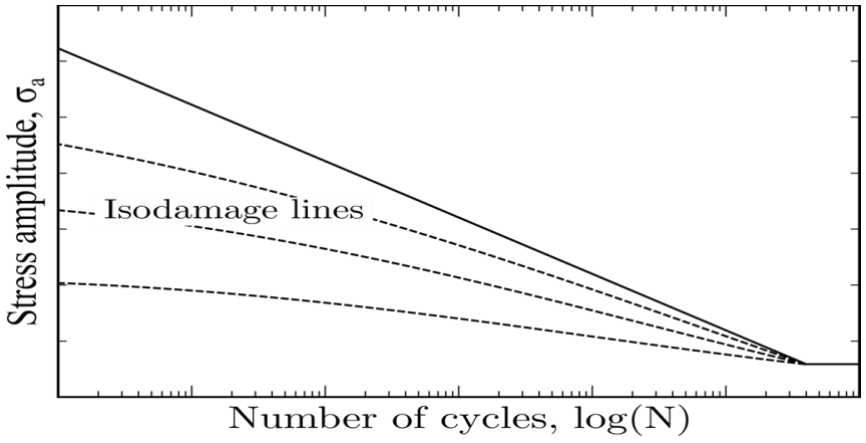

Figure 19: The nonlinear isodamage curve model [Rege & Pavlou, 2017].

$$\log(n_{i-1,i}) = \log(N_f) - \frac{\log(N_f) - \log(N_i)}{D_{i-1}^{1/q(\sigma_i)}} \tag{3.92}$$

$$D_i = \left[\frac{\tan(\theta_i)}{\tan(\theta_f)}\right]^{q(\sigma_i)} = \left[\frac{\log(N_f) - \log(N_i)}{\log(N_f) - \log(n_{i-1,i} + n_i)}\right]^{q(\sigma_i)} \tag{3.93}$$

The N_i is the constant amplitude fatigue life at the stress amplitude σ_i. The N_f is the number of cycles at the fatigue limit. The $q(\sigma_i)$ is a function of the stress amplitude for the current load step i, which is best determined from experimental data, but can also be estimated by using Equation (3.94). The σ_s is the value of the stress amplitude at the point where the straight S-N curve intersects the stress axis. Rege and Pavlou proposed that a value of $b = -0.75$ will be suitable for most steel grades. This was verified by comparing the model predictions to experimental data [Rege & Pavlou, 2017].

$$q(\sigma_i) = (a\sigma_i)^b = (2\frac{\sigma_i}{\sigma_s})^{-0.75} \tag{3.94}$$

The model predictions were compared to those of Subramanyans [Subramanyan, 1976]. For the high-to-low loading tests, the suggested model was found to be more conservative than the model of Subramanyan. However, for low-to-high loading tests, the results showed no significant differences. Which means, although, the model is an improvement when compared to the linear isodamage curve model, it still has disadvantages. Firstly, if the stress amplitude changes a lot, then it will become tiresome to use as it requires the consecutive Equations (3.92) and (3.93). Secondly, S-N curves in design standards are often bilinear, meaning they cannot be used with the suggested model [Rege & Pavlou, 2017].

Zhu et al. discussed that the model of Rege and Pavlou does not actually improve the fatigue life predictions for C35 and P355NL1 steels when compared to the model of Subramanyan. Their reason being that the exponent $q(\sigma_i)$ only depends on the stress amplitude and not on the loading history. From there they suggested a new expression for the damage exponent $q(\sigma_i)$ which is expressed in Equation (3.95).

$$q = l \log n_i + s \log \varepsilon_{a,i} \tag{3.95}$$

The $\varepsilon_{a,i}$ is the strain amplitude at the i_{th} loading step. The l is the load sequence weighted coefficient, and the s is the load weighted coefficient. These characterize the mutual contributions of the stress amplitude and the loading history and should be determined from a regression analysis to data from two-level block loading fatigue tests. The Equation (3.95) needs to be substituted into the Equations (3.92) and (3.93) to calculate the fatigue life under multi-level block loading [Zhu et al., 2019].

Pavlou proposed in 2018, a new model that was based on the isodamage lines model, called the S-N fatigue damage envelope. The proposal was that the area bounded by the N-axis, the S-axis, and the S-N curve, reflects the macroscopic consequences of the damage mechanisms for any pair (S, n). This is shown in Figure 20. The damage envelope (Figure 20, gray area) for any material is bounded by the bilinear curve HOK that corresponds to D = 0, and the S-N curve HK that corresponds to D = 1. For the sake of convenience, it is better to use dimensionless

quantities for the coordinate axes, and so σ_i^* is used for the S-axis, and n_i^* is used for the N-axis. They are expressed in Equation (3.96).

$$\sigma_i^* = \frac{\sigma_i - \sigma_f}{\sigma_u - \sigma_f} \qquad n_i^* = \frac{n_i}{N_i} \tag{3.96}$$

The σ_i is the stress amplitude of a specific loading block. The σ_f is the fatigue limit of the material, and lastly, the σ_u is the ultimate tensile stress. In Figure 20, the damage evolution of a four-step loading sequence is shown [Pavlou, 2018].

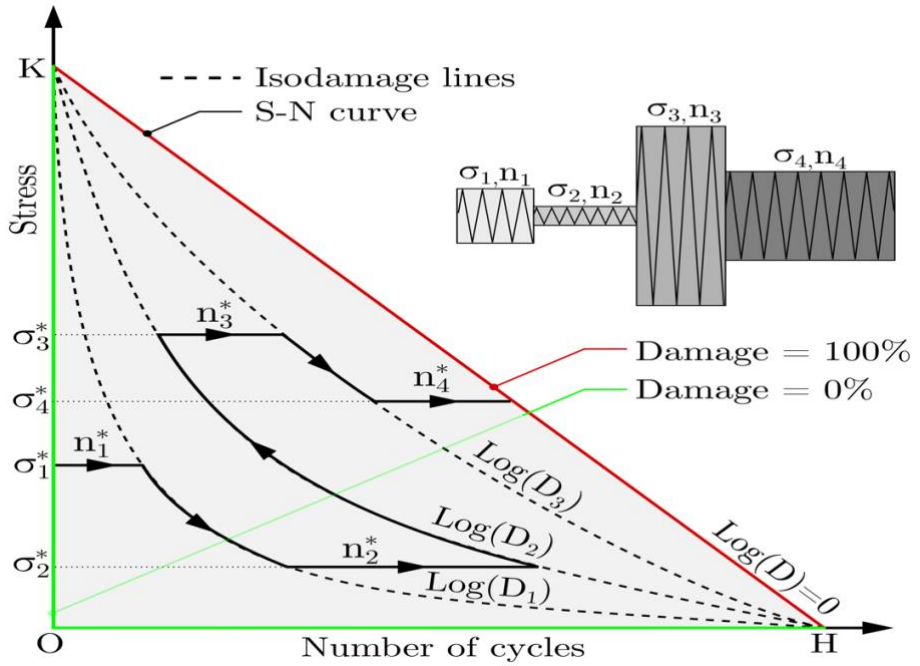

Figure 20: Illustration of the damage envelope and the concept of the isodamage lines [Pavlou, 2018].

Pavlou presented that the isodamage lines can be derived from a steady state heat transfer analysis with a commercial finite element package. The predictions of the suggested theory were compared to experimental data available in the literature, and they were in good agreement. To use the damage envelope concept for multi-axial fatigue, S-N curves obtained from specimens loaded under multi-axial fatigue stress, should be used to derive the fatigue damage envelope. Compared to the previous model by Rege and Pavlou [Rege & Pavlou, 2017], Pavlou's model does not need any parameters fitted and is valid for all types of S-N curves, linear and nonlinear [Pavlou, 2018].

Batsoulas presented the concept of hyperbolic isodamage lines. The goal was to account for the invalidity of the straight S-N isodamage lines observed when near the axes. The hyperbolic curves as expressed as:

$$log\frac{\sigma}{\sigma_f'} = c\,(log\frac{N}{N_e})^{-1} \tag{3.97}$$

σ_f' is the coefficient for the fatigue strength. The N_e is the minimum number of cycles needed for damage initiation, and the c is a constant. The isodamage lines are defined by a $\log(\sigma / \sigma_f')$ versus a $\log(n / N_e)$ diagram and the points along the $\log(\sigma / \sigma_f')$ versus the $\log(N / N_e)$ are the points of failure. In Figure 21, the concept of the hyperbolic isodamage line is shown. An important note about the isodamage lines model, is that their points are apexes of equivalent rectangles. For instance, in the Figure 21, the area of the rectangle [OABC] is equal to the area of the rectangle [OA´B´C´]. This means, the fatigue damage associated with a certain isodamage line can be expressed as [Batsoulas, 2016]:

$$D_i = \frac{[OABC]}{[OAFE]} = \frac{\log\left(\frac{\sigma_i}{\sigma_f'}\right)\log\left(\frac{n_i}{N_e}\right)}{\log\left(\frac{\sigma_i}{\sigma_f'}\right)\log\left(\frac{N_i}{N_e}\right)} \tag{3.98}$$

The damage accumulation for a multi-level loading sequence can be determined as

$$\left(\left(\left(\frac{n_1}{N_1}\right)^{\varphi_{1,2}} + \frac{n_2}{N_2}\right)^{\varphi_{2,3}} + \cdots + \frac{n_i}{N_{i-1}}\right)^{\varphi_{i-1,i}} + \frac{n_i}{N_i} = 1 \quad with \quad \varphi_{i-1,i} = \frac{\log\left(\frac{\sigma_{i-1}}{\sigma_f'}\right)}{\log\left(\frac{\sigma_i}{\sigma_f'}\right)} \tag{3.99}$$

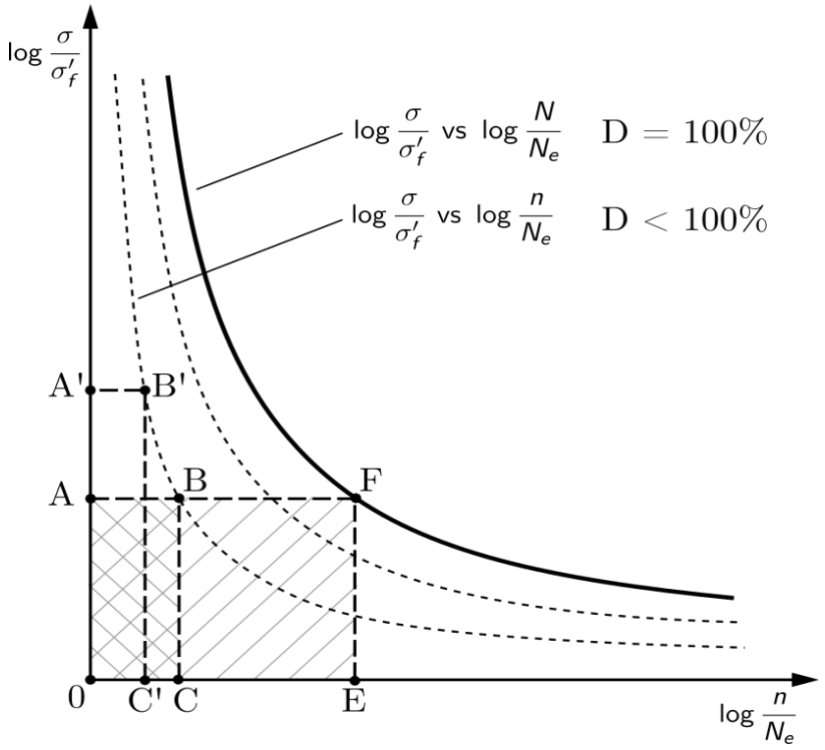

Figure 21: Illustration of the Hyperbolic isodamage line concept [Batsoulas, 2016].

A modified model of the hyperbolic isodamage concept was presented by Xia et al. where they combined it with the model of Ye and Wang which is based on the exhaustion of static

toughness. Basically, this model modifies the exponent $\varphi_{i-1,i}$ to [Ye & Wang, 2001] [Xia et al., 2020]

$$\varphi_{i-1,i} = \left(\frac{\log\left(\frac{\sigma_{i-1}}{\sigma_f'}\right)}{\log\left(\frac{\sigma_i}{\sigma_f'}\right)}\right)\left(\frac{\log(N_f)-\log(N_i)}{\log(N_f)-\log(N_{i-1})}\right) \tag{3.100}$$

3.3.8 Continuum Damage Mechanics Based Models

Continuum damage mechanics (CDM) is about the mechanical behavior of a deteriorating medium at the continuum scale. The foundations for CDM were made by Kachanov and Rabotnov [Kachanov, 1958] [Rabotnov, 1970]. It was first applied to fatigue life prediction by Chaboche. He suggested a nonlinear continuum damage (NLCD) model to explain the progressive deteriorating process before the macroscopic crack initiation. His model generalizes the NLDR model of Marco and Starkey and the DCA model of Manson and Halford supported by CDM [Marco & Starkey, 1954] [Manson & halford, 1981]. The model was first described by Chaboche and later reviewed by Chaboche and Lesne [Chaboche, 1974] [Chaboche & Lesne, 1988]. Equation (3.101) shows the damage expressed for uniaxial loading. The Equation (3.102) expresses the number of cycles for a macroscopic crack initiation N_F (the failure criterion).

$$D = 1 - \left[1 - \left(\frac{n}{N}\right)^{\frac{1}{1-\alpha}}\right]^{\frac{1}{1-\beta}} \quad with \quad \alpha = 1 - a\left\langle\frac{\sigma_a - \sigma_{l_0}(1-b\bar{\sigma})}{\sigma_u - \sigma_{max}}\right\rangle \tag{3.101}$$

$$N_F = \frac{1}{(1+\beta)(1-\alpha)}\left[\frac{\sigma_{max}-\bar{\sigma}}{M_0(1-b\bar{\sigma})}\right]^{-\beta} \tag{3.102}$$

$\alpha, \beta,$ and the M_0 are the material constants. The σ_{l_0} is the fatigue limit for fully reversed conditions, σ_a is the stress amplitude, σ_{max} is the maximum stress, and σ_u is the ultimate tensile strength. Definition for the symbol $\langle\rangle$ is that the $\langle x\rangle = 0$ when $x < 0$ and $\langle x\rangle = x$ when the $x > 0$. There are some major advantages to the NLCD model. Firstly, it considers the damage growth below the initial fatigue limit if the material is damaged. Secondly, it can consider the interaction effects by using an additional variable that considers the strain hardening. Thirdly, the damage is only dependent on the mean stress. Finally, the material parameters can be obtained from conventional S-N curves. To apply the model for multi-axial loading conditions, a multi-axial fatigue criterion must be added since the damage D is a scalar variable written in uniaxial form [Chaboche, 1974] [Chaboche & Lesne, 1988]. Sun et al. were successful in using the NLCD model and showing its practicability with an effective stress in an online damage calculation framework for a steam turbine [Sun et al., 2017].

3.3.8.1 Models Based on Chaboche's Nonlinear Continuum Damage Model

Oller et al. proposed a thermo-elasto-plastic-damage model that establishes a connection between the residual material strength and the damage threshold evolution. They proposed a new state variable of fatigue $f_{red}\ (N, \sigma_{max}, R, \theta)$, which they called the reduction function, to model

the nonlinear damage behavior seen in fatigue. Where the N is the current number of cycles, the σ_{max} is the maximum applied stress, the R is the stress ratio σ_{min} / σ_{max}, and the θ is the temperature. This state variable modifies the discontinuity threshold surface $F^D\left(S_{ij}, d\right)$ (damage or yield). Therefore, the influence of the number of cycles is implicitly incorporated in this fatigue damage model. Their method is different from that of the model by Chaboche and Lesne where the number of cycles is specifically defined in the fatigue damage model [Chaboche & Lesne, 1988]. Meaning that fatigue phenomena can be introduced in the manner of classical constitutive damage formulations [Oller et al., 2005].

Dattoma et al. introduced a new nonlinear uniaxial model based on the model of Chaboche [Chaboche, 1974]. They introduced a new expression for the exponent α:

$$\alpha = 1 - \frac{1}{H} \langle \frac{\sigma_a - \sigma_f}{\sigma_u - \sigma_a} \rangle^a \tag{3.103}$$

where the H and the a are parameters that must be experimentally obtained. The α is chosen in a way that makes it a monotonically decreasing function of the stress to consider the load interaction effects and that it is equal to 1 should the applied stress be below the fatigue limit. Dattoma et al. proposed that, for a multi-level loading sequence, the cumulative damage can be determined as

$$D_i = 1 - \left[1 - \left(\frac{N_i + n_i}{N_{f_i}}\right)^{\frac{1}{1-\alpha_i}}\right]^{\frac{1}{1+\beta}} \tag{3.104}$$

where the N_{f_i} is the number of cycles to failure at the stress amplitude $\sigma_{a,i}$. The N_i corresponds to an equivalent number of cycles applied with the stress amplitude $\sigma_{a,i}$ that inflicts the same amount of damage as caused by n_{i-1} number of cycles at the stress amplitude $\sigma_{a,i-1}$. When the load spectrum contains several cycles below the fatigue limit, the value of the α is equal to 1. The damage increment is expressed as

$$D_i = 1 - \left[1 - W_i\right]^{\frac{1}{1+\beta}} \tag{3.105}$$

with

$$W_i = \left[1 - (D_{i-1})^{1+\beta}\right] \exp\left[\left(\frac{n_i}{(M_0/\sigma_i)^\beta}\right)(1 + \beta)\right]$$

The CDM-based model by Dattoma et al. can be applied for complex, multi-level loading sequences. It considers the damage caused by cycles below the fatigue limit and all the parameters can be determined from an S-N curve. The verification of the model was experimental data from two-level and multi-level rotating bend experiments on 30NiCrMoV12 steel. For the multi-level loading conditions Dattoma et al. considered a load history of a railway axle that runs onto a European line for 3000 kilometers. They also performed fatigue tests with low-to-high and high-

to-low, and random loading sequences on cylindrical specimens. The results of the experiments were in good agreement with the model [Dattoma et al., 2006]. Giancane et al. compared the model predictions to experiments performed on the same steel grade (30NiCrMoV12) for three different cylindrical experiments. One smooth specimen, and two notched specimens with different geometries in the notch. They concluded that the suggested CDM model produces satisfactory predictions for the fatigue life of complex geometries. Although, they also mentioned that the model's major disadvantage is its requirement to know the S-N curve for every considered geometry and for different load conditions [Giancane et al., 2010].

Zhang et al. presented another modified model based on the model of Chaboche and Lesne [Chaboche & Lesne, 1988]. In the original version, all cycles below the fatigue limit are considered damaging once D > 0. However, it has been shown that low amplitude cycles between 75% to 95% of the fatigue limit can increase the fatigue strength of the material, and thereby increasing the fatigue life [Sinclair, 1952] [Xi & Songlin, 2008] [Xi & Songlin, 2009]. It is important to note that the low amplitude cycles still do damage to the material, while also strengthening it. Therefore, omitting the low amplitude cycles results in a very conservative estimation. Zhang et al. proposed a strengthening function f_s to consider low amplitude cycles:

$$f_s = \begin{cases} 1 & \sigma_i \in [0,\sigma_F] \\ \exp(m'\sigma_i) & \sigma_i \in [\sigma_F,\sigma_0] \end{cases} \tag{3.106}$$

where the m' is the strengthening coefficient that is related to the material properties and can be determined through experiments. The σ_F is the lower limit of strengthening stress. The damage can then be determined by multiplying Equation (3.101) with the strengthening function defined in Equation (1.106). Zhang et al. also proposed the use of a membership function based on fuzzy logic mathematics to calculate whether low amplitude cycles cause damage or induce strengthening. The model was verified through experimental data of multi-level loading including low amplitude cycles below the fatigue limit. They verified that the new model has better performance than the NLCD model with errors between 14.96% and 21.5% for Chaboche's model and 2.5% and 8.38% for the model of Zhang et al. [Zhang et al., 2018].

3.3.8.2 Thermo-Mechanical Principle Model's

Bhattacharya and Ellingwood discussed in 1998 that the models available at the time introduced unknown material constants in damage growth quantification which made their use either very difficult or impossible. They also discussed that the thermodynamics based CDM models of damage growth lack continuity with the first principles of thermodynamics and mechanics, and they presented an overview of these models and their disadvantages. To overcome these disadvantages, they introduced a new thermodynamic framework for a CDM-based model to structural deterioration. Based on the first principles of thermodynamics, a coupled set of partial differential equations for damage growth in deformable bodies was determined. Under the assumption of uniaxial loading and isotropic damage growth, an expression for the fatigue damage could be derived from the differential equations. For strain-controlled loading, the fatigue damage after n number of cycles is

$$D_n = 1 - (1 - D_0)\left(\frac{\frac{1}{1+\frac{1}{M'}}\Delta\varepsilon_{p0}^{1+(1/M')} - \Delta\varepsilon_{p1}^{1/M'}\Delta\varepsilon_{p0} + C}{\frac{1}{1+\frac{1}{M'}}\Delta\varepsilon_{p}^{1+(1/M')} - \Delta\varepsilon_{p1}^{1/M'}\Delta\varepsilon_{p} + C}\right)^n \tag{3.107}$$

where the D_0 is the initial damage. The M' is the exponent for cyclic hardening. The $\Delta\varepsilon_p$ is the plastic strain range, and the $\Delta\varepsilon_{p0}$ is the threshold plastic strain range. The ε_{p1} is the plastic strain range corresponding to the strain where the reloading curve cuts the monotonic strain-axis. By using Equation (3.107), it is possible to calculate the number of cycles to crack initiation by using the conditions expressed in Equation (3.108) if the critical damage D_c is determined. The N_I is the number of cycles to macroscopic crack initiation [Bhattacharya & Ellingwood, 1998] [Bhattacharya & Ellingwood, 1999].

$$\begin{cases} D_{N_I-1} < D_c \\ D_{N_I} \geq D_c \end{cases} \tag{3.108}$$

Li et al. introduced a damage model based on the accumulation of the micro-plastic strain (usually assumed to be zero), the strain energy density release rate, and the current damage state. This model was developed to evaluate the damage accumulation in bridges under traffic loading. They began with a general constitutive model that was developed by Krajcinovic and Lemaitre [Krajcinovic & Lemaitre, 1987]. The model expresses the fatigue damage rate for high-cycle fatigue damage and is shown in Equation (3.109) [Li et al., 2001].

$$\dot{D} = \frac{R_v \sigma_{eq}^2 \left|\sigma_{eq} - \bar{\sigma}_{eq}\right|^{\beta}}{B\,(1-D)^{\alpha}} \langle \dot{\sigma}_{eq} \rangle \tag{3.109}$$

The R_v being the triaxiality function that models the influence of the triaxiality ratio (σ_H/σ_{eq} with σ_H being the hydrostatic stress) on damage and rupture. The σ_{eq} is the von Mises equivalent stress. The α defines the nonlinearity of the damage function and is a function of the stress range. The rate of damage $\dot{D}$ = 0 if the $\sigma^* < \sigma_f$ with the σ_f being the fatigue limit. The σ^*, is defined as the damage equivalent stress and was defined by Krajcinovic and Lemaitre as the stress where the damage acts in the same manner as the von Mises stress acts for plasticity [Krajcinovic & Lemaitre, 1987]. Based on the Equation (3.109), Li et al. introduced the damage model in Equation (3.110),

$$D_{i+1} = 1 - \left\{ (1 - D_i)^{\alpha_1+1} - \frac{(\alpha_1+1)N_{bl}^i}{B(\beta+3)} \sum_{j=1}^{m_{rb}} \left[\left(\sigma_j + 2\sigma_{mj}\right)\sigma_j \right]^{\frac{\beta+3}{2}} (1 - D_i)^{\alpha_1 - \alpha_j} \right\}^{\frac{1}{\alpha+1}} \tag{3.110}$$

With the

$$\alpha_i = k_a \sigma_i + \alpha_0 \tag{3.111}$$

The B, β, k_a and the α_0 are all material parameters that can be obtained from the S-N curve. The m_{rb} is the number of cycles with the maximum stress in the representative block above the fatigue limit. The N_{bl} is the number of loading blocks, the σ_{mj} and the σ_j are the mean stress and the stress range for the j_{th} cycle. This damage model has been introduced and

successfully applied for fatigue damage assessment of the Tsing Ma Bridge under various loading conditions in several research papers [Li et al., 2001] [Chan et al., 2001] [Li et al., 2002] [Xu et al., 2009]. The Equation (3.109) has also been used by other researchers, as the basis for other cumulative damage models with the purpose of fatigue damage assessment of long span bridges [Xu et al., 2012] [Wang et al., 2018]. These models are very similar to the model of Li et al. expressed in Equation (3.110) (Li et al., 2001].

3.3.8.3 Damage Stress Concept Based Models

Mesmacque et al. introduced the damage stress model (DSM) based on the CDM model. The DSM is based on the idea that if the physical state of the damage does not change, the fatigue life depends only on the loading conditions. The remaining fatigue life of a structure loaded for n_i number of cycles, with a stress amplitude σ_i, is equal to $N_{iR} = N_i - n_i$. The remaining life corresponds to an admissible stress level $\sigma_{ed,i}$ on the S-N curve. This is shown in Figure 22. The stress $\sigma_{ed,i}$ is called the damage stress after n_i number of loading cycles. That means, the damage stress is described as the stress corresponding to the instantaneous remaining life on the S-N curve [Mesmacque et al., 2005].

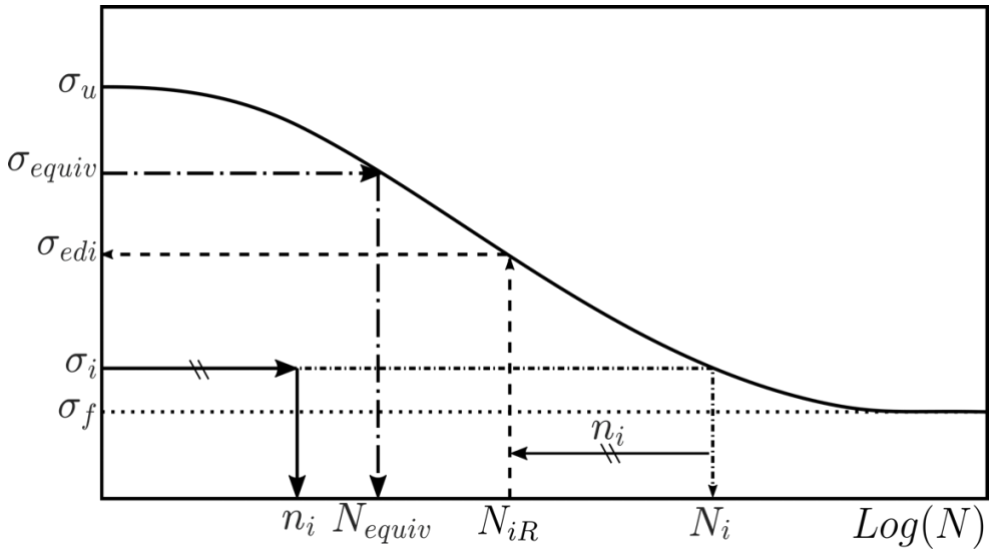

Figure 22: Illustration of the Damage Stress Model's parameters [Mesmacque et al., 2005].

They proposed a new damage parameter and expressed it as

$$D_i = \frac{\sigma_{ed,i} - \sigma_i}{\sigma_u - \sigma_i} \tag{3.112}$$

where the σ_u is the ultimate stress. For multi-level loading, the damage can be transferred to level $i + 1$ by using Equation (3.113). Then it is possible to determine the number of cycles N_{equiv} (shown in Figure 22) at the level $i + 1$, equivalent to n_i cycles at level i. The remaining lifetime after n_{i+1} number of load cycles with a stress amplitude of σ_{i+1} will then be $N_{i+1} - n_{i+1}$. The equivalent damage stress σ_{equiv} at the level $i + 1$ can be determined by using Equation (3.113). To begin with, when $D = 0$, the damage stress $\sigma_{ed} = \sigma_i$. When $D = 1$, the damage stress $\sigma_{ed} = \sigma_u$, and failure will occur.

$$D_i = \frac{\sigma_{ed,i} - \sigma_i}{\sigma_u - \sigma_i} = \frac{\sigma_{equiv} - \sigma_{i+1}}{\sigma_u - \sigma_{i+1}} \quad (3.113)$$

Mesmacque et al. compared their model with Miner's rule for two-level and four-level block loading sequences. For two-level block loading sequence, the differences between the experimental data and the results were, with the DSM between 7.7% and 89% and with Miner's rule, they were between 16.8% and 155%. For the four-level block loading sequence, the difference between experimental data and the results were, with the DSM between 2.5% and 6.5%, and with Miner's rule they were between 4.7% and 75.1% [Mesmacque et al., 2005]. Aid et al. then continued to compare the model to Miner's rule for multi-level block loading sequences and a random block loading sequence on both steel and aluminum alloys. Their conclusion was similar, that fatigue lives estimated with the DSM will deviate significantly less from experimental data compared to predictions based on Miner's rule [Aid et al., 2011]. Siriwardane et al. applied the DSM to predict the fatigue lives of riveted railway bridges. They considered both uniaxial and multi-axial fatigue. They discovered a difference of 10 to 15 years between the lifetimes predicted with the DSM and Miner's rule. Siriwardane et al. suggested that the DSM should be used if stress histories are known [Siriwardane et al., 2008]. Adasooriya and Siriwardane continued the work of Siriwardane et al. to estimate the fatigue life of corroded bridge members. They suggested a method that consists of the stress history, a full range S-N curve that also represents corrosive environment, and the DSM to predict the fatigue life of corroded structures. Their conclusion was that the suggested method is suitable for fatigue life assessment of structures subjected to uniform corrosion [Siriwardane et al., 2008] [Adasooriya & Siriwardane, 2014].

Aid et al. presented an improvement to the DSM, originally developed for uniaxial loading, to bi-axial random loading applied to cruciform specimens. To apply the DSM in multi-axial fatigue, an equivalent stress criterion must be used. They compared the DSM, couple with the von Mises (DSM-VM) [Pitoiset & Preumont, 2000], Crossland (DSM-CR) (Crossland, 1956], and Sines (DSM-SI) [Sines, 1959] criteria. The DSM-CR and the DSM-SI both gave satisfying results. To conclude, they recommended the DSM-SI model, due to its lowest average deviation of the lifetime predictions when compared to the experimental data [Aid et al., 2012].

Shen et al. suggested that two additional relations be used. Equation (3.114) suggested in the work of Robert [Robert, 1992], and Equation (3.115) called Gerber's parabola so that a single S-N curve is enough [Shen et al., 2020].

$$\frac{\tau_{-1}(N)}{\sigma_{-1}(N)} = 0.56 \quad (3.114)$$

$$\frac{\sigma_a}{\sigma_{-1}} \left(\frac{\sigma_m}{\sigma_u}\right)^2 = 1 \quad (3.115)$$

3.3.8.4 Models Based on Material Degradation

Experimental studies have reported that static mechanical properties (Young's modulus E, the yield stress $\sigma_{0.2}$, the ultimate tensile strength σ_{UTS}, etc.) of non-damaged material differ from that of post-fatigue static properties. This material degradation as a function of the cycle ratio n / N has been implemented to develop models for fatigue damage accumulation [Ye & Wang, 2001] [Cadenas et al., 2009].

Ye and Wang presented a new damage accumulation model based on the exhaustion of static toughness and the dissipation of cyclic plastic strain energy during fatigue [Ye & Wang, 2001]. Building on the experimental data from their work [Ye & Wang, 2001], they concluded

that, as the material continues to be exposed to more fatigue cycles, the materials ability to absorb energy (meaning the static toughness) will decrease. That means, the internal energy of the material increases, which in turn, causes material damage like the formation of internal defects (cracks and voids), phase changes, translation of dislocations, and development of residual stress. Ye and Wang expressed the damage as irreversible dissipation of cyclic plastic strain energy that causes fatigue fracture when it reaches a critical value. The scalar damage value D is shown in Equation (3.116).

$$D_i = -\frac{D_{N_f-1}}{ln\, N_i}\ln(1-\frac{n_i}{N_i}) \quad with \quad D_{N_i-1} = 1-\frac{\sigma_a^2}{2EU_{T0}} \tag{3.116}$$

Where the E is Young's modulus, the U_{T0} is the static toughness of the material in its original undamaged state. The σ_a is the stress amplitude, and the n_i and N_i are same as usual. The D_{N_f-1} is the damage variables critical value [Ye & Wang, 2001].

Lv et al. presented a modified version of the damage model by Ye and Wang. Based on the works of Corten and Dolan [Corten & Dolan, 1956], and Morrow [Morrow, 1986], they presented a load interaction factor in Equation (3.116) to consider the load sequence effects. Then, Equation (3.117) is expressed as

$$D = -\frac{D_{N_f-1}}{ln\, N_i}\ln(1-\frac{n_i}{N_i})(\frac{\sigma_i}{\sigma_{max}}) \tag{3.117}$$

when assuming that $D_{N_f-i}/D_{N_f-(i-1)} \approx 1$, for high cycle fatigue, the number of cycles to failure for multi-level block loading can be determined by using the Equation (3.118) [Lv et al., 2014]. When the interaction factor in the exponent is left out of Equation (3.118), then it is reverted to being the original model by Ye and Wang [Ye & Wang, 2001].

$$D = \frac{n_i}{N_i} + \left[\left[\left(\frac{n_1}{N_1}\right)^{\frac{\ln(N_2)}{\ln(N_1)}\frac{\sigma_1}{\sigma_2}} + \frac{n_2}{N_2}\right]^{\frac{\ln(N_3)}{\ln(N_2)}\frac{\sigma_2}{\sigma_3}} + \cdots + \frac{n_{i-1}}{N_{i+1}}\right]^{\frac{\ln(N_i)}{\ln(N_{i-1})}\frac{\sigma_{i-1}}{\sigma_i}} = 1 \tag{3.118}$$

Lv et al. used the experimental data from two-level block loading experiments on smooth and notched specimens of 16Mn and C45 grade steel to verify their modified model for damage accumulation. By adding an interaction factor, the original model's predictions were improved, meaning the load interaction effects cannot be ignored [Lv et al., 2014].

Another method of approach for material degradation was suggested by Böhm et al. [Böhm et al., 2014]. They introduced a model of fatigue damage accumulation that was based on the theoretical assumptions taken from psychology called the Ebbinghaus forgetting curve. It is an exponential function that explains the decline of memory retention at times when a person does not make the effort to retain them. To explain the material degradation caused by fatigue, the function of time, had to be converted into a function of the number of cycles. They expressed material memory as

$$m = (a-c)^e - \frac{N_f}{d} + c \tag{3.119}$$

where the m is the material memory performance. The a is the rate of memorization, the d is the reciprocal value of the forgetting rate given in number of cycles, and the c is the functions horizontal asymptote. By introducing a new material memory concept expressed in Equation (3.119), Böhm et al. derived the function for damage accumulation expressed in Equation (3.120). The $N_f = \sum_i n_i$ is the total number of cycles to failure. The N_i and the n_i are the same as usual [Böhm et al., 2014] [Böhm et al., 2015].

$$D = \sum_{i=1}^{j} \frac{N_f - e^{\frac{n_i}{d}}}{d\,(1 - e^{-\frac{N_f}{d}})N_i} \tag{3.120}$$

Peng et al. combined the concept of the material memory with the concept of the S-N curve model. The residual S-N curve explains the remaining life of a component or material, after it has been stressed with a number of cycles. That gives the residual S-N curve the same slope as the S-N curve of the original, undamaged material, but with a different S-intercept. Peng et al. hypothesized that the slope of the residual S-N curve is the same as the S-N curve of the original, undamaged material b, but as the fatigue damage continues to increase, the slope of Δb will also increase. The slope ratio $b/\Delta b$ is considered to represent the accumulation of fatigue damage. Based on the approach of material memory degradation, a coefficient for the decay, α, is defined, which is related to the slope ratio $b/\Delta b$. The memory degradation approach is therefore used to model the changes in the residual S-N curve. This is expressed in Equation (3.121) for the i_{th} loading block [Peng et al., 2018].

$$b/\Delta b = \alpha_i = \frac{e^{-\frac{n_i}{N_i}} - e^{-1}}{1 - e^{-1}} \tag{3.121}$$

By using the relation in Equation (3.121), Peng et al. derived a new cumulative fatigue damage rule expressed as Equation (3.122):

$$D = \sum_1^i \frac{n_i}{N_i}\ x\ \prod_{j=1}^{i-1} \left(\frac{N_i}{N_{i+1}}\right)^{(\prod \frac{e^{-\frac{n_i}{N_i}} - e^{-1}}{1 - e^{-1}}) - 1} \tag{3.122}$$

The results they obtained from this damage model were then compared to the results obtained from the model of Kwofie and Rahbar [Kwofie & Rahbar, 2103] and Miner's rule [Corten & dolan, 1956] for two-level multi block loading. They concluded that the suggested model had better performance compared to its counterparts due to the scalar damage variable being more sensitive to the changes in load level [Peng et al., 2018].

Zhou et al. did also propose a cumulative fatigue damage model that was based on the concept of the material memory [Zhou et al., 2020]. Their damage model is expressed in Equation (3.123).

$$D_i = \left(\frac{1 - e^{-\frac{n_i}{N_i}}}{1 - e^{-1}}\right)^{\zeta(\sqrt{\sigma_{max,i}\sigma_{a,i}})^{\delta}} \tag{3.123}$$

The ζ and the δ are fitting parameters. Zhou et al. suggested a value of δ = -5.78 on 18 two-level block loading experiments on steel grade 30NiCrMoV12 [Dattoma et al., 2006]. They completely left out the ζ when determining the remaining life, and there was no reason given for this. Furthermore, they also assumed that their proposed value of δ = -5.78 can be used for all metals shown in their study [Zhou et al., 2020].

3.3.8.5 Energy-Based Rules

Damage rules that are based on strain energy for high-cycle fatigue have their origin from observations that the plastic energy dissipation ΔW^p during cyclic loading, can be used as a criterion for low-cycle fatigue failure [Lefebvre et al., 1981] [Kujawski & Ellyin, 1984]. However, this approach is only limited to low-cycle fatigue, and the reason is, as the magnitude of the strain range $\Delta\varepsilon$ decreases, the plastic component $\Delta\varepsilon^p \rightarrow 0$, and that means the plastic strain energy density $\Delta W^p \rightarrow 0$. Ellyin along with other co-workers have suggested a new criterion that they called the total strain energy density ΔW^t, which is a combination of the damaging plastic strain energy density ΔW^p, and the elastic strain energy associated with the tensile mode ΔW^{e+}, that causes crack growth [Ellyin & Kujawski, 1985] [Golos & Ellyin, 1987] [Ellyin, 1987] [Golos & Ellyin, 1988]. That is why they made a unified model for both low and high-cycle fatigue. In this approach, the fatigue life is a function of the total energy input and is explained by a power law relation that is shown in a linear curve in a double logarithmic plot that looks like the S-N curve. This is illustrated in Figure 23. The power law relation is expressed in Equation (3.124) [Golos & Ellyin, 1988].

$$\Delta W^t = \Delta W^e + \Delta W^p = \kappa N^\alpha + C \tag{3.124}$$

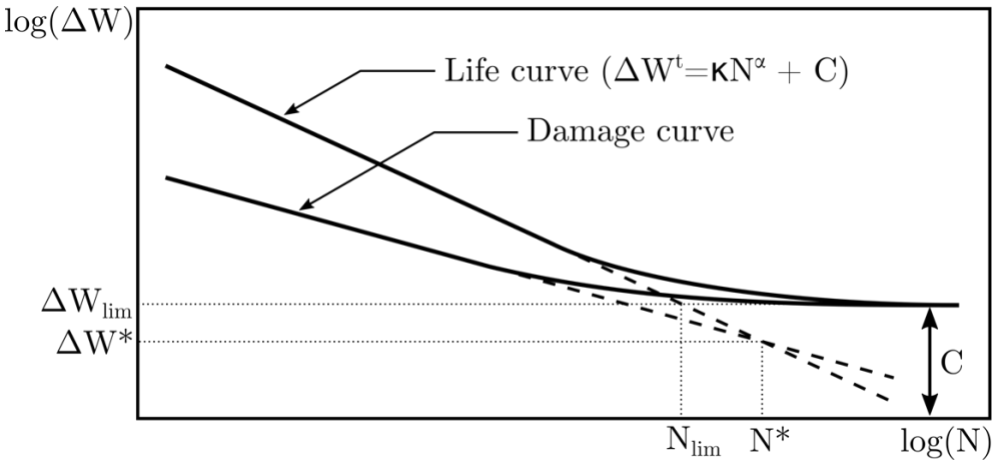

Figure 23: Critical damage and life curves intersection at the reduce fatigue limit [Golos & Ellyin, 1988].

There are three material parameters, the κ, the α, and the C. The constant C is the part of the tensile mode elastic energy input and is related to the fatigue limit strain energy density ΔW_{lim} of the material. They also introduced a critical damage curve (see Figure 23) in terms of the total strain energy density that present the transition between the crack initiation and the following crack propagation stage [Golos & Ellyin, 1988]. Furthermore, they developed a criterion for fatigue that can be used to calculate the fatigue life in the case of a multi-block loading. The remaining life in the i_{th} load block can be calculated as

$$\left\{\left[\left(\frac{n_1}{N_1}\right)^{\frac{\log\left(\frac{N_2}{N^*}\right)}{\log\left(\frac{N_1}{N^*}\right)}}+\frac{n_2}{N_2}\right]^{\frac{\log\left(\frac{N_3}{N^*}\right)}{\log\left(\frac{N_2}{N^*}\right)}}+\cdots+\frac{n_{i-1}}{N_{i-1}}\right\}^{\frac{\log\left(\frac{N_i}{N^*}\right)}{\log\left(\frac{N_{i-1}}{N^*}\right)}}+\frac{n_i}{N_i}=1 \qquad (3.125)$$

where the $\Delta W^* < \Delta W_{lim}$ and its value can be determined from the intersection of the extrapolated life curve $\Delta W - N_f$ with the critical damage curve (see Figure 23). The value of the N^* corresponds to the value of the ΔW^* on the N axis of the life curve $\Delta W - N_f$ and is called the reduced fatigue limit [Golos & Ellyin, 1987].

Park et al. presented a modified model of the strain energy density model from Equation (3.124) to describe the fatigue behavior of an anisotropic rolled AZ31 magnesium alloy, and so they applied a parameter that considers the plastic strain energy consumed by the mean strain. This is expressed in Equation (3.126). The $f(\varepsilon_m)$ is the plastic strain energy that is associated with the mean strain and the γ is a material constant. They compared their model with experimental data and concluded that it was in good agreement [Park et al., 2008].

$$\Delta W^t = \Delta W^{e+} + \Delta W^p + \left\{\frac{f(\varepsilon_m)}{N_f}\right\}^{\gamma} = \kappa N^{\alpha} + C \qquad (3.126)$$

Ellyin and Golos extended the total train energy density to also include multi-axial conditions under, almost, proportional fatigue loading [Ellyin & Golos, 1988]. Macha and Sonsino published a review of energy based multi-axial fatigue failure criteria, where they concluded that criteria that include the strain energy density in the fracture plane, or the critical plane are the most promising [Macha & Sonsino, 1999].

Lagoda et al. verified that the normal strain energy density in the critical plane is an efficient parameter for high-cycle fatigue life prediction under cyclic or random non-proportional loading. They also suggested a new parameter for the strain energy density that enables us to distinguish between the positive strain energy density that happens in a tension path, and the negative strain energy density that happens in a compression path. Compared to previous methods that only accounted for the amplitude of the stresses, the strains, and the dissipated energy, the suggested strain energy density parameter also accounts for the history of the accounted parameter [Lagoda et al., 1999]. The parameter was used in a fatigue life calculation algorithm that was validated with experimental data from studies on cast irons and steels [Lagoda, 2001] [Lagoda, 2001].

Jahed and Varvani-Farahani presented an energy-based fatigue life prediction model for metallic components [Jahed & Varvani-Farahani, 2006]. The model can make estimations for the upper and lower bounds of the experimental fatigue life, and it was originally proportional multi-axial loading conditions, as well as tension and torsion. The number of cycles to failure N_F is expressed in Equation (3.127).

$$N_F = \frac{\Delta E_A}{\Delta E} N_A + \frac{\Delta E_T}{\Delta E} N_T \qquad (3.127)$$

The ΔE_A is the energy from pure tensile loading, and the ΔE_T is the energy from pure torsion loading. The ΔE is the total elastic-plastic energy. Later they extended this method to include non-proportional loading as well [Jahed & Varvani-Farahani, 2007]. Gu et al. used the methods by Jahed and Varvani-Farahani to predict the fatigue life of a mining truck welded frame, and their results were in good agreement with experimental data [Gu et al., 2016].

Scott-Emuakpor et al. performed fully reversed rotating bending tests, and axial tension-compression tests for 6061-T6 aluminum [Scott-Emuakpor et al., 2004] [Scott-Emuakpor et al., 2005] [Scott-Emuakpor et al., 2007] [Scott-Emuakpor, 2007] [Scott-Emuakpor et al., 2008]. Their results showed that the experimental fatigue lives for the rotating bending tests, were 20% higher than for the tension-compression tests. This was due to the gradient effect of the normal stress [Papadopoulos & Panoskaltsis, 1996]. They suggested and modified a uniaxial, energy-based criteria for high-cycle tension-compression fatigue that considers the gradient effect and the effects of the mean stress. They assumed that the strain energy needed to fracture a material in monotonic loading, is the same as the strain energy needed to cause fatigue failure, meaning that during cyclic loading, hysteresis energy slowly builds up with each cycle until the built-up amount is equal to the fracture energy obtained from a static test [Stowell, 1966]. The energy needed to cause fracture is expressed in Equation (3.128].

$$W_f = \sigma_f \left(\varepsilon_f - \frac{\sigma_f}{2E}\right) - \sigma_0 \varepsilon_0 (cosh \frac{\sigma_f}{\sigma_0} - 1) \tag{3.128}$$

The σ_f is the true stress at fracture, and the ε_f is the true strain at fracture. The ε_0 is a curve fit parameter, and the σ_0 is expressed in Equation (3.129) as

$$\sigma_0 = \frac{\sigma_f - \sigma_y}{\ln\left(\frac{\varepsilon_f}{0.002}\right)} \tag{3.129}$$

Where the σ_f is the true fracture stress, and the ε_f is the true strain at fracture. The σ_y is the yield stress. The model predictions have been compared to experimental data from Ti 6Al-4V and Al 6061-T6 specimens and were in good agreement. Scott-Emuakpor et al. further modified the model to also consider multi-axial and transverse shear loading [Scott-Emuakpor et al., 2010].

Their model is based on the idea that the strain energy density is the same for each cycle, however this is thought to overly simplify the matter [Feltner & Morrow, 1961]. Experimental data for axial and torsional loading, has shown that, the strain energy density decreases slightly from the constant level at around 90% of the predicted fatigue life, and then there is a rapid energy increase until failure occurs [Ozaltun et al., 2011] [Wertz et al., 2012]. Letcher et al. proposed a new material property called the "critical lifetime" which happens when the steady-state value of the cyclic strain energy density deviates by 5% [Letcher et al., 2012]. To determine the lifetime predictions in an intelligent manner, Scott-Emuakpor et al. included the concept of the critical lifetime into the strain energy density model [Scott-Emuakpor et al., 2010].

Djebli et al. presented an energy-based model of the DSM by Mesmacque et al. [Mesmacque et al., 2005]. They proposed a new damage parameter D_i that is expressed in Equation (3.130).

$$D_i = \frac{W_{ed,i} - W_i}{W_u - W_i} \tag{3.130}$$

The $W_{ed,i}$ is the energy from the damage stress. The W_i is the energy from the applied stress, and the W_u is the energy corresponding to the ultimate stress of the material. The fatigue lifetime prediction is like the original DSM. The curve is rescaled into a W-N curve, instead of using an S-N curve. For high-cycle fatigue, the Basquin function $W = \kappa N^{\alpha}$ can be used to model the curve. When the characteristic $\sigma_a - N$ is used, the stress amplitude axis σ_a, should be replaced with W_a, where the $W_a = \sigma_a/(2E)$ [Lagoda et al., 1999] [Djebli et al., 2013].

Peng et al. presented a new model called the fatigue driving energy (FDE) model. The FDE consists of a combination of the FDS model by Kwofie and Rahbar [Kwofie & rahbar, 2013], and of the strain energy density (SED) model. Their goal was to overcome several of the weaknesses in the original FDS model. Consider a two-level low-to-high block loading sequence, where the consumed life fraction by the first block is a very small fraction. Calculating the equivalent fatigue driving stress for the second load block, with a higher stress, would be impossible. More so, an equivalent fatigue driving stress does not always correspond to equivalent damage. Peng et al. presented a new fatigue damage accumulation model that is expressed in Equation (3.131)

$$D = \frac{W_D - W_{D_0}}{W_{D_c} - W_{D_0}} = \frac{N^{-2b\frac{n}{N}} - 1}{N^{-2b} - 1} \tag{1.131}$$

with

$$W_D = \frac{1}{2E}\sigma^2 N^{-2b\frac{n}{N}} \quad \rightarrow \quad \begin{cases} W_{D_0} = \frac{\sigma^2}{2E}, \ \frac{n}{N} = 0 \\ W_{D_c} = \frac{A^2}{2E}, \ \frac{n}{N} = 1 \end{cases} \tag{1.132}$$

where the W is the SED, and the W_D is the FDE. The W_{D_0} is the SED for the undamaged original state of the material, and the W_{D_c} is the critical SED (where D = 1). The A is a material constant, and b is the exponent of the Basquin equation. The damage accumulation approach in Equation (3.131) was extended to consider load interaction effects by the addition of a load interaction factor. As a result, the remaining lifetime for multi-level block loading is expressed in Equation (1.133)

$$\frac{n_i}{N_i} = 1 - \frac{1}{-2b\ln(N_i)} \ln\left(\left(N_i^{-2b} - 1\right)\left(\frac{N_{i-1}^{-2b\left[\frac{n_{i-1}}{N_{i-1}} + 1 - \frac{n_{i-1}}{N_{i-1}}\right]} - 1}{N_{i-1}^{2b} - 1} \right)^{\frac{\sigma_{i-2}}{\sigma_{i-1}} x \frac{\sigma_{i-1}}{\sigma_{i-1}}} + 1 \right) \tag{3.133}$$

Peng et al. used data from five experimental datasets for different geometric shapes, to compare the lifetime predictions of the presented model (both with and without considering the load interaction effects), with the prediction of Miner's rule. The proposed model based on the FDE model, resulted in more accurate lifetime predictions, compared to the predictions of Miner's rule [Peng et al., 2016].

4. Experimental Verification of Fatigue Models

4.1 Introduction

The experimental work was performed in the machine lab at Kjølv Egelands hus, at the University of Stavanger, Faculty of Science and Technology, in Norway. The goal of this experimental work is to perform fatigue tests on S355J2+N grade steel under two-level block loading. The results from these tests will then be compared to calculations of the theoretical remaining fatigue life based on a linear model (Miner's rule) and a nonlinear model (Rege and Pavlou model).

4.2 Properties and Composition of S355J2+N

Before the testing program could be made, we had to determine the mechanical and chemical properties of the S355J2+N grade steel. From there an S-N curve is used to decide the stress levels in the fatigue testing program.

The steel was provided by Ovako, however there was two material sheets provided by the company for this steel. Therefore, it was unclear which one belonged to the specimens of this work and we had to perform a tensile test to determine the material properties. The full results of tensile test are given in Appendix C. Table 1 is a list of the material properties from the tensile test. Table 2 is the material chemical composition.

Table 1: Mechanical properties

Young's modulus (E) GPa	Yield Strength (f_y) MPa	Tensile strength (f_u) MPa
202	470	600

Table 2: Chemical composition of S355J2+N

C %	Si %	Mn %	P %	S %	Cr %	Ni %	Mo %	Ti %	Al %	N %	CEV %
0,15	0,21	1,19	0,011	0,009	0,07	0,12	0,03	0,001	0,021	0,0101	0,40

4.3 Experimental Fatigue Test

4.3.1 Specimen

Figure 24: S355J2+N specimen.

The dimensions of the specimen are 270 mm in total length, 20 mm diameter for the outer parts (handles), it is not very visible in the Figure 24, however the specimen is not symmetric. The left side (until the polished midpart) is 105 mm, while the right side (until the polished midpart) is 95 mm. The middle part is 70 mm in length and 10.02 mm in diameter.

4.3.2 Instron 5985 Dual Column Floor Frames Tensile Testing Machine

Due to the amount of people doing experimental work, the fatigue testing machine of the university was fully booked. Therefore, the fatigue test had to be performed on an Instron 5985 tensile testing machine.

Figure 25: Instron Tensile Testing Machine.

4.3.3 Preparation for Fatigue Testing

Before fitting the specimen to the machine, the grips need to be changed to be of a geometry and size that are made for the size (of the handles) of the specimen. In this case, we used grips that were made for bar shaped specimens and of size between 16 mm to 22 mm. The machine is the lifted, and the bar fitted into the bottom part.

Figure 26: Installing the specimen to bottom grips.

Then the upper part of the machine is lowered, and the grips are tightened on the specimen. From the handles, around 1 cm is left outside of the grips on both upper and lower side. This is to ensure that when the grips are tightened, the specimen will not slip loose, invalidating the test result, risking injury of bystanders in case of steel parts getting thrown, and possibly causing damages to the machine. It is very important to ensure that the grips are tightened before commencing testing.

Figure 27: Lowering the upper part of the machine to specimen.

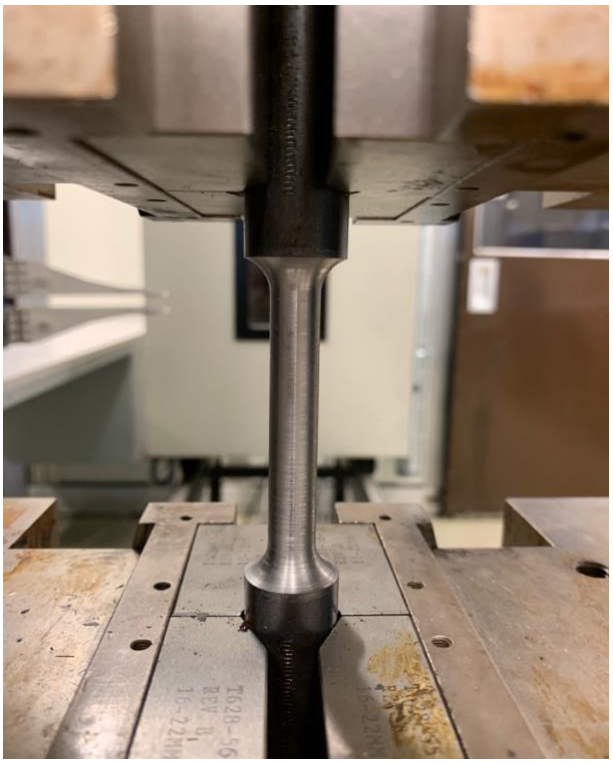

Figure 28: 1 cm protruding on both ends and tightened grips.

4.3.4 Testing Program

After the tensile test, we had determined the material properties of the specimen and could therefore use an S-N curve to decide the testing program. The S-N curve in Figure 29 was used to make the program. The program was made by Professor Dimitrios Pavlou. Due to lack of time, and scheduling of the machine with other people, it was necessary to be safe that our fatigue tests do not occur in the fatigue limit range.

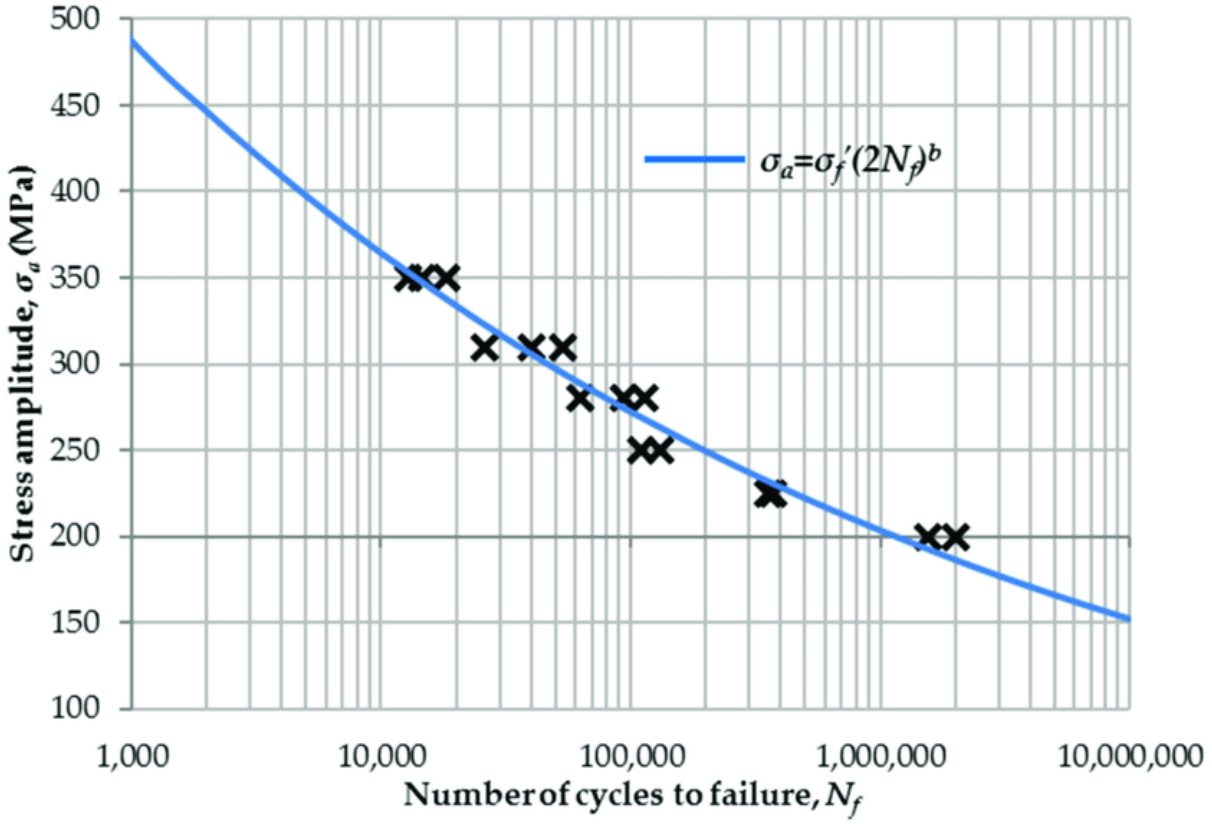

Figure 29: Semi-log S-N curve for S355J2+N grade steel [Milovanovic et al., 2022].

After finding an S-N curve for our material, the professor made the testing program for a two-level block loading test.

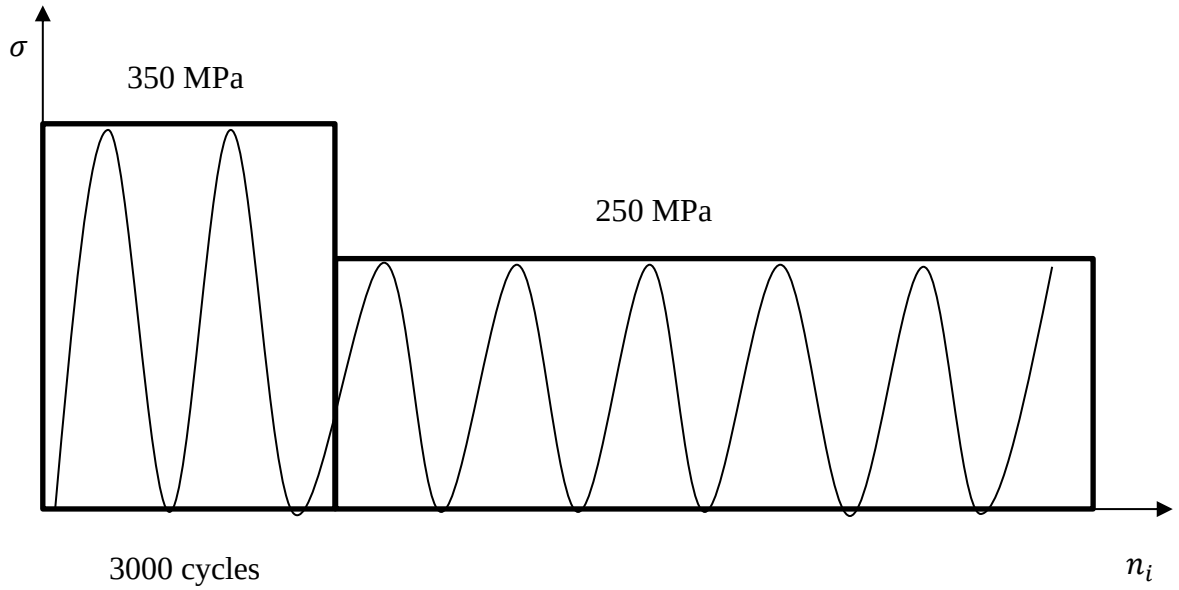

Figure 30: Two-level block loading test (1).

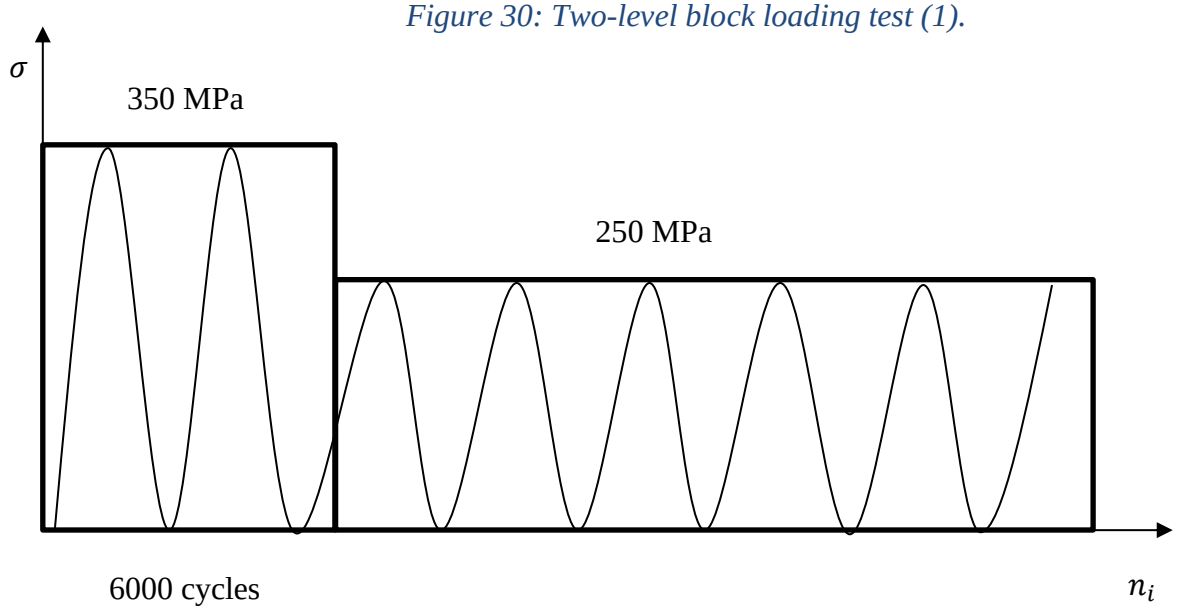

Figure 31: Two-level block loading test (2).

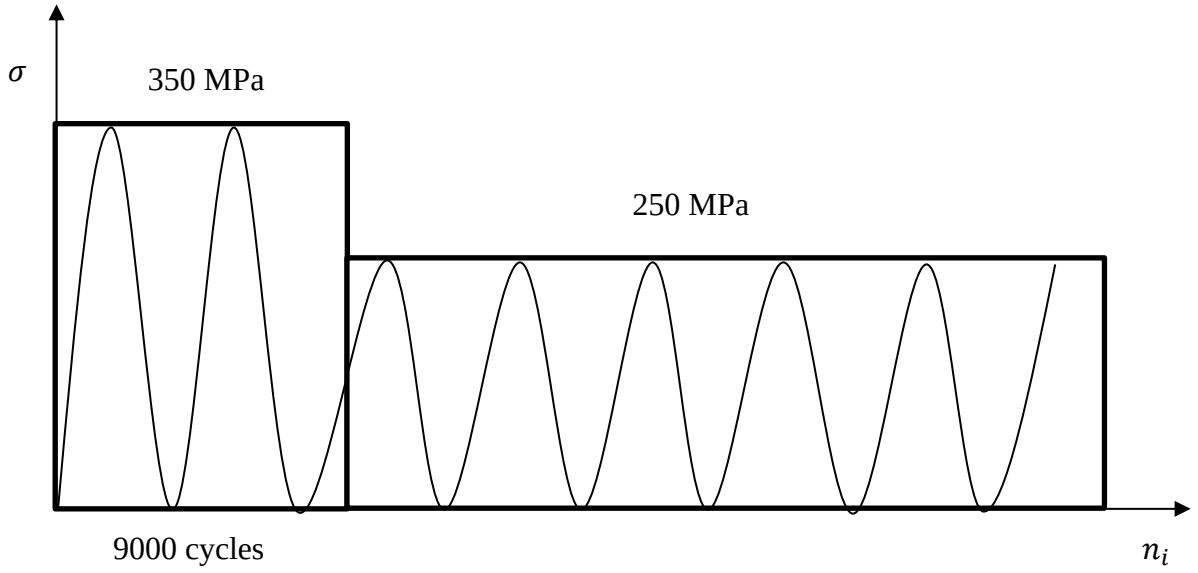

Figure 32: Two-level block loading test (3).

The test program was divided into two parts, high-to-low fatigue tests, and low-to-high fatigue tests. Beginning with high-to-low tests, it was planned that we would test with a minimum stress of 0 MPa to a maximum stress of 350 MPa, for a number of 3000 cycles, during the first block. For the second block we would test with minimum stress of 0 MPa to a maximum stress of 250 MPa, to go until failure. For the second test everything is the same except first block will be 6000 cycles, and likewise for the third test, everything is the same, except first block will go to 9000 cycles.

For the low-to-high tests, we reverse the loading sequence and begin the first block with a minimum stress of 0 MPa to a maximum stress of 250 MPa, for a number of 3000 cycles. For second block minimum stress of 0 MPa to a maximum stress of 350 MPa, to go until failure. The 5th test is the same, except first block will go until 6000 cycles, and 6th test is also the same, except first block will go until 9000 cycles.

To have data that is usable and that we can make curves from, it was planned two specimens per part of the program. Meaning for the high-to-low part of the program, it would be six specimens, and for the low-to-high part, it would also be six specimens. A total of 12 specimens.

4.3.5 Fatigue Life Testing

The tensile testing machine is not a fatigue testing machine; therefore, it was not able to go down to 0 MPa, and we had to start the test with an offset stress to not risk damaging the machine. The lab supervisor of this work, Johan Andreas Håland Thorkaas, suggested that we start with an offset of 50 MPa and that we would be safe. The first deviation from the program then, was that we could not test with minimum stress of 0 MPa and had to test with minimum stress of 50 MPa.

That meant we also had to change the rest of the program so we would not be testing with too low stress levels. Therefore, the maximum stresses were also increased by 50 MPa and the maximum stresses became 400 MPa (first block) and 300 MPa (second block) respectively for the high-to-low tests and inversed for the low-to-high tests.

Once the planning of the stress levels was done, we had to figure out which speeds the test could be run on the tensile testing machine. Due to the Instron machine not being made for fatigue tests, we had to test out a specimen and see which speeds could be input and observe the behavior of the machine and the sounds it made. This was so we didn't run the tests at too high speeds and risk damaging the machine, potentially risking other project works. We tried a few different speeds, and at the end an input speed of 70 mm/min was decided upon with the supervision of Johan. This gave a frequency of approximately 1,5 Hz.

The fatigue tests have to be done in six different parts due to not being able to run the tests continuously. This was either due to scheduling crashes with other student works or due to being worried about damages to the machine and having to stop and inspect for any faults.

4.3.5.1 Testing

The first part of the test began Thursday 13th April around 8 am in the morning. It went very smoothly. There were no issues. After 3000 cycles, the load changed to 300 MPa and the second block started. We first estimated that, based on the data from the S-N curve (see Figure 29), the test would not run long past 200 000 cycles. Therefore, an upper bound of 300 000 cycles were set since we were sure the test would not run that long. This was a mistake, as we estimated with the stress in the program, and not the equivalent stress amplitude of the S-N curve. The test continued until it reached 300 000 cycles and then stopped on Saturday 15th of April around 10:30 am. It was coordinated with Johan and his superiors that I could supervise the test alone during weekends, but I could not touch the machine or the specimen, aside from pushing the emergency stop button in case of an emergency. I could on the other hand control the machine from the

computer should that be necessary. Usually, it was not. The most important part of this project work was to put the specimen in the machine, start the machine, and then to just watch over. I was not allowed to operate on my own, and therefore project work completely halted during weekends.

Part two of the test began on the next week, as we had to plan how to continue. The specimen lasted over 300 000 cycles and did not break. So, with the supervision of Professor Pavlou, it was decided we would continue with a max stress = 350 MPa (not 300 MPa). An important note is that we are done with the first block, and every other part of the test (part 2 until part 6) will be in the second block. Part two lasted for a number of 257 819 cycles. This took approximately 48 hours. This time, the machine did start to make strange clicking sounds from the lower part (see Figure 25) where the motor and the bands are located. Once the rhythm of the machine was broken and it started being out of rhythm, Johan suggested we stop and look for any faults.

Part three of the test started soon after part two. We checked the machine but did not find any faults. It was decided that we have to stop if the machine starts going out of rhythm as that could damage the hydraulics of the machine. After 257 036 and approximately 48 hours, we decided to stop the machine again because the clicking type sounds from the motor and belts came back. To oil the hydraulics, we had to open the upper part of the grips and run the machine up and down a couple of times. This was so the oil could be applied evenly to the hydraulic arms of the machine.

The fourth part of the test were similar to the two previous. The machine ran 142 369 cycles, and when the noises came back, we stopped, checked for faults, opened upper grips to run machine up and down and oil the hydraulic arms. This part lasted around 26 hours.

The fifth part seemed fine until there was a power outage at cycle 23 261. The sixth and last part of the test was the longest one. At this point it was decided by the lab supervisor Johan that if the specimen does not break soon, we would have to stop as the toll on the machine would be too much, and we would actually break it. The sixth part ran for 327 174 cycles and lasted 58,68 hours. Table 3 (see Appendix A) is a summary of all the tests.

An important thing to note, is that the Instron machine was also not able to hit the peak and bottoms of the programmed loads, meaning when max stress = 400 MPa it would go above that (by ca. 30 MPa) and when min stress = 50 MPa, it would go almost 30 MPa below that. This then gives us completely different numbers than the ones used to determine the fatigue life of the specimens for each test.

4.3.6 Theoretical Fatigue Life Calculations

The theoretical calculations of the fatigue life were planned to be both linear and nonlinear. In Appendix B, all calculations are shown. To begin with, we use the planned program to determine the mean stress and the stress amplitude.

$$\sigma_{mean} = \frac{(\sigma_{max} + \sigma_{min})}{2} \tag{4.1}$$

$$\sigma_a = \frac{(\sigma_{max} - \sigma_{min})}{2} \tag{4.2}$$

After we have determined the mean stress and the stress amplitude, we use the modified Goodman to determine the equivalent stress amplitude.

$$\sigma_{eq} = \frac{(\sigma_a)}{1-(\frac{\sigma_{mean}}{\sigma_u})} \tag{4.3}$$

Once we have found the equivalent stress amplitude for both load block 1 and load block 2, we can use the S-N curve to find the number of cycles until failure, N_1 and N_2 for load block 1 and 2, respectively. Then we can use Miner's rule (linear rule) to predict the remaining life.

$$\frac{n_1}{N_1} + \frac{n_2}{N_2} = 1 \tag{4.4}$$

$$n_2 = 1 - \left(\frac{n_1}{N_1}\right) * N_2 \tag{4.5}$$

For this work it was decided that the nonlinear model that would be used for fatigue life prediction would be Rege-Pavlou model [Rege & Pavlou, 2017]. This is due its simple application of needing only one parameter. The σ_1 and σ_2 are the equivalent stress amplitude 1 and 2, respectively.

$$\left(\frac{n_1}{N_1}\right)^{\left(\frac{\sigma_2}{\sigma_1}\right)^{0,75}} + \frac{n_2}{N_2} = 1 \tag{4.6}$$

$$\frac{n_2}{N_2} = 1 - \left(\frac{n_1}{N_1}\right)^{\left(\frac{\sigma_2}{\sigma_1}\right)^{0,75}} \tag{4.7}$$

4.3.6.1 Experimental Fatigue Life Calculation

Due to the test not really going as planned. It is not a two-block, but a three-block loading sequence. Therefore, it is different from the theoretical calculations because the testing program was made for a two-block loading sequence. The only difference is the addition of a n_i/N_i to each model, otherwise everything is the same. Calculating with Miner's rule (linear rule) gives us

$$\frac{n_1}{N_1} + \frac{n_2}{N_2} + \frac{n_3}{N_3} = 1 \tag{4.8}$$

$$n_3 = 1 - \left(\frac{n_1}{N_1}\right) - \left(\frac{n_2}{N_2}\right) * N_3 \tag{4.9}$$

and calculating with Rege-Pavlou model gives us

$$\left(\frac{n_1}{N_1}\right)^{\left(\frac{\sigma_2}{\sigma_1}\right)^{0,75}} + \left(\frac{n_2}{N_2}\right)^{\left(\frac{\sigma_3}{\sigma_2}\right)^{0,75}} + \frac{n_3}{N_3} = 1 \tag{4.10}$$

$$\frac{n_3}{N_3} = 1 - \left(\frac{n_1}{N_1}\right)^{\left(\frac{\sigma_2}{\sigma_1}\right)^{0,75}} - \left(\frac{n_2}{N_2}\right)^{\left(\frac{\sigma_3}{\sigma_2}\right)^{0,75}} \quad (4.11)$$

5. Results

5.1 Results from The Fatigue Test

In table 3 (see Appendix A) the results from the fatigue test are summarized.

Table 3: Result from fatigue test

Test	Numbers of cycles (n_i)	Maximum stress σ_{max} (MPa)	Minimum Stress σ_{min} (MPa)	Time (hours)
Part 1-1	3000	429.23	18.52	-
Part 1-2	300 000	333.17	16.08	48.58
Part 2	257 819	386.42	14.80	47.74
Part 3	257 036	384.54	18.19	48.02
Part 4	142 369	384,9	18.84	26.23
Part 5	23 261	386.06	19.33	4.26
Part 6	327 174	388.16	20.04	58.68
Total	1 310 659	-	-	233.51

5.2 Results from The Fatigue Life Calculations

5.2.1 Linear Result (Miner's rule)

This section will summarize the calculations. See Appendix B for the full list of calculations and results.

Part 1: High-to-low

$$\frac{n_2}{N_2} = \frac{3\,368\,750}{3\,500\,000} = 0{,}9625 \tag{5.1}$$

Part 2: High-to-low

$$\frac{n_2}{N_2} = \frac{3\,237\,500}{3\,500\,000} = 0{,}925 \tag{5.2}$$

Part 3: High-to-low

$$\frac{n_2}{N_2} = \frac{3\,106\,250}{3\,500\,000} = 0{,}8875 \tag{5.3}$$

Part 4: Low-to-high

$$\frac{n_2}{N_2} = \frac{79\,931}{80\,000} = 0{,}99914 \tag{5.4}$$

Part 5: Low-to-high

$$\frac{n_2}{N_2} = \frac{79\,862}{80\,000} = 0{,}99829 \tag{5.5}$$

Part 6: Low-to-high

$$\frac{n_2}{N_2} = \frac{79\,794}{80\,000} = 0{,}99743 \tag{5.6}$$

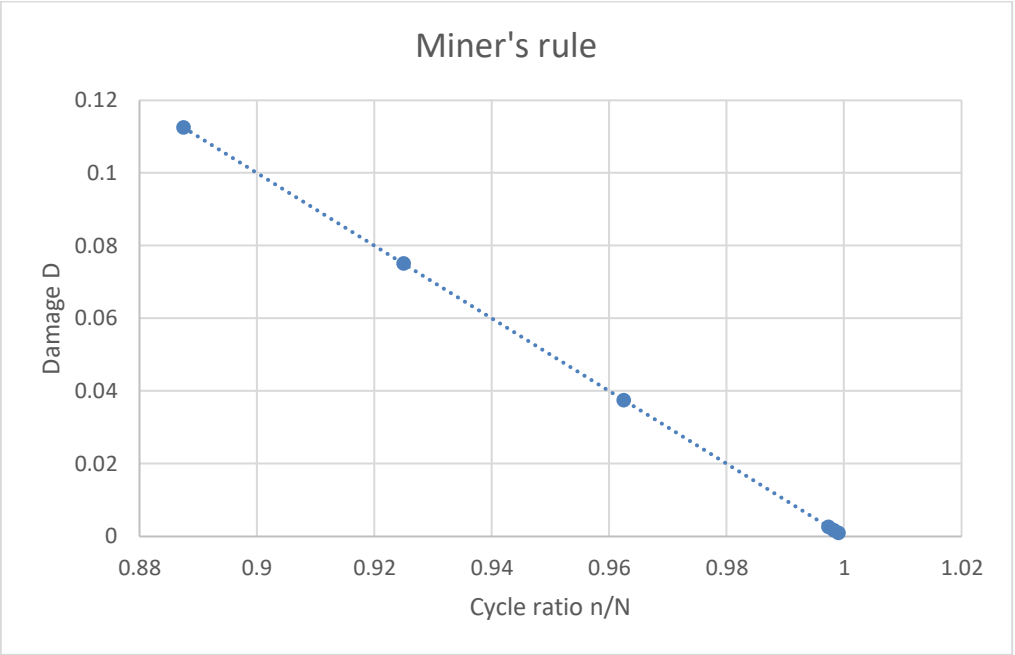

Figure 33: Miner's rule for two-level block loading sequence (linear rule).

5.2.2 Nonlinear Results (Rege and Pavlou model)

Part 1: High-to-low

$$\frac{n_2}{N_2} = 1 - \left(\frac{3000}{80\,000}\right)^{\left(\frac{176,471}{280}\right)^{0,75}} \tag{5.7}$$

$$\frac{n_2}{N_2} = 0,788$$

Part 2: High-to-low

$$\frac{n_2}{N_2} = 1 - \left(\frac{6000}{80\,000}\right)^{\left(\frac{176,471}{280}\right)^{0,75}} \tag{5.8}$$

$$\frac{n_2}{N_2} = 0,706$$

Part 3: High-to-low

$$\frac{n_2}{N_2} = 1 - \left(\frac{9000}{80\,000}\right)^{\left(\frac{176,471}{280}\right)^{0,75}} \tag{5.9}$$

$$\frac{n_2}{N_2} = 0,644$$

Part 4: Low-to-high

$$\frac{n_2}{N_2} = 1 - \left(\frac{3000}{3\,500\,000}\right)^{\left(\frac{280}{176{,}471}\right)^{0{,}75}} \qquad (5.10)$$

$$\frac{n_2}{N_2} = 1$$

Part 5: Low-to-high

$$\frac{n_2}{N_2} = 1 - \left(\frac{6000}{3\,500\,000}\right)^{\left(\frac{280}{176{,}471}\right)^{0{,}75}} \qquad (5.11)$$

$$\frac{n_2}{N_2} = 0{,}999$$

Part 6: Low-to-high

$$\frac{n_2}{N_2} = 1 - \left(\frac{9000}{3\,500\,000}\right)^{\left(\frac{280}{176{,}471}\right)^{0{,}75}} \qquad (5.12)$$

$$\frac{n_2}{N_2} = 0{,}999$$

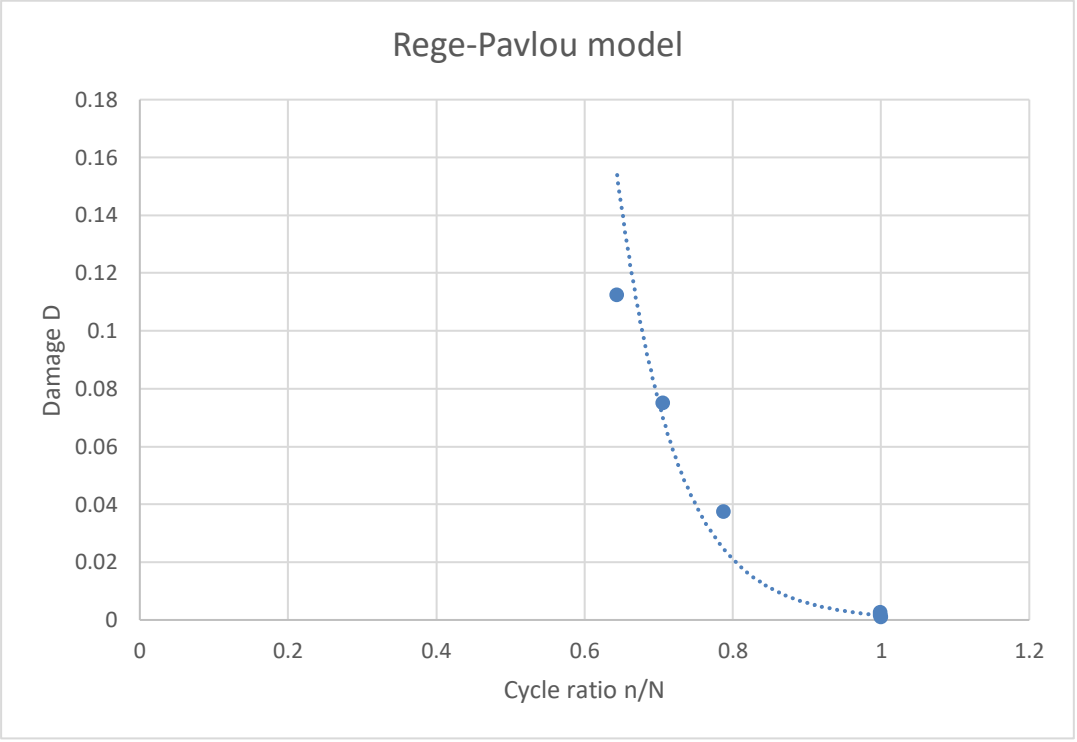

Figure 34: Rege-Pavlou model two-level block loading sequence (nonlinear rule).

5.2.3 Results from Experimental Fatigue Test

Since the actual test deviated from the program and had to be done as a three-level block loading sequence, we calculate the experimental fatigue life in three blocks.

Miner's rule

$$n_3 = 1 - \left(\frac{3000}{80\,000}\right) - \left(\frac{300\,000}{3\,500\,000}\right) * 450\,000 = 471696 \tag{5.13}$$

$$\frac{n_3}{N_3} = 0{,}954$$

Figure 39 illustrates the fatigue damage with Miner's rule

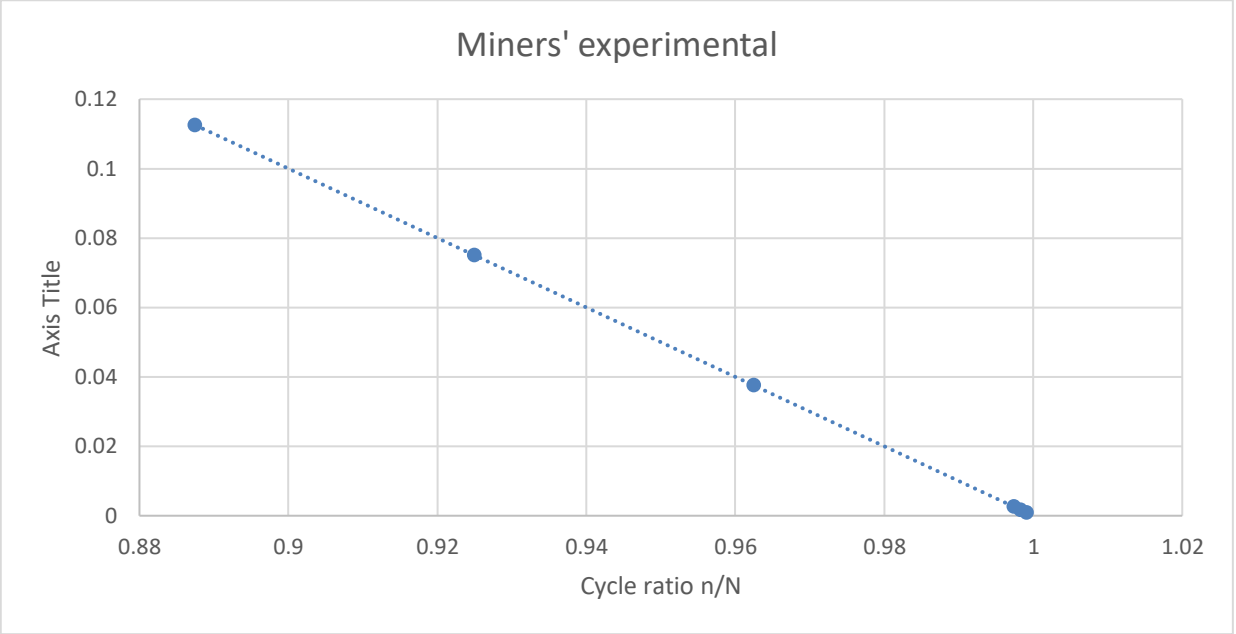

Figure 35: Experimental fatigue damage results (Miner's rule).

Rege and Pavlou Model

$$\frac{n_3}{N_3} = 1 - \left(\frac{3000}{80\,000}\right)^{\left(\frac{176{,}471}{280}\right)^{0{,}75}} - \left(\frac{300\,000}{3\,500\,000}\right)^{\left(\frac{225}{176{,}741}\right)^{0{,}75}} \tag{5.14}$$

$$\frac{n_3}{N_3} = 0{,}117$$

Figure 40 illustrates the fatigue damage with Rege and Pavlou model

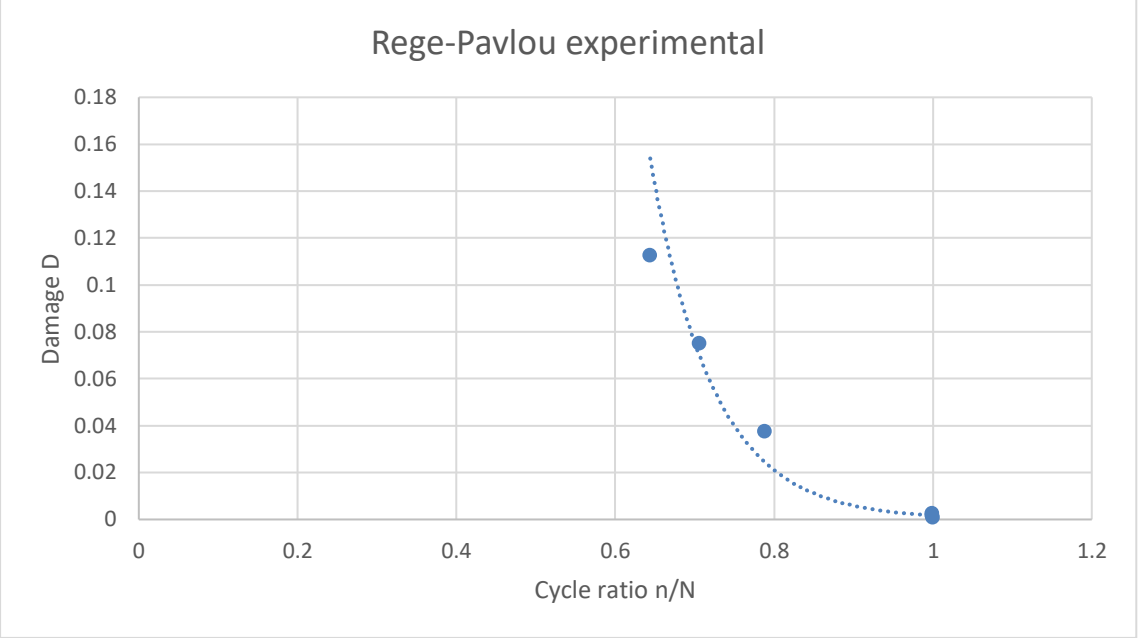

Figure 36: Experimental fatigue damage results (Rege and Pavlou model).

6. Discussion

6.1 Discussion about The Results

As can be seen from the Equations (5.1) to (5.14) the fatigue life of the high-to-low block loading sequences are higher than those of the low-to-high block loading sequences. Also, from Figure 33 to Figure 36 the fatigue damages (cycle ratios) of the tests respective of load sequence, are illustrated. Comparing Miner's rule to that of the model by Rege and Pavlou we see that the cycle ratios are not very different for the low-to-high block loading sequences. However, we see that for the high-to-low block loading sequences, the nonlinear model offers more conservative values and is therefore the safer (better) model.

For the experimental fatigue results, the nonlinear model of Rege and Pavlou has offered a much more conservative value than the Miner's rule. This makes sense when comparing it to the number of cycles the specimen has been through, as only around half the fatigue life has been consumed.

6.2 Discussion about The Experimental Work

The experimental program for this thesis was made so that we would be able to make a curve of the results of the actual experiments and compare them with the theoretical results. This would be done both linearly and nonlinearly. Unfortunately, due to not being able to test with a fatigue testing machine, the experimental work didn't make much progress. An actual fatigue testing machine can test with speed of 6 Hz and upwards. The fatigue testing machine in the machine lab at UiS can do fatigue tests at 10 Hz. On the other hand, the Instron machine is in no way made for fatigue testing. Instead of testing at 10 Hz, the tests of this project were done at around 1,5 Hz which is almost 10 times slower. After almost 10 days of testing, the specimen did not break. Assuming that it did break on the 10^{th} day, I would still need 120 days to be able to test all 12 specimens. Which is simply impossible, considering the time available to work on a thesis is one semester, and there are other projects that need to work on the machine as well.

6.3 Discussion about Structural Health Monitoring

This section will be discussing Real-time Structural Health Monitoring and the future aspects of it.

Real-time Structural Health Monitoring is being used to increase the safety, the lifetime, the performance as well as, to reduce the cost of maintenance (over time) to the structures in our society. These methods can be used on all types of structures both civil and mechanical. As we face a growing world population, and climate change is becoming an increasingly bigger issue. Maintaining our structures health and safety and lowering costs and resource consumption is vital for our future. Therefore, the field of Structural health monitoring will be just as much if not even more important in the times ahead. The real-time aspect of Structural Health Monitoring will enable us to detect fracture or any other damages real-time. This will enable us to act quicker, have better control over all of our structures and save costs in the long run. From the literature review of this thesis a framework made with the supervision of Professor Dimitrios Pavlou, will be presented in Table 4.

Table 4: Framework for Real-time Structural Health Monitoring

Real-time strain measurements ⬇
Transformation to stresses history ⬇
Transformation to cyclic loads with the aim of Rainflow Counting method ⬇
Calculation of equivalent stress amplitude for each loading cycle ⬇
Calculation of the damage due to each loading cycle ⬇
Damage summation of all the loading cycle.

7. Conclusion

7.1 Conclusion

During the work of this master's thesis, a brief overview of Structural Health Monitoring Methods has been given, and with Professor Dimitrios Pavlou's supervision, a framework has been suggested for Real-time Structural Health Monitoring (see Table 4). An overview of fatigue damage model has been given. This overview contains both linear models and nonlinear models. It is not an exhaustive overview, but it does provide an overview of the most recent linear and nonlinear models. There are very many fatigue damage model, and new models are being continuously made. With each models seemingly outperforming its predecessor.

A fatigue test has been performed and analyzed for S355J2+N grade steel for different stress ratios. The results of the fatigue test are given in Appendix A and the calculations are explained in Appendix B as well as chapter 4 and presented in chapter 5. The theoretical calculation of the remaining fatigue life is done both linearly (with Miner's rule) and nonlinearly (with Rege-Pavlou model). Based on the theoretical results, while the differences between the fatigue life is minimal for both models in low-to-high fatigue testing. For high-to-low fatigue testing, the nonlinear model gives more conservative values, than the linear one. This is also shown in the result from the experimental data, that the nonlinear experimental calculation is more conservative than the linear calculation. The graphs for the cycle ratios of the linear and nonlinear results have been obtained although they do not look entirely correct. The x-axis is not correct and will not act as stress ratio. Instead, it is just points that the damage ratios are tied to, which has to be wrong.

As far as the goals of this thesis project described in chapter 1.2 is concerned, to conclude, a brief overview of SHM methods has been given, and an overview of fatigue damage accumulation models has been given. Calculations have been done with both linear and nonlinear models, but the fatigue tests were not completed at all. Not only was the fatigue work unable to get anywhere due to the Instron machine not being able to test at speeds higher than 1.5 Hz, not even the one single tested specimen broke. The program was to be testing 12 specimens. It is very important to conclude that no further fatigue testing should ever be done on the Instron tensile testing machine. It is not a machine made for fatigue testing, but a machine for tensile tests.

7.2 Future Work

To continue the work of this thesis, the following objectives are suggested:

- Early planning to ensure that the tests can be done on the actual fatigue testing machine, that way more tests can be completed in a shorter amount of time.
- Use of strain gauges to ensure real-time data collection about any changes in the specimen during testing.
- It would maybe be relevant to perform uniaxial tests and include torsional loading, a more complex load sequence would mimic real life conditions better.

References

Adasooriya, N. D.; Siriwardane, S. C. Remaining fatigue life estimation of corroded bridge members. *Fatigue Fract. Eng. Mater. Struct.* **2014**, *37*, 603-622. [CrossRef]

Aeran, A.; Siriwardane, S. C.; Mikkelsen, O., Langen, I. An accurate fatigue damage model for welded joints subjected to variable amplitude loading. *IOP Conf. Ser. Mater. Sci. Eng.* **2017**, *276*. [CrossRef]

Aeran, A.; Siriwardane, S. C.; Mikkelsen, O.; Langen, I. A new nonlinear fatigue damage model based only on S-N curve parameters. *Int. J. Fatigue* **2017**, *103*, 327-341. [CrossRef]

Aid, A.; Amrouche, A.; Bouiadjra, B. B.; Benguediab, M., Mesmacque, G. Fatigue life prediction under variable amplitude loading based on a new damage model. *Mater. Des.* **2011**, *32*, 183-191. [CrossRef]

Aid, A.; Bendouba, M.; Aminallah, L.; Amrouche, A.; Benseddiq, N.; Benguediab, M. An equivalent stress process for fatigue life estimation under multiaxial loadings based on a new non linear damage model. *Mater. Sci. Eng. A* **2012**, *538*, 20-27. [CrossRef]

Aktan, A. E.; Tsikos, C. J.; Catbas, F. N.; Grimmelsman, K.; Barrish, R. Challenges and opportunities in bridge health monitoring. SHM-**2000**, pp. 461-473.

ASTM International. ASTM 1823-13. Standard Terminology Relating to Fatigue and Fracture Testing. **2013,** In Annual book of ASTM standards, pp. 1-25. West Conshohocken, PA.

Batsoulas, N. D. Cumulative Fatigue Damage: CDM-Based Engineering Rule and Life Prediction Aspect. *Steel Res. Int.* **2016**, *87*, 1670-1677. [CrossRef]

Bhattacharya, B.; Ellingwood, B. A Damage Mechanics Based Approach to Structural Deterioration and Reliability; Nuclear Regulatory Commission. Washington, DC, USA, 1998.

Bhattacharya, B.; Ellingwood, B. A new CDM-based approach to structural deterioration. Int. J. Solids Struct. **1999**, *36*, 1757-1779. [CrossRef]

Boardman, B.; Deere, and Company. Fatigue resistance of steels. In ASM Hand-book Committee, editor, Properties and Selection: Irons, Steels, and High-Performance Alloys. **1990**, ASM International.

Böhm, E.; Kurek, M.; Junak, G.; Cies´la, M.; Lagoda, T. Accumulation of Fatigue Damage Using Memory of the Material. *Procedia Mater. Mater. Sci.* **2014,** *3*, 2-7. [CrossRef]

Böhm, E.; Kurek, M.; Lagoda, T. Accumulation of fatigue damage for block-type loads with use of material memory function. *Solid State Phenom.* **2015**, *224*, 39-44. [CrossRef]

Cadenas, P.; Amrouche, A.; Mesmacque, G.; Jozwiak, K. Effect of the residual fatigue damage on the static and toughness properties. In *Damage and Fracture Mechanics: Failure Analysis of Engineering Materials and Structures*; Springer: Berlin/Heidelberg, Germany, **2009**, pp. 323-330. [CrossRef]

Chaboche, J. L.; Lesne, P. M. A Non-Linear Continuous Fatigue Damage Model. *Fatigue Fract. Eng. Mater. Struct.* **1988**, *11*, 1-17. [CrossRef]

Chaboche, J. L. *Une loi Différentielle D'endommagement de Fatigue avec Cumulation non Linéaire; Office Nationale d'Etudes et de Recherches Aérospatiales*: Paris, France, 1972.

Chang, F. K.; Prosser, W. H.; Schulz, M. J. Editorial: Letter of introduction from Editors of Structural Health Monitoring. *Structural Health Monitoring.* **2002**, *1*, 3-4. [CrossRef]

Chang, P. C.; Flatau, A.; Liu, S. C. Review Paper: Health Monitoring of Civil Infrastructure. *Structural Health Monitoring*. **2003**, *2*, 257-267. [CrossRef]

Chan, T. H.; Li, Z. X.; Ko, J. M. Fatigue analysis and life prediction of bridges with structural health monitoring data – Part II: Application. *Int. J. Fatigue* **2001**, *23*, 55-64 [CrossRef]

Chen, X.; Jin, D.; Kim, K. S. Fatigue life prediction of type 304 stainless steel under sequential biaxial loading. *Int. J. Fatigue* **2006**, *28*, 289-299. [CrossRef]

Chmelko, V.; Garan, M.; 14th IMEKO TC10 workshop on technical Diagnostics, Tools and techniques for system reliability, maintainability and safety, 2016, Milan, Italy.

Costa, J. D.; Ferreira, J. A.; Borrego, L. P.; Abreu, L. P. Fatigue behaviour of AA6082 friction stir welds under variable loadings. *Int. J. Fatigue* **2012**, *37*, 8-16. [CrossRef]

Crossland, B. Effect of large hydrostatic pressures on the torsional fatigue strength of an alloy steel. In Proceedings of the International Conference on fatigue of Metals, *Institution of Mechanical Engineers*, London, UK, **1956**, Volume 138, p. 12.

Czepiel, E. J. Bridge Management Systems, **1994**, Literature review and Search by the Infrastructure Technology Institute at Northwestern University. [CrossRef]

Dang-Van, K.; Macro-micro approach in high cycle multiaxial fatigue. In McDowell, D. and Ellies, R., editors, STP1191-EB Advances in Multiaxial Fatigue, ASTM International, West Conshohockeren, PA, **1994**, pp. 7-36.

Dang-Van, K.; Maitournam, M. H. Rolling contact in railways: modelling, simulation and damage prediction, **2003**, Fatigue and Fracture of Engineering Materials and Structures, 26:939-948

Dantas, R. G. R. Fatigue life estimation of steel half-pipes bolted connections for onshore wind towers applications, **2019**, [Master's thesis]. *University of Porto*.

Dattoma, V.; Giancane, S.; Nobile, R.; Panella, F. W. Fatigue life prediction under variable loading based on a new non-linear continuum damage mechanics model. *Int. J. Fatigue* **2006**, *28*, 89-95. [CrossRef]

Derriso, M. M.; Faas, P.; Calcaterra, J.; Barnes, J. H.; Sotomayer, W. Structural health monitoring applications for current and future aero-space vehicles. *Proc. 3rd Int.* Workshop on Structural Health Monitoring, Stanford, CA. **2001**, pp. 3-11.

Desimone, H.; Bernasconi, A.; Berreta, S. On the application of dang van criterion to rolling contact fatigue. **2006**, Wear 260, pp. 567-572.

Djebli, A.; Aid, A.; Bendouba, M.; Amrouche, A.; Benguediab, M.; Benseddiq, N. A non-linear energy model of fatigue damage accumulation and its verification for Al-2024 aluminium alloy. *Int. J. Non-Linear Mech.* **2013**, *51*, 145-151. [CrossRef]

Dowdell, D.; Leipholz, H.; Topper, T. The modified life law applied to SAE-1045 Steel. *Int. J. Fract.* **1986**, *31*, 29-36. [CrossRef]

El Aghoury, I.; Galal, K. A fatigue stress-life damage accumulation model for variable amplitude fatigue loading based on virtual target life. *Eng. Struct.* **2013**, *52*, 621-628. [CrossRef]
Ellyin, F. Fatigue Life Prediction Under Multiaxial Stress Conditions. *Development in Engineering Mechanics*, Selvadurai, A.P.S., Ed.; Elsevier Science Publishers BV: Amsterdam, The Netherlands, **1987**, pp. 133-158.

Ellyin, F.; Golos, K. Multiaxial fatigue damage criterion. *J. Eng. Mater. Technol.* **1988**, *110*, 63-68. [CrossRef]

Ellyin, F.; Kujawski, D. A multiaxial fatigue criterion including mean-stress effect. In McDowell, D. and Ellis, R., editors, STP1191-EB Advances in Multiaxial Fatigue, ASTM International, West Conshohocken, PA, **1993**, pp. 7-36.

Ellyin, F.; Kujawski, D. An energy-based fatigue failure criterion. *Microstruct. Mech. Behav. Mater.* **1985**, *2*, 591-600.

Enright, M. P.; Frangopol, D. M. Reliability based lifetime maintenance of aging highway bridges. SPIE-3995, **2000**, pp. 4-13.

Feltner, C. E.; Morrow, J. D. Microplastic strain hysteresis energy as a criterion for fatigue fracture. *J. Fluids. Eng. Trans. ASME* **1961**, *83*, 15-22. [CrossRef]

Fernandes, A.; de Castro, P.; Moura Branco, C. Fadiga de Estruturas Soldadas. **1999**, Funda c ao Calouste Gulbenkian, Lisboa.

Findley, W. N. A theory for the effect of mean stress on fatigue of metals under combined torsion and axial load or bending. [Providence] *Engineering Materials Research Laboratory*, **1958**, Division of Engineering, Brown University.

Fuhr, P. L. Wireless interrogation of instrumented structures. In. Ansari, F. editors, Condition Monitoring of Materials and Structures, *Engineering Mechanics Conf.* 2000, Austin, Texas. US, pp. 148-163.

Galea, S. C.; Baker, A. A. Smart structures approaches for health monitoring of aircraft structures. Proc. of SPIE Vol. 4235, *Smart Materials and MEMS*, **2000**, Melbourne, Australia, pp. 4235-4239.

Gao, H.; Huang, H. Z.; Lv, Z.; Zuo, F. J.; Wang, H. K. An improved Corten-Dolan's model based on damage and stress state effects. *J. Mech. Sci. Technol.* **2015**, *29*, 3215-3223 [CrossRef]

Gao, H.; Huang, H. Z.; Zhu, S. P.; Li, Y. F.; Yuan, R. A modified nonlinear damage accumulation model for fatigue life prediction considering load interaction affects. *Sci. World J.* **2014**, 164378. [CrossRef]

Giancane, S.; Nobile, R.; Panella, F. W.; Dattoma, V. Fatigue life prediction of notched components based on a new nonlinear continuum damage mechanics model. *Procedia Eng.* **2010**, *2*, 1317-1325. [CrossRef]

Golos, K.; Ellyin, F. A Total Strain Energy Density Theory for Cumulative Fatigue Damage. *J. Press. Vessel. Technol.* **1988**, *110*, 36. [CrossRef]

Golos, K.; Ellyin, F. Generalization of cumulative damage criterion to multilevel cyclic loading. *Theor. Appl. Fract. Mech.* **1987**, *7*, 169-176. [CrossRef]

Grover, H. An observation concerning the cycle ratio in cumulative damage. In *Symposium on Fatigue of Aircraft Structures*; ASTM International: West Conshohocken, PA, USA, **1960**.

Gu, Z.; Mi, C.; Ding, Z.; Zhang, Y.; Liu, S.; Nie, D. An energy based fatigue life prediction of a mining truck welded frame. *J. Mech. Sci. Technol.* **2016**, *30*, 3615-3624. [CrossRef]

Hashin, Z.; Rotem, A. A cumulative damage theory of fatigue failure. *Mater. Sci. Eng.* **1978**, *34*, 147-160. [CrossRef]

Hectors, K.; De Waele, W. Cumulative Damage and Life Prediction Models for High-Cycle Fatigue of Metals: A Review. Metals. **2021,** *11*, 204. [CrossRef]

Hunter, M. S.; Fricke, W. G. Metallographic aspects of fatigue behavior of aluminium. In *American Society for Testing and Materials*; AMER SOC Testing Materials 100 BARR Harbor DR: West Conshohocken, PA, USA, **1954**, *54*, 717-736.

Inoma, J. E.; Pavlou, D. G.; Zec, J. Implementation of linear, double-linear, and nonlinear fatigue damage accumulation rules for fatigue life prediction of offshore drilling top-drive tie-rods. In *IOP Conference Series: Material science and Engineering*; Institute of Physics. Publishing: Bristol, UK, **2019**, *700*. [CrossRef]

Itoh, T.; Chen, X.; Nakagawa, T.; Sakane, M. A simple model for stable cyclic stress-strain relationship of type 304 stainless steel under nonproportional loading. *J. Eng. Mater. Technol. ASME* **2000**, *122*, 1-9. [CrossRef]

Jahed, H.; Varvani-Farahani, A.; Noban, M.; Khalaji, I. An energy-based fatigue life assessment model for various metallic materials under proportional loading and non-proportional loading loading conditions. *Int. J. Fatigue* **2007**, *29*, 647-655. [CrossRef]

Jahed, H.; Varvani-Farahani, A. Upper and lower fatigue life limits model using energy-based fatigue properties. *Int. J. Fatigue* **2006**, *28*, 467-473. [CrossRef]

Jiao, J.; Lei, H.; Chen, Y. F. Numerical simulation and experimental study on constant amplitude fatigue behavior of welded cross plate-hollow sphere joints. *J. Southeast Univ. (Engl.Ed.)* **2018**, *34*, 62-70. [CrossRef]

Kachanov, L. M. Time of the rupture process under creep conditions, Izy Akd. *Nank SSR Otd Tech Nauk* **1958**, *8*, 26-31.

Kaechele, L. Review and Analysis of Cumulative Fatigue Damage Theories; Technical Report August; *The RAND Corporation*: Santa Monica, CA, USA, **1963**.
Kallmeyer, A. R.; Krgo, A.; Kurath, P. Evaluation of HCF Multiaxial Fatigue Life Prediction Methodologies for Ti-6Al.4V. *Journal of Engineering Materials and technology, 124*, 1-12.

Kamal, M.; Rahman, M. M. Advances in fatigue life modeling: A review. Renewable and Sustainable Energy Reviews, **2018**, *82*, 940-949.

Keller, E.; Ray, A. Real-Time Health Monitoring of Mechanical Structures. Structural health Monitoring. **2003**, *2*, 191-203. [CrossRef]

Kujawski, D.; Ellyin, F. A cumulative damage theory for fatigue crack initiation and propagation. *Int. J. Fatigue* **1948**, *6*, 83-88. [CrossRef]

Kwofie, S.; Rahbar, N. A fatigue driving stress approach to damage and life prediction under variable amplitude loading. *Int. J. Damage Mech.* **2013**, *22*, 393-404. [CrossRef]

Kwofie, S.; Rahbar, N. An equivalent driving force model for crack growth prediction under different stress ratios. *Int. J. Fatigue* **2011**, *33*, 1199-1204. [CrossRef]

Lagoda, T. energy models for fatigue life estimation under biaxial random loading. Part I: The model elaboration. *Int. J. Fatigue* **2001**, *23*, 467-480. [CrossRef]

Lagoda, T. energy models for fatigue life estimation under biaxial random loading. Part II: The Verification of the model. *Int. J. Fatigue* **2001**, *23*, 481-489. [CrossRef]

Lagoda, T.; Macha, E.; Bedkowski, W. X. A critical plane approach based on energy concepts: Application to biaxial random tension-compression high-cycle fatigue regime. *Int. J. Fatigue* **1999**, *21*, 431-443. [CrossRef]

Lee, Y. L.; Barkey, M. E.; Kang, H. T. Metal Fatigue Analysis Handbook – Practical Problem-Solving Techniques for Computer-Aided Engineering, **2012**, Elsevier.

Lee, Y. L.; Pan, J.; Hathaway, R. B.; Barkey, M. E. Fatigue Testing and Analysis: Theory and Practice; 2014, *Butterworth-Heinemann*: Oxford, UK.

Lefebvre, D.; Neale, K. W.; Ellyin, F. A criterion for low-cycle fatigue failure under biaxial states of stress. *J. Eng. Mater. Technol. Trans. ASME* **1981**, *103*, 1-6. [CrossRef]

Leipholz, H. H. E. Lifetime predictions for metallic specimens subjected to loading with varying intensity. *Mech. Mater. Struct. Theor.* **1985**, *20*, 239-246.

Leipholz, H. On the modified S-N curve for metal fatigue prediction and its experimental verification. *Eng. Fract. Mech.* **1986**, *23*, 495-505. [CrossRef]

Leipholz, H.; Topper, T.; El Menoufy, M. Lifetime prediction for metallic components subjected to stochastic loading. *Com- put. Struct.* **1983**, *16*, 499-507. [CrossRef]

Lemke, J. A remote vibration monitoring system using wireless internet data transfer. SPIE-3995, pp. 436-445.

Letcher, T.; Shen, M. H.; Scott-Emuakpor, O.; George, T.; Cross, C. An energy-based critical fatigue life prediction method for Al6061-T6. *Fatigue Fract. Eng. Mater. Struct.* **2012**, *35*, 861-870. [CrossRef]

Li, Z. X.; Chan, T. H., Ko, J. M. Evaluation of typhoon induced fatigue damage for Tsing Ma Bridge. *Eng. Struct.* **2002**, *24*, 1035-1047. [CrossRef]

Li, Z. X.; Chan, T. H.; Ko, J. M. Fatigue damage model for bridge traffic under traffic loading: Application made to Tsing Ma Bridge. *Theor. Appl. Fract. Mech.* **2001**, *35*, 81-91. [CrossRef]

Liu, Q.; Gao, Y.; Li, Y.; Xue, Q. Fatigue life prediction based on a novel improved version of the Corten-Dolan model considering load interaction effect. *Eng. Struct.* **2020**, *221*, 111036. [CrossRef]

Lv, Z.; Huang, H. Z.; Zhu, S. P.; Gao, H.; Zuo, F. A modified nonlinear fatigue damage accumulation model. *Int. J. Damage Mech.* **2014**, *24*, 168-181. [CrossRef]

Macha, E.; Sonsino, C. M. Energy criteria of multiaxial fatigue failure. *Fatigue Fract. Eng. Mater. Struct.* **1999**, *22*, 1053-1070. [CrossRef]

Manson, S.; Freche, J.; Ensign, C. Application of a Double Linear Damage Rule to Cumulative Fatigue Damage; *Technical Report; Manson:* 1967, West Conshohocken, PA, USA.

Manson, S. S.; Halford, G. R. Practical implementation of the double linear damage rule and damage curve approach for treating cumulative fatigue damage. *Int. J. Fract.* **1981**, *17*, 169-192. [CrossRef]

Manson, S. Interfaces between creep, fracture, and fatigue. *Int. J. Fract. Mech.* **1966**, *2*, 328-363. [CrossRef]

Maktouf, W.; Ammar, K.; Naceur, I. B.; Sai, K. Multiaxial high-cycle fatigue criteria and life prediction: Application to gas turbine blade. *International Journal of Fatigue*, **2016**, *92*, 25-35.

Marco, S. M.; Starkey, W. l. A concept of fatigue damage. *Trans. ASME* **1954**, *76*, 627-632.

Margetin, M.; Durka, R.; Chmelko, V. Multiaxial fatigue criterion based on parameters from torsion and axial S-N curve, **2016**, *10*, 146-152.

Marsh, B. K. J.; Mackinnon, J. A. Random-loading and block loading fatigue tests on sharply notched midl steel specimens. *J. Mech. Eng. Sci.* **1968**, *10*, 48-58. [CrossRef]

McDowell, D.; Ellis, J. Overviw in McDowell, D. and Ellis, R., editors, Advances in Multiaxial Fatigue, *ASTM International*, **1994**, West Conshohocken, PA, pp. 1-4.

McDiarmid, D. A general criterion for high cycle multiaxial fatigue failure. Fatigue and fracture of engineering Materials and Structures, **1991**, *14*, 429-453.

McDiarmid, D. A shear stress based critical-plane criterion of multiaxial fatigue failure for design and life prediction. Fatigue and Fracture of Engineering materials and structures, **1994**, *17*, 1475-1484.

Mesmacque, G.; Garcia, S.; Amrouche, A.; Rubio-Gonzalez, C. Sequential law in multiaxial fatigue, a new damage indicator. *Int. J. Fatigue* **2005**, *27*, 461-467. [CrossRef]

Milovanovic, V.; Arsic, D.; Milutinovic, M.; Zivkovic, M.; Topalovic, M. A comparison study of fatigue behavior of S355J2+N, S690QL and X37CrMoV5-1 steel. Metals, **2022**, *12*, 1199.

Mita, A. Emerging needs in Japan for health monitoring technologies in civil and building streuctures. *SHM*, **2000**, 56-67.

Morrow, J. D. The effect of selected syb-cycle sequences in fatigue loading histories.Random Fatigue Life Predict. **1986**, *72*, 43-60.

Natke, H. G.; Cempel, C. Model-aided diagnosis of mechanical systems, fundamentals, detection, localization, assessment, Springer-Verlag, Berlin.

Oller, S.; Salomon, O.; Onate, E. A continuum mechanics model for mechanical fatigue analysis. *Comput. Mater. Sci*. **2005**, *32*, 175-195 [CrossRef]

Oshima, T.; Rahman, M.; Mikami, S.; Yamazaki, T.; Takada, N.; Lesko, J.; Kriz, R. Application of smart materials ans systems to long-term bridge health monitoring. SPIE-3995, 2000, pp. 253-263.

Ozaltun, H.; Shen, M. H.; George, T., Cross, C. An Energy based fatigue life protection framework for in-service structural components. *Exp. Mech*. **2011**, *51*, 707-718. [CrossRef]

Papadopoulos, I. V.; Panoskaltsis, V. P. Invariant formulation of a gradient dependent multiaxial high-cycle fatigue criterion. *Eng. Fract. Mech*. **1996**, *55*, 513-528. [CrossRef]

Park, S. H.; Hong. S. G.; Lee, B. H., Lee, C. S. Fatigue life prediction of rolled AZ31 magnesium alloy using an energy-based model. *Int. j. Mod. Phys*. B **2008**, *22*, 5503-5508. [CrossRef]

Pavlou, D. A phenomenological fatigue damage accumulation rule based on hardness increasing, for the 2024-T42 aluminium. *Eng. Struct.* **2002**, *24*, 1363-1368. [CrossRef]

Pavlou, D. G. The theory of the S-N fatigue damage envelope: Generalization of linear, double-linear, and non-linear fatigue damage models. *Int. J. fatigue* **2018**, *110*, 204-214. [CrossRef]

Peeters, B.; Maeck, J.; De Roeck, G. Monitoring of the Z24 bridge: separating temperature effects from damage. 2000, pp. 377-386.

Peng, Z.; Huang, H. Z.; Zhou, J.; Li, Y. F. A new cumulative fatigue damage rule based on dynamic residual S-N curve and material memory concept. Metals 2018, 8, 456. [CrossRef]

Peng, Z.; Huang, H. Z., Zhu, S. P.; Gao, H.; Lv, Z. A fatigue driving energy approach to high-cycle fatigue life estimation under variable amplitude loading. *Fatigue Fract. Eng. Mater. Struct.* **2016**, *39*, 180-193. [CrossRef]

Pitoiset, X.; Preumont, A. Spectral methods for multiaxial random fatigue analysis of metallic structures. *Int. J. fatigue* **2000**, *22*, 541-550. [CrossRef]

Prine, D. W. Problems associated with nondestructive evaluation of bridges. BIRL, Northwestern Univ. Industrial research Lab. [CrossRef]

Rabotnov, Y. N. Creep problems in structural members. *J. Appl. Mech. Mar*. **1979**, *37*, 249. [CrossRef]

Rahman, M. S.; Oshima, T.; Mikami, S.; Yamaaki, T.; Tamba, I. Diagnosis of aged bridge by using intelligent monitoring system. SHM, 2000, pp. 484-493.

Rao, J. S.; Pathak, A., Chawla, A. Blade life: A comparison by cumulative damage theories. *J. Eng. Gas. Turbines power* **2001**, *123*, 886-892. [CrossRef]

Rege, K.; Pavlou, D. G. A one-parameter nonlinear fatigue damage accumulation model. *Int. J. Fatigue* **2017**, *98*, 234-246. [CrossRef]

Richart, f. E.; Newmark, N. M. A hypothesis for the determination of cumulative damage in fatigue. I ncivil engineering classics; Newmark, N. M., Ed.; ASCE: Reston, VA, USA, 1948, pp. 279-312.

Robert, J. L. Contribution a L'etude de la fatigue multi axiale sous Sollicitations Periodique ou Aleatoires. Ph.D. Thesis, Institut National des sciences appliquees, Lyon France, 1992.

Schijve, J. Fatigue of structures and materials. Kluwer Academic Publishers, United States of America.

Shütz, W. A history of fatigue. Engineering Fracture Mechanics, 54, 263-300

Scott-Emuakpor, O. E. Development of a novel energy-based method for multi-axial fatigue assessment. Ph.D. thesis, The Ohio State University, 2007.

Scott-Emuakpor, O. E.; Shen, H.; George, T.; Cross, C. An energy-based uniaxial fatigue life prediction method for commonly used gas turbine engine materials. *J. Eng. Gas. Turbines. Power* **2008**, *130*, 062504. [CrossRef]

Scott-Emuakpor, O.; George, T.; Cross, C.; Shen, M. H. Multi-axial fatigue life prediction via a strain-energy method. AIAAJ. **2010**, *48*, 63-72. [CrossRef]

Scott-Emuakpor, O.; Herman Shen, M. H., Cross, C.; Calcaterra, J.; George, T. A promising new energy-based fatigue life prediction framework. *Proc. ASME Turbo Expo* **2005**, *4*, 397-404. [CrossRef]

Scott-Emuakpor, O.; Herman Shen, M. H.; Cross, C.; Calcaterra, J.; George, T. Development of an improved high cycle fatigue criterion. In *ASME Turbo Expo*; ASME: Vienna, Austria, **2004**; pp. 1-8 [CrossRef]

Scott-Emuakpor, O.; Shen, M. H., George, T.; cross, C.; Calcaterra, J. Development of an improved high cycle fatigue criterion. *J. Eng. Gas. Turbines Power* **2007**, *129*, 162-169. [CrossRef]

Shen, C.; Talha, A.; Hamdi, A.; Benseddiq, N. A new cumulative fatigue damage model under biaxial loading. *Proc. inst. Mech. Eng. Part L J. mater. Des. Appl*. **2020**, *234*, 962-973. [CrossRef]

Si-Jian, L.; Wer, L.; Da,-Qing, T., Jun-Bi, L. A new fatigue damage accumulation model considering loading history and loading sequence based on damage equivalence. *Int. J. damage Mech.* **2018**, *27*, 707-728. [CrossRef]

Sinclair, G. An investigation of the coaxing effect in fatigue of metals, Technical Report; Illinois University: Urbana, IL, USA, 1952

Sines, G. Behavior of metals under complex static and alternating stresses. Met. Fatigue 1959, 1, 146-169.

Sines, G. Failure of materials under combined repeated stresses with superimposed static stresses. National Advisory Committee for Aeronautics.

Siriwardane, S.; Ohga, M.; Dissanayake, R.; Taniwaki, K. Application of new damage indicator-based sequential law for remaining fatigue life estimation of railway bridges. *J. Constr. Steel Res*. **2008**, *64*, 228-237. [CrossRef]

Socie, D. Critical plane approaches for multiaxial fatigue damage assessment. In McDowell, D and Ellis, R., editors, STP1191-EB Advances in Multiaxial Fatigue, pages 7-36 ASTM International, West Conshohocken, PA, 1993.

Socie, D. Multiaxial stress-life technical background, 2018.

Spitzer, R.; Corten, H. T. Effect of loading sequence on cumulative fatigue damage of 7075-T6 aluminium alloy. In proceedings of the American Society for Testing snd Materials; ASTM Philadelphia, PA USA, 1956, 61, 719-731.

Stowell, E. Z. a study of energy criterion for fatigue. Nucl. Eng. Des. 1966, 3, 32-40 [CrossRef]

Strasser, E. G. A modular, wireless, damage monitoring system for structures. Ph.D Dissertation, Dept. Civ.Eng., 1998, Stanford, Palo Alto, USA.

Subramanyan, S. A cumulative damage rule based on the knee point of the S-N curve. *J. eng. Mater. Technol.* **1976**, *98*, 316-321. [CrossRef]

Sun, Y.; Lu, S.; Meng, Q.; Wang, X. Online damage model os team turbine based on continuum damage mechanics. On proceedings of the Chinese Control Conference, CCC Dalian, China, 2017, 10392-10397. [CrossRef]

Theil, N. Fatigue life prediction method for the practical engineering use taking in account the effect of the overload blocks. *Int. J. Fatigue* **2016**, *90*, 23-35. [CrossRef]

Todoroki, A., Shimamura, Y.; Inada, T. Plug and monitor system via ethernet with drstributed sensors and ccd camera. SHM, 2000, pp. 571-580.

Van der Auweraer, H.; Peeters, B. International Projects on Structural health monitoring: An overview. SHM, 2003, 2, 341-358. [CrossRef]

Van Lieshout, P.; den besten, J.; Kaminski, M. Validation of the corrupted dang van multiaxial fatigue criterion applied to turret bearings of from offloading buoys. Ships and Offshore structures, 2017, 12, 521-529.
Wang, H.; Qin, S.; Wang, Y. Nonlinear cumulative damage model and application to bridge fatigue life evaluation. *Adv. Struct. Eng*. **2018**, *21*, 1402-1408. [CrossRef]

Weaver, J.; Gupta, S.; Woods, T.; The effects of test speed on fatigue life of Nitinol wire in rotary bend. 10.1520/STP155920120213

Wertz, J.; Shen, M. H., Scott-Emuakpor, O.; George, T.; Cross, C. An energy-based torsional shear fatigue lifting method. *Exp. Mech*. **2012**, *52*, 705-715. [CrossRef]

Xi, L.; Songlin, Z. Changes in mechanical properties of vehicle compoenents after strengthening under low amplitude loads below the fatigue limit. *Fatigue Fract. Eng. Mater. Struct*. **2009**, *32*, 847-855, [CrossRef]

Xi, L.; Songlin, Z. Strengthening of transmission gear under low amplitude loads. *Mater. Sci. Eng.* A **2008**, *488*, 55-63. [CrossRef]

Xia, F. L.; Zhu, S. P.; Liao, D.; Dantas, R.; Correia, J. A.; De Jesus, A. M. Isodamage curve-based fatigue damage accumulation model considering the exhaustion of static toughness. *Eng. Fail. Anal.* **2020**, *115*, 104575 [CrossRef]

Xue, Q.; Du, X.; Wang, S.; An improved fatigue life prediction model based on loading sequence. *Sci*. **2019**, *40*, 88-93. [CrossRef]

Xu, J.; Shang, D. G.; Sun, G. Q.; Chen, H.; Liu, E. T. Fatigue life prediction for GH4169 superalloy under multiaxial variable amplitude loading. *J. technol*. **2012**, *38* 1462-1466.

Xu, Y. L.; Chen, Z. W.; Xia, Y. fatigue assessment of multi-loading suspension bridges using continuum damages model. *Int. j. Fatigue* **2012**, *40*, 27-35. [CrossRef]

Xu, Y. L.; Liu, T. T.; Zhang, W. S. Buffeting-induced fatigue damage assessment of along suspension bridge. *Int. J. fatigue* **2009**, *31*, 575-586. [CrossRef]

Yamamoto, Y.; Mita, A.; Okada, K. Intranet-based remote monitoring system for construction site proc. Annual meeting of the archit. Inst. pp. 417-418.

Yang, X.; Yao, W.; Duan, C. The review of ascertainable fatigue cumulative damage rule. *Eng. Sci.* **2003**, *5*, 82-87.

Ye, D.; Wang, Z. A new approach to low-cycle fatigue damage based on exhaustion of static toughness and dissipation of cyclis plastic strain energy during fatigue. *Int. J. Fatigue* **2001**, *23*, 679-687. [CrossRef]

Ye, D.; Wang, Z. Change characteristics of static mechanical property parameters and dislocation structures of 45# medium carbon structural steel during fatigue failure process. *Mater. Sci. Eng*. A **2001**, *297*, 54-61. [CrossRef]

Yuan, R.; Li, H.; Huang, H. Z.; Zhu, S. P.; Gao, H. A nonlinear fatigue damage accumulation model considering strength degradation and it applications to fatigue reliability analysis. *Int. J. Damage Mech.* **2015**, *24*, 646-662. [CrossRef]

Yung-Li, L.; Tjhung, T. Chapter 3 – Ranflow cycle counting techniques, Metal fatigue analysis handbook, **2012**, 89-114. [CrossRef]

Zhang, J.; F, X.; Lin, J.; Liu, Z.; Liu, N.; Wu, B. Study on damage accumulation and life prediction with loads below fatigue limit based on a modified nonlinear model. Materials **2018**, 11, 2298. [CrossRef]

Zhao, S. B. Study on the accuracy of fatigue life predictions by the generally used damage accumulation theory. *J. Mech. Strength* **2000**, *22*, 206-209.

Zhou, J.; Huang, H. Z.; Barnabart, M. V.; Huang, G.; Li, Y. F. A novel linear cumulative fatigue damage model based on the degradation of material memory. *Int. J. Damage Mech*. **2020**, *29*, 610-625. [CrossRef]

Zhu, S. P.; Hao, Y. Z.; de Oliveira Correia, J. A.; Lesiuk, G.; de Jesus, A. M. Nonlinear fatigue damage accumulation and life prediction of metals: A comparative study. *Fatigue Fract. Eng. Mater. Struct.* **2019**, *42*, 1271-1282. [CrossRef]

Zhu, S. P.; Huang, h. Z.; Liu, Y.; He, L. P.; Liao, Q. A practical method for determining the Corten-Dolan exponent and its application to fatigue life prediction. *Int. J. Turbo JET Engines* **2012**, *29*, 79-87. [CrossRef]

Zhu, S. P.; Huang, H. Z.; Xie, L. Y. Nonlinear fatigue damage cumulative model and the analysis of the strength degradation based on the double parameter fatigue criterion. China *Mech. Eng*. **2008**, *19*, 2753-2761.

Zhu, S. P.; Liao, D.; Liu, Q.; Correia, J. A.; de Jesus, A. M. Nonlinear fatigue damage accumulation. Isodamage curve-based model and life prediction aspects. *Int. J. Fatigue* **2019**, *128*, 105185. [CrossRef]

Appendix A: Experimental Fatigue Test Data

The test was done in 6 different parts, due to not being able to do it in one go. Either due to scheduling issues with other bachelor or master's thesis students, or due to the risk of damaging the Instron machine. The machine also was not able to hit peaks or bottoms accurately and therefore, there were deviations from the programmed loads. Part 1 is divided into two, because it changes after 3000 cycles from the first block to the second block. Its time is combined for both parts.

The test was programmed in three different loads for a number of cycles.

First block: Max stress = 400 MPa, Min stress = 50 MPa, for a number of 3000 cycles.

Second block: Max stress = 300 MPa, Min stress = 50 MPa, for a number of 300 000 cycles.

Third block: Max stress = 350 MPa, Min stress = 50 MPa, to go until failure.

Test	Numbers of cycles (n_i)	Maximum stress σ_{max} (MPa)	Minimum Stress σ_{min} (MPa)	Time (hours)
Part 1-1	3000	429.23	18.52	-
Part 1-2	300 000	333.17	16.08	48.58
Part 2	257 819	386.42	14.80	47.74
Part 3	257 036	384.54	18.19	48.02
Part 4	142 369	384,9	18.84	26.23
Part 5	23 261	386.06	19.33	4.26
Part 6	327 174	388.16	20.04	58.68
Total	1 310 659	-	-	233.51

Appendix B: Calculations

Miner's rule (with modified Goodman) (linear):

$$\sigma_{mean} = \frac{(\sigma_{max} + \sigma_{min})}{2}$$

$$\sigma_a = \frac{(\sigma_{max} - \sigma_{min})}{2}$$

$$\sigma_{eq} = \frac{(\sigma_a)}{1 - (\frac{\sigma_{mean}}{\sigma_u})}$$

$$\frac{n_1}{N_1} + \frac{n_2}{N_2} = 1$$

$$n_2 = 1 - \left(\frac{n_1}{N_1}\right) * N_2$$

$$\frac{n_1}{N_1} + \frac{n_2}{N_2} + \frac{n_3}{N_3} = 1$$

$$n_3 = 1 - \left(\frac{n_1}{N_1}\right) - \left(\frac{n_2}{N_2}\right) * N_3$$

Rege-Pavlou model (nonlinear):

$$\left(\frac{n_1}{N_1}\right)^{\left(\frac{\sigma_2}{\sigma_1}\right)^{0,75}} + \frac{n_2}{N_2} = 1$$

$$\frac{n_2}{N_2} = 1 - \left(\frac{n_1}{N_1}\right)^{\left(\frac{\sigma_2}{\sigma_1}\right)^{0,75}}$$

$$\left(\frac{n_1}{N_1}\right)^{\left(\frac{\sigma_2}{\sigma_1}\right)^{0,75}} + \left(\frac{n_2}{N_2}\right)^{\left(\frac{\sigma_3}{\sigma_2}\right)^{0,75}} + \frac{n_3}{N_3} = 1$$

$$\frac{n_3}{N_3} = 1 - \left(\frac{n_1}{N_1}\right)^{\left(\frac{\sigma_2}{\sigma_1}\right)^{0,75}} - \left(\frac{n_2}{N_2}\right)^{\left(\frac{\sigma_3}{\sigma_2}\right)^{0,75}}$$

Fatigue Life Calculation (linear) (Miner's rule)

Test 1: High-to-low block loading.

$$\sigma_{mean} = \frac{(\sigma_{max} + \sigma_{min})}{2}$$

$$\sigma_{mean1} = \frac{(400 + 50)}{2} = 225\ MPa$$

$$\sigma_a = \frac{(\sigma_{max} - \sigma_{min})}{2}$$

$$\sigma_{a1} = \frac{(400 - 50)}{2} = 175\ MPa$$

$$\sigma_{eq} = \frac{(\sigma_a)}{1 - (\frac{\sigma_{mean}}{\sigma_u})}$$

$$\sigma_{eq1} = \frac{(175)}{1 - (\frac{225}{600})} = 280\ MPa$$

$$n_1 = 3000$$

$$N_1 = 80000$$

$$\sigma_{mean2} = \frac{(300 + 50)}{2} = 175\ MPa$$

$$\sigma_{a2} = \frac{(300 - 50)}{2} = 125\ MPa$$

$$\sigma_{eq2} = \frac{(125)}{1 - (\frac{175}{600})} = 176{,}471\ MPa$$

$$N_2 = 3\ 500\ 000$$

$$\frac{n_1}{N_1} + \frac{n_2}{N_2} = 1$$

$$n_2 = 1 - \left(\frac{n_1}{N_1}\right) * N_2$$

$$n_2 = 1 - \left(\frac{3000}{80\,000}\right) * 3\,500\,000 = 3\,368\,750$$

$$\frac{n_2}{N_2} = \frac{3\,368\,750}{3\,500\,000} = 0{,}9625$$

The procedure is the same for the 5 other tests

Test 2: High-to-low block loading. Only change is

$$n_1 = 6000$$

$$n_2 = 1 - \left(\frac{n_1}{N_1}\right) * N_2$$

$$n_2 = 1 - \left(\frac{6000}{80\,000}\right) * 3\,500\,000 = 3\,237\,500$$

$$\frac{n_2}{N_2} = \frac{3\,237\,500}{3\,500\,000} = 0{,}925$$

Test 3: High-to-low block loading.

$$n_1 = 9000$$

$$n_2 = 1 - \left(\frac{n_1}{N_1}\right) * N_2$$

$$n_2 = 1 - \left(\frac{9000}{80\,000}\right) * 3\,500\,000 = 3\,106\,250$$

$$\frac{n_2}{N_2} = \frac{3\,106\,250}{3\,500\,000} = 0{,}8875$$

Test 4: Then the loads are reversed. Low-to-high block loading.

$$\sigma_{mean} = \frac{(\sigma_{max} + \sigma_{min})}{2}$$

$$\sigma_{mean1} = \frac{(300 + 50)}{2} = 175\ MPa$$

$$\sigma_a = \frac{(\sigma_{max} - \sigma_{min})}{2}$$

$$\sigma_{a1} = \frac{(300 - 50)}{2} = 125\ MPa$$

$$\sigma_{eq} = \frac{(\sigma_a)}{1 - (\frac{\sigma_{mean}}{\sigma_u})}$$

$$\sigma_{eq1} = \frac{(125)}{1 - (\frac{175}{600})} = 176{,}471\ MPa$$

$$n_1 = 3000$$

$$N_1 = 3\ 500\ 000$$

$$\sigma_{mean2} = \frac{(400 + 50)}{2} = 225\ MPa$$

$$\sigma_{a2} = \frac{(400 - 50)}{2} = 175\ MPa$$

$$\sigma_{eq2} = \frac{(125)}{1 - (\frac{175}{600})} = 280\ MPa$$

$$N_2 = 80\ 000$$

$$\frac{n_1}{N_1} + \frac{n_2}{N_2} = 1$$

$$n_2 = 1 - \left(\frac{n_1}{N_1}\right) * N_2$$

$$n_2 = 1 - \left(\frac{3000}{3\ 500\ 000}\right) * 80\ 000 = 79\ 931$$

$$\frac{n_2}{N_2} = \frac{79\ 931}{80\ 000} = 0{,}99914$$

Test 5: Low-to-high block loading.

$$n_1 = 6000$$

$$N_1 = 3\ 500\ 000$$

$$N_2 = 80\ 000$$

$$n_2 = 1 - \left(\frac{n_1}{N_1}\right) * N_2$$

$$n_2 = 1 - \left(\frac{6000}{3\ 500\ 000}\right) * 80\ 000 = 79\ 862$$

$$\frac{n_2}{N_2} = \frac{79\ 862}{80\ 000} = 0{,}99829$$

Test 6: Low-to-high block loading.

$$n_1 = 9000$$

$$N_1 = 3\ 500\ 000$$

$$N_2 = 80\ 000$$

$$n_2 = 1 - \left(\frac{n_1}{N_1}\right) * N_2$$

$$n_2 = 1 - \left(\frac{9000}{3\ 500\ 000}\right) * 80\ 000 = 79\ 794$$

$$\frac{n_2}{N_2} = \frac{79\ 794}{80\ 000} = 0{,}99743$$

Fatigue Life Calculation (nonlinear) (Rege-Pavlou model)

Test 1: High-to-low block loading.

$$\left(\frac{n_1}{N_1}\right)^{\left(\frac{\sigma_2}{\sigma_1}\right)^{0,75}} + \frac{n_2}{N_2} = 1$$

$$\frac{n_2}{N_2} = 1 - \left(\frac{n_1}{N_1}\right)^{\left(\frac{\sigma_2}{\sigma_1}\right)^{0,75}}$$

$$\frac{n_2}{N_2} = 1 - \left(\frac{3000}{80\,000}\right)^{\left(\frac{176,471}{280}\right)^{0,75}}$$

$$\frac{n_2}{N_2} = 0,788$$

Test 2: High-to-low block loading.

$$\left(\frac{n_1}{N_1}\right)^{\left(\frac{\sigma_2}{\sigma_1}\right)^{0,75}} + \frac{n_2}{N_2} = 1$$

$$\frac{n_2}{N_2} = 1 - \left(\frac{n_1}{N_1}\right)^{\left(\frac{\sigma_2}{\sigma_1}\right)^{0,75}}$$

$$\frac{n_2}{N_2} = 1 - \left(\frac{6000}{80\,000}\right)^{\left(\frac{176,471}{280}\right)^{0,75}}$$

$$\frac{n_2}{N_2} = 0,706$$

Test 3: High-to-low block loading.

$$\left(\frac{n_1}{N_1}\right)^{\left(\frac{\sigma_2}{\sigma_1}\right)^{0,75}} + \frac{n_2}{N_2} = 1$$

$$\frac{n_2}{N_2} = 1 - \left(\frac{n_1}{N_1}\right)^{\left(\frac{\sigma_2}{\sigma_1}\right)^{0,75}}$$

$$\frac{n_2}{N_2} = 1 - \left(\frac{9000}{80\ 000}\right)^{\left(\frac{176{,}471}{280}\right)^{0{,}75}}$$

$$\frac{n_2}{N_2} = 0{,}644$$

Test 4: Low-to-high block loading.

$$\left(\frac{n_1}{N_1}\right)^{\left(\frac{\sigma_2}{\sigma_1}\right)^{0{,}75}} + \frac{n_2}{N_2} = 1$$

$$\frac{n_2}{N_2} = 1 - \left(\frac{n_1}{N_1}\right)^{\left(\frac{\sigma_2}{\sigma_1}\right)^{0{,}75}}$$

$$\frac{n_2}{N_2} = 1 - \left(\frac{3000}{3\ 500\ 000}\right)^{\left(\frac{280}{176{,}471}\right)^{0{,}75}}$$

$$\frac{n_2}{N_2} = 1$$

Test 5: Low-to-high block loading.

$$\left(\frac{n_1}{N_1}\right)^{\left(\frac{\sigma_2}{\sigma_1}\right)^{0{,}75}} + \frac{n_2}{N_2} = 1$$

$$\frac{n_2}{N_2} = 1 - \left(\frac{n_1}{N_1}\right)^{\left(\frac{\sigma_2}{\sigma_1}\right)^{0{,}75}}$$

$$\frac{n_2}{N_2} = 1 - \left(\frac{6000}{3\ 500\ 000}\right)^{\left(\frac{280}{176{,}471}\right)^{0{,}75}}$$

$$\frac{n_2}{N_2} = 0{,}999$$

Test 6: Low-to-high block loading.

$$\left(\frac{n_1}{N_1}\right)^{\left(\frac{\sigma_2}{\sigma_1}\right)^{0,75}} + \frac{n_2}{N_2} = 1$$

$$\frac{n_2}{N_2} = 1 - \left(\frac{n_1}{N_1}\right)^{\left(\frac{\sigma_2}{\sigma_1}\right)^{0,75}}$$

$$\frac{n_2}{N_2} = 1 - \left(\frac{9000}{3\ 500\ 000}\right)^{\left(\frac{280}{176,471}\right)^{0,75}}$$

$$\frac{n_2}{N_2} = 0,999$$

Fatigue life calculation of performed experiment

Until now, we have calculated the fatigue life of the planned tests (theoretical values). Now we calculate the actual damage done to specimen. Test was done in 3 parts.

The test was programmed in three different loads for a number of cycles.

First block: Max stress = 400 MPa, Min stress = 50 MPa, for a number of 3000 cycles.

Second block: Max stress = 300 MPa, Min stress = 50 MPa, for a number of 300 000 cycles.

Third block: Max stress = 350 MPa, Min stress = 50 MPa, to go until failure.

$$\sigma_{mean3} = \frac{(350 + 50)}{2} = 200\ MPa$$

$$\sigma_{a3} = \frac{(350 - 50)}{2} = 150\ MPa$$

$$\sigma_{eq3} = \frac{(150)}{1 - (\frac{175}{600})} = 225\ MPa$$

$$N_3 = 450\ 000$$

Miner's rule

$$\frac{n_1}{N_1} + \frac{n_2}{N_2} + \frac{n_3}{N_3} = 1$$

$$n_3 = 1 - \left(\frac{n_1}{N_1}\right) - \left(\frac{n_2}{N_2}\right) * N_3$$

$$n_3 = 1 - \left(\frac{3000}{80\,000}\right) - \left(\frac{300\,000}{3\,500\,000}\right) * 450\,000 = 471696$$

$$\frac{n_3}{N_3} = 0{,}954$$

Rege-Pavlou model

$$\sigma_{eq1} = \frac{(175)}{1 - (\frac{225}{600})} = 280\ MPa$$

$$\sigma_{eq2} = \frac{(125)}{1 - (\frac{175}{600})} = 176{,}471\ MPa$$

$$\sigma_{eq3} = \frac{(150)}{1 - (\frac{175}{600})} = 225\ MPa$$

$$\left(\frac{n_1}{N_1}\right)^{\left(\frac{\sigma_2}{\sigma_1}\right)^{0,75}} + \left(\frac{n_2}{N_2}\right)^{\left(\frac{\sigma_3}{\sigma_2}\right)^{0,75}} + \frac{n_3}{N_3} = 1$$

$$\frac{n_3}{N_3} = 1 - \left(\frac{3000}{80\,000}\right)^{\left(\frac{176{,}471}{280}\right)^{0,75}} - \left(\frac{300\,000}{3\,500\,000}\right)^{\left(\frac{225}{176{,}741}\right)^{0,75}}$$

$$\frac{n_3}{N_3} = 0{,}117$$

Furthermore, this was what we programmed into the machine, but due to the machine not being able to hit actual max and min stress values, we also calculate with the number from Appendix A.

Test	Numbers of cycles (n_i)	Maximum stress σ_{max} (MPa)	Minimum Stress σ_{min} (MPa)	Time (hours)
Part 1-1	3000	429.23	18.52	-
Part 1-2	300 000	333.17	16.08	48.58
Part 2	257 819	386.42	14.80	47.74
Part 3	257 036	384.54	18.19	48.02
Part 4	142 369	384,9	18.84	26.23
Part 5	23 261	386.06	19.33	4.26
Part 6	327 174	388.16	20.04	58.68
Total	1 310 659	-	-	233.51

$\boldsymbol{\sigma_{mean}}$ (MPa)	$\boldsymbol{\sigma_a}$ (MPa)	$\boldsymbol{\sigma_{eq}}$ (MPa)
438,49	419,97	1560,16
341,21	325,13	753,80
393,82	379,02	1102,97
393,63	375,44	1091,59
394,32	375,48	1095,33
395,72	376,39	1105,55
398,18	378,14	1124,18

Graphs

Miner's rule

n_2/N_2	n_1/N_1
0,9625	0,0375
0,925	0,075
0,8875	0,1125
0,99914	0,00085714
0,99829	0,00171429
0,99743	0,00257143

Rege-Pavlou

0,788	0,0375
0,706	0,075
0,644	0,1125
1	0,00085714
0,999	0,00171429
0,999	0,00257143

Graph with Miner's rule

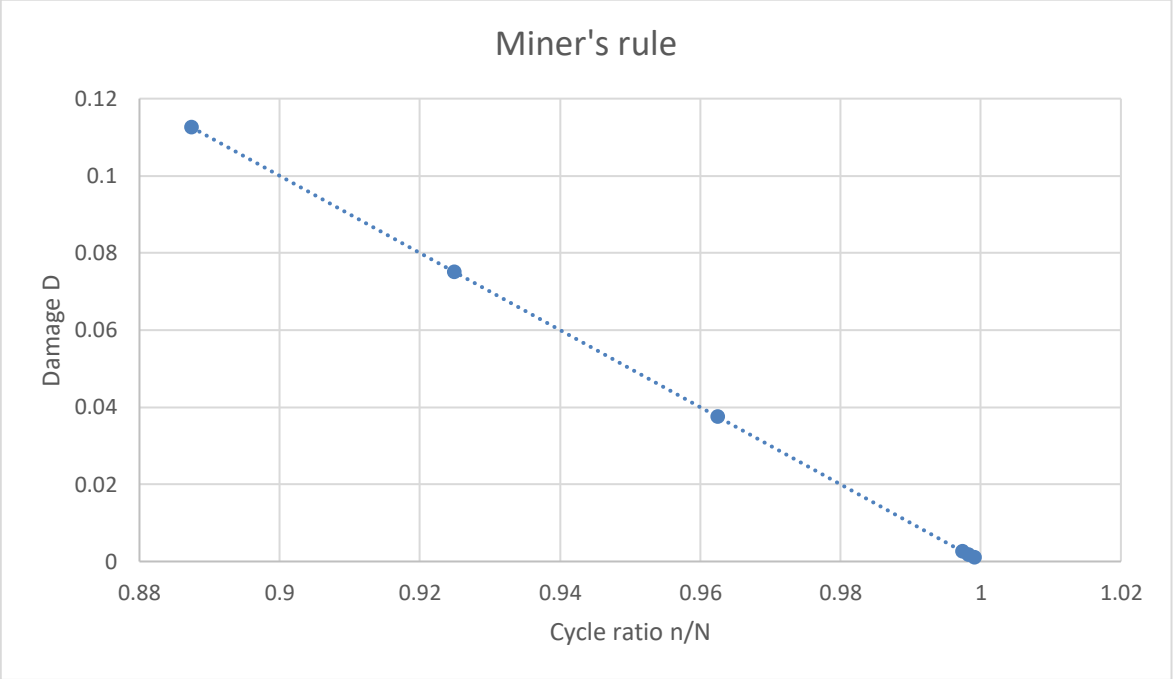

Graph with Rege-Pavlou

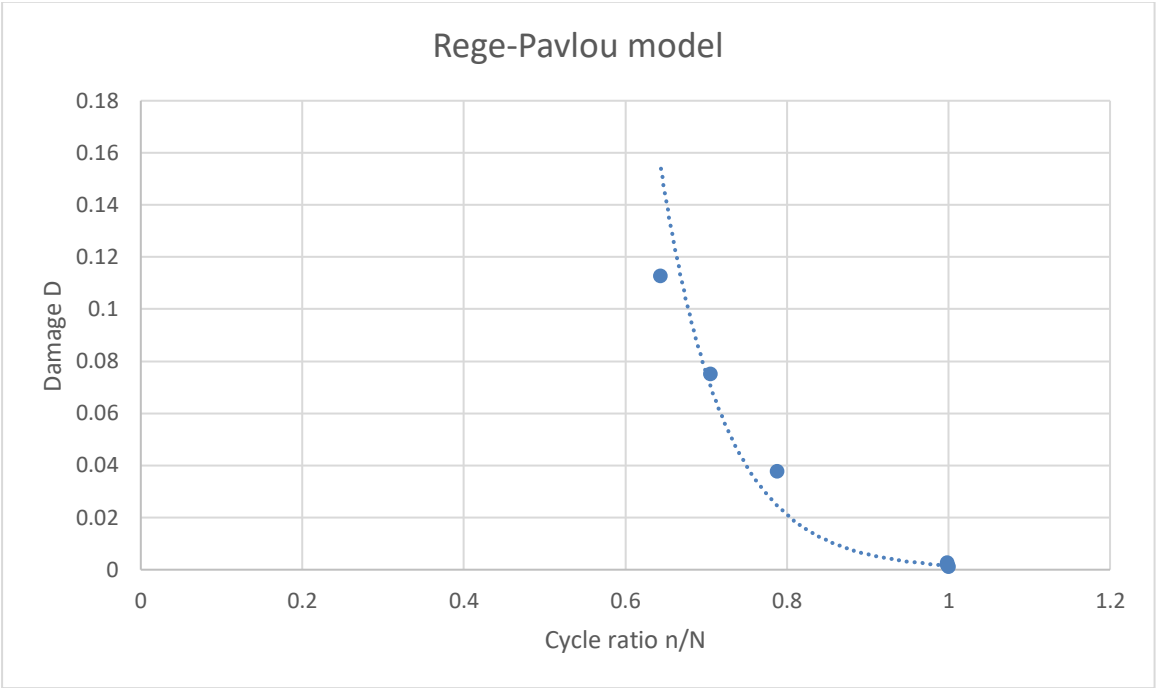

Experimental fatigue curve (Miner's rule)

Result of experiment with Miner's rule n3/N3= 0,954

Graph with experimental result (Miner's rule)

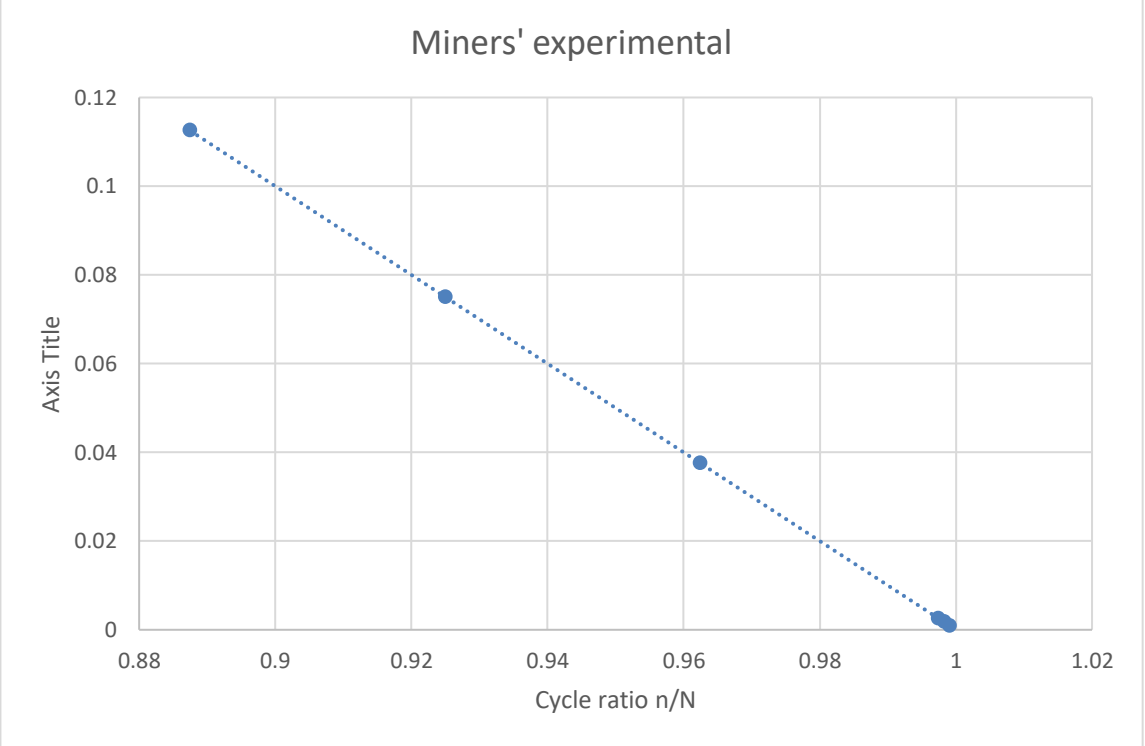

Experimental fatigue curve (Rege-Pavlou model)

Result from experiment with Rege-Pavlou model n3/N3 = 0,117

Graph with Rege-Pavlou model

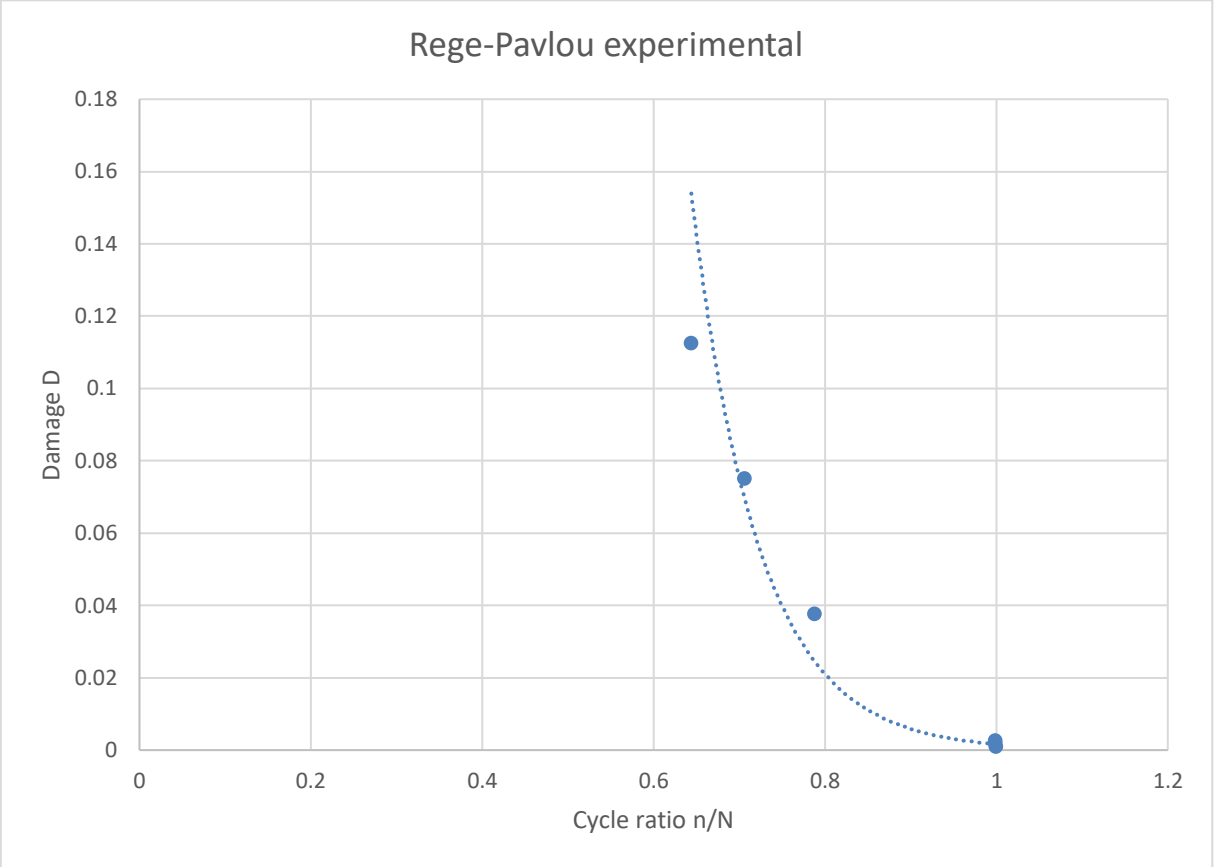

Appendix C: Tensile Test Results

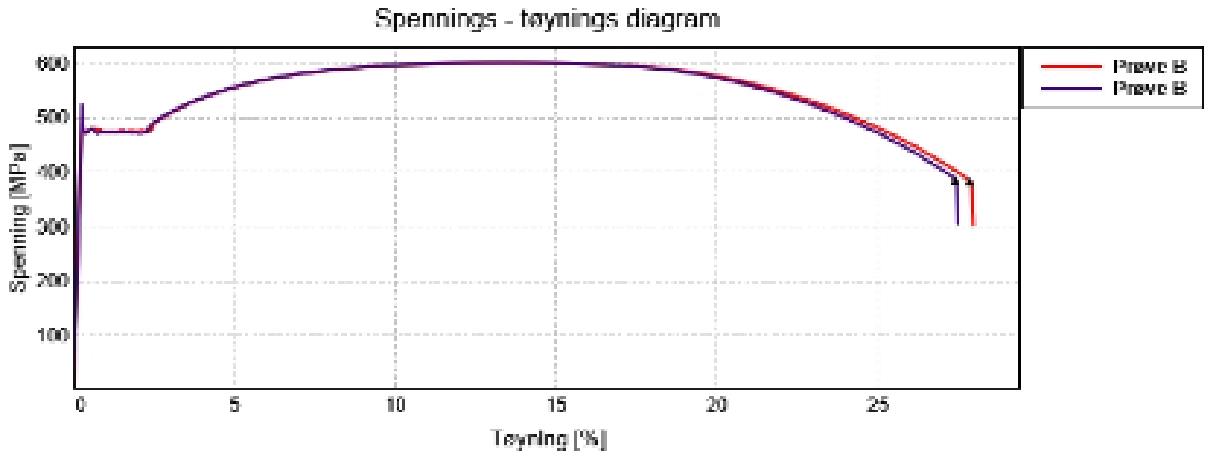

	Prøvenavn	E-modul [GPa]	ReH [MPa]	ReL [MPa]	Rp0.2 [MPa]	Strekkfasthet, Rm [MPa]	Spenning ved brudd [MPa]	Tøyning ved brudd, A [%]
2	Prøve B	202	506	471	470	600	383	27.9
3	Prøve B	200	524	470	470	601	386	27.4